A Linear Data-Driven System Identification Methodology for an Active/Passive Solar Thermal Storage System and Application to a Solar House

Amélie Allard

A Thesis
in the Department
of
Building, Civil and Environmental Engineering

Presented in Partial Fulfillment of the Requirements
for the Degree of Master of Applied Science (Building Engineering) at
Concordia University
Montreal, Quebec, Canada

July 2013

CONCORDIA UNIVERSITY
School of Graduate Studies

This is to certify that the thesis prepared

By: Amélie Allard

Entitled: A Linear Data-Driven System Identification Methodology for an Active/Passive Solar Thermal Storage System and Application to a Solar House

and submitted in partial fulfillment of the requirements for the degree of

Master of Applied Science (Building Engineering)

complies with the regulations of the University and meets the accepted standards with respect to originality and quality.

Signed by the final examining committee:

Dr. R. Zmeureanu Chair

Dr. L. Wang Examiner

Dr. S. Williamson Examiner

Dr. A. Athienitis Supervisor

Approved by _____
Chair of Department or Graduate Program Director

_____
Dean of Faculty

Date _____

ABSTRACT

A Linear Data-Driven System Identification Methodology for an Active/Passive Solar Thermal Storage System and Application to a Solar House

Amélie Allard

This thesis presents a methodology developed to identify a parametric model of a thermally-activated building system (TABS) using a system identification (SI) tool. The model was identified with collected data from an energy efficient solar single-family residential building, the Ecoterra™ house located in Eastman, Quebec. The TABS is a ventilated concrete slab (VCS) serving as an energy storage medium for active and passive solar gains in the basement. The system uses the structural mass of the house to store active solar gains collected by the building-integrated photovoltaic/thermal (BIPV/T) roof and passive solar gains entering the living space through the energy efficient windows.

A data-driven system identification approach is used. Identifying a linear model and obtaining a low-order polynomial model were the main identification criteria. The thesis addresses the issues of the monitoring sensor accuracy on the model parameters, how physical knowledge of the VCS dynamic system can be considered during its validation and how the identification assumptions guide the future use of the model.

This thesis also demonstrates that the identified linear polynomial model is an efficient tool to carry out redesign studies and possible control studies. Improved BIPV/T roof designs are compared based on increased solar energy utilization potential and potential increase of collected thermal energy stored into the VCS. The effect of modifying the BIPV/T roof angle and including a glazing section are analyzed and

discussed, demonstrating the use of the identified transfer function model of the VCS as a more efficient and quicker alternative to whole building detailed simulations, particularly for comparing design and operation options on a relative basis.

ACKNOWLEDGEMENTS/REMERCIEMENTS

Je voudrais remercier Dr. Andreas K. Athienitis, mon superviseur, de m'avoir permis de faire cette maîtrise au sein de son groupe de recherche. Sa passion pour son sujet de recherche est admirable tout comme le sont les pas de géants qu'il fait faire au domaine des bâtiments solaires intelligents à consommation énergétique nulle. Je tiens à lui exprimer toute ma gratitude puisqu'il a accepté la façon que j'ai choisie pour compléter cette maîtrise. Celle-ci m'a permis de travailler tout en restant proche de mes deux jeunes enfants et de leurs donner toute l'attention dont ils avaient besoin.

José, je voudrais te remercier pour les connaissances que tu m'as transmises au cours de nos collaborations. Je crois que tes intérêts pour l'art, la culture, la politique, la littérature et l'histoire sont des atouts et je te considère comme un grand scientifique.

Guillaume, je n'aurais jamais pu terminer cette maîtrise sans ton aide, ta patience et ton amour. Le support moral que tu m'as donné jour et nuit ne sera jamais oublié. Je suis choyée de vivre à tes côtés cette existence si riche. J'ai encore mille projets à partager avec toi.

Isabelle et Geneviève, je ne peux soumettre ce mémoire sans souligner les bienfaits des longs kilomètres que j'ai partagés avec vous, de foulée en foulée. Vous m'êtes très chères.

Finalement, René et Hélène, je vous remercie de m'avoir enseigné qu'une grande satisfaction émane des projets complétés.

TABLE OF CONTENTS

LIST OF FIGURES

LIST OF TABLES

NOMENCLATURE

Symbols

A_W	Total glazing area of the three basement south facing windows
$A(q)$	Polynomials in terms of q^{-1}
a	Collares-Pereira and Rabl coefficients for hourly clearness index calculations.
$B(q)$	Polynomials in terms of q^{-1}
b	Collares-Pereira and Rabl coefficients for hourly clearness index calculations
C_F1	BIPV/T fan current amp sensor
CFM	Volumetric flow rate at the entry manifold of the ventilated concrete slab
C_p , $C_{p,air}$, Cp_{air}	Specific heat, specific heat of air
$C_{p,conc}$	Specific heat of concrete
$e(t)$	Disturbance at time t
$F\ 0\text{-}3$	VCS inlet manifold air temperature sensor
$F\ 0\text{-}4$	VCS outlet manifold air temperature sensor
F_{dir}	South facade direct solar radiation portion
F_{diff}	South facade diffuse solar radiation portion
G	Data recorded by south facing vertical pyranometers
$G_{tot.roof}$	Total incident solar radiation on roof surfaces
$G_{BIPV/T}$, G_{SG} , G_{TEXT}	Transfer functions
h_s	Sunset hour angle
$h_{c,pv/t}$	Convective heat transfer coefficient, top and bottom surfaces of the BIPV/T channels

$h_{c,vcs}$	Convective heat transfer coefficient, inside surfaces of the ventilated concrete slab channels
I	BIPV/T fan electrical current
I_o	Extraterrestrial normal solar radiation
I_b	Incident beam solar radiation
I_{ds}	Incident sky diffuse solar radiation
I_{dg}	Ground reflected diffuse solar radiation
K_t	Daily average clearness index
k_t	Hourly clearness index
k_d	Hourly diffuse clearness index
k_b	Beam clearness index
k	Extinction coefficient of each layer of glass for the triple-glazed windows
$L_{BIPV/T}$	BIPV/T roof effective length
L_{roof}	BIPV/T roof length
$\dot{m}, \dot{m}_{air}$	Volumetric flow rate of the heated air drawn from the BIPV/T roof
n	Day number
n_g	Refraction index of each layer of glass for the triple glazed windows
n_a , n_{b1} , n_{b2} , n_{b3} , n_k	Orders and time delay parameters for the polynomial model system identification procedure
PV_{eff}	Electric efficiency of PV panels
$Q_{BIPV/T}$	Active solar gains of the ventilated concrete slab.
Q_{SG}	Passive solar gains of the ventilated concrete slab
$\dot{Q}_{act}$	Rate at which BIPV/T solar thermal energy is actively transmitted into the VCS
$\dot{Q}_{coll}$	Thermal energy collected from the BIPV/T roof

$\dot{Q}_{avail,stor}$	Thermal energy available for storage in the ventilated concrete slab
q	Forward shift operator
q^{-1}	Backward shift operator
R1. R2, R3, R4, R5	Five BIPV/T roof configurations
s	Laplace transform operator
$T_{air\text{-}in}$, $T_{air\text{-}out}$	Inlet and outlet air temperature of the BIPV/T roof
$T_{outlet,bipv/t}$	Exit air temperature from the BIPV/T roof
T_{ext}	Outdoor temperature
T_{IN_VCS}, T_{OUT_VCS}	Air temperature at the entry and exit manifolds of the ventilated concrete slab
T_{SURF_VCS}, $T_{VCS,surf}$	Surface temperature of the ventilated concrete slab
t	Current time for hourly clearness index calculations
u_2	Passive heat charging input of the ventilated concrete slab dynamic system
$u_{2,dir}$	Direct solar radiation part of passive heat-charging input of the ventilated concrete slab dynamic system
$u_{2,diff}$	Diffuse solar radiation part of passive heat-charging input of the ventilated concrete slab dynamic system
u_3	Exterior temperature input of the ventilated concrete slab dynamic system
$\dot{V}$	BIPV/T fan volumetric flow rate
$\dot{V}_{tot,conc}$	Total volume of concrete in the ventilated slab
$v_{air,pvt}$	Air velocity (m/s) inside the BIPV/T roof cavities
$W_{BIPV/T}$	BIPV/T roof width
y	Surface temperature output of the ventilated concrete slab dynamic system
$y(t)$	Output variable at time t
$y(n)$	Measured output value

$\hat{y}(n)$	Output value calculated by the model
$\bar{y}$	Arithmetic mean of the model output
z	z-transform operator

Greek letters

β	Tilt angle of the surface
Δq_{air}	Total energy lost by the air when it travels across one of the VCS control volumes
$\Delta q_{air\_to\_slab}$	Energy lost to the slab by the air when it travels across one of the VCS control volumes
$\Delta q_{air\_to\_soil}$	Energy lost to the ground by the air when it travels across one of the VCS control volumes
ΔT	Temperature change
ρ_{air}	Density of air
ρ_{conc}	Density of concrete
θ	Incidence angle of the sun-rays on the surface
$\theta_{a,b}$	Parameters of the A(q) and B(q) polynomials determined during system identification
τ_{diff}	Effective diffuse solar transmittance of the glazing system
ω	Earth's spin rate
ψ	Orientation of the surface

Abbreviations and Acronyms

AI	Artificial intelligence
ANN	Artificial neural network
ARX	Auto-regressive model with exogenous input
ASHRAE	American Society of Heating, Refrigeration and Air-Conditioning Engineers
BB	Black-box

BIPV/T	Building-integrated photovoltaic/thermal
CMHC	Canadian Mortgage and Housing Corporation
GPC	Generalized predictive control
HQ	Hydro-Québec
HVAC	Heating, ventilation and air-conditioning
MISO	Multiple-input/single-output
PI	Proportional-integral
PV	Photovoltaic
RFH	Radiant floor heating
RMS	Root mean square
SBRN	Solar Building Research Network
SI	System identification
TABS	Thermally-activated building systems
VCS	Ventilated concrete slab

1 INTRODUCTION

1.1 Background

In January 2013, Hydro-Québec electricity grid experienced the largest demand load in its history. At this time, the national peak electricity demand reached 39 120 MW[1]. Year after year, this peak demand increases. In a context in which residential buildings consume approximately 30% of the energy produced by Hydro-Québec, finding ways to reduce their energy consumption and shift in time their peak daily demands is crucial while designing buildings. These efforts will potentially release an important portion of the electricity produced for other purposes such as the electrification of transportation systems.

Thermal systems in high performance buildings must be designed and controlled rigorously. This allows to maintain comfortable indoor conditions while reducing the energy consumption and cutting down the building peak loads. In that context, the control of solar systems solar plays an important role. Furthermore, the use of simple physical models of such systems allows exploring ways to optimize the solar energy use. Therefore, the subject of this thesis is the development of a methodology to identify a simplified model of a solar thermal storage system in order to build control strategies to optimize its energy storage capacity.

A system identification methodology using monitored data from an existing energy efficient solar house will be presented in order to develop a model of a structural

[1] Reference: LaPresse.ca, http://www.lapresse.ca/le-soleil/affaires/consommation/201301/24/01-4614837-consommation-historique-delectricite-hydro-quebec-a-eu-chaud.php.

active/passive solar thermal storage system. The ventilated concrete slab of the Ecoterra™ house is used as the demonstration and validation example.

1.1.1 Ecoterra™ Project

The Ecoterra™ house was the first of 15 demonstration projects to be built as part of the Equilibrium™ Sustainable Housing Demonstration Initiative sponsored by the Canadian Mortgage and Housing Corporation (CMHC) and launched in 2006.

The Ecoterra™ house was built using seven prefabricated modular sections in 2007 in the Alouette Homes factory. Expertise was provided by the NSERC Solar Building Research Network (SBRN) and support by, among others, Natural Resources Canada, CHMC, Hydro-Quebec and Regulvar.

Figure 1.1: Ecoterra™ house, Eastman, Quebec.

The Ecoterra™ house is a single family detached dwelling. It is two storeys high and includes a basement. Its total heated floor area (including the basement) is 211.1m^2. It was assembled on-site in Eastman (Québec) and has been occupied since August 2009. Figure 1.2 shows a schematic about the integration of its main energy systems.

In agreement with the performance monitoring needs of the CMHC Equilibrium Initiative as well as the requirements of all parties involved in the project, the house was equipped by SBRN with over 150 sensors measuring mainly climate variables, indoor conditions, temperatures, energy consumption of HVAC equipment, and flow rates. The collected data is stored in a central database accessible via the web.

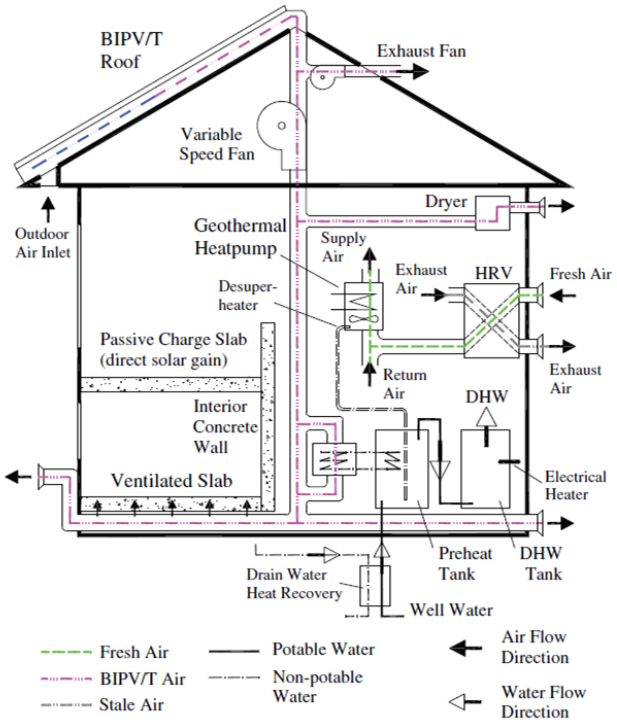

Figure 1.2: Ecoterra™ energy systems. (Source: Y. Chen, Athienitis, & Galal, 2010).

The house was designed to produce as much energy as it consumes on a yearly basis. The design approach respected passive solar and bioclimatic principles. Several energy efficiency measures were also applied and energy production systems were integrated.

The house orientation, its fenestration and its thermal mass were selected in order to optimize the capture, storage and utilization of passive solar energy. The Ecoterra™ house was built with windows covering 42% of its south facade. Most of its thermal mass

is distributed in the south portion of the house and helps to dampen the interior temperature swings. An innovative ventilated concrete slab is located in the basement (Figure 1.3). It uses the structural mass of the slab as a thermal storage device where the transmitted direct solar gains and thermal energy from the solar thermal collectors are, in that order, passively and actively accumulated. Active thermal gains are stored in the concrete mass of the slab by circulating heated air across an assembly of embedded channels.

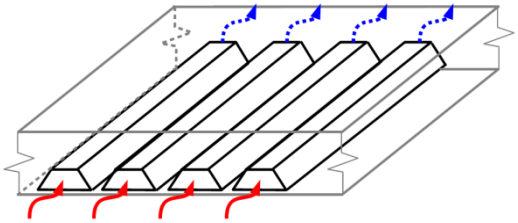

Figure 1.3: Schematic of the ventilated concrete slab.

Its main energy systems were selected and designed in order to reduce the amount of energy dedicated to space heating and domestic hot water. The list of energy efficiency measures in the house includes a ground source heat pump and a drain water heat recovery system. As a result, this house consumes about 11% of the amount a typical Canadian home consumes for space heating and 20% of what it consumes for domestic hot water.

The main system allowing the production of energy is its photovoltaic/thermal roof. This system was designed to be incorporated directly into the building envelope. The building-integrated photovoltaic/thermal (BIPV/T) roof permits the collection of solar thermal energy and the production of electricity. The electricity generated can be used locally or exported to the utility grid.

1.2 BIPV/T Roof - Ventilated Concrete Slab System

The BIPV/T roof is the main solar energy collection system of the Ecoterra™ house (Figure 1.4). It forms the main south-facing roof section and its cover is made of amorphous silicon photovoltaic panels having a total rated capacity of 2.8 kW attached (with adhesive and screws at the top) to a metal layer. Air can enter soffit openings and can be drawn under this layer by a variable speed fan. As the air travels though the cavity underneath the PV panels and metal roof, it gathers thermal energy while acting as a cooling fluid for the PV panels. This heated air can later be used to preheat the domestic hot water system, to dry clothes or to actively charge the ventilated concrete slab located in the basement.

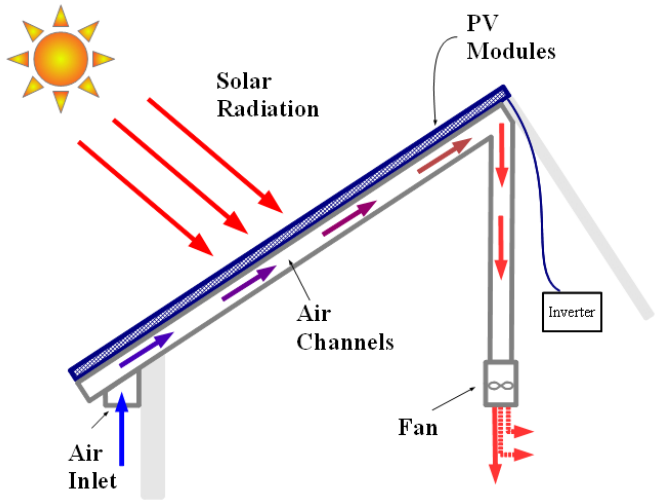

Figure 1.4: Schematic of a BIPV/T roof.

The BIPV/T roof is thermally coupled to the ventilated concrete slab (VCS) of the basement where the thermal energy collected can be actively injected. Chen (2009, p. 91) listed the requirements that were established prior to its design:

- Store the thermal energy collected across the BIPV/T roof.
- Avoid exceeding the limit of comfort for a floor surface temperature.

- Release the stored energy at a desirable rate to avoid overheating of the space.
- Serve as a structural element.

1.3 Studies on the Ecoterra™ House

The Ecoterra™ house is a key demonstration project of the NSERC Solar Buildings Research Network and CMHC which has already contributed to the completion of various building engineering studies focusing on subjects such as net-zero energy homes, building-integrated photovoltaic/thermal systems, thermal storage systems, building design tools, building controls and low-energy building design optimization. In the past few years, several SBRN graduate students have made this demonstration project the main topic and/or reference model for a variety of studies. In addition, it forms an important Canadian case study for IEA Task 40 (http://task40.iea-shc.org/).

First, Candanedo (2010) used monitored data of the Ecoterra™ house to carry out a comparison of two models he created for transient and steady state evaluations of air-based open-loop BIPV/T systems. Recently, O'Brien (2011) assessed the Ecoterra™ design process and the design tools employed in its development.

The conclusions and work included in the two following master thesis are significant supporting work for this thesis.

1.3.1 Previous Studies on the Ventilated Concrete Slab of Ecoterra™

Y. Chen et al. (2010) described the design of the innovative type of ventilated concrete slab built in the basement floor of the house and its connection to the BIPV/T system. Y. Chen completed a related master thesis at Concordia (2009). Y. Chen et al.

assessed the performance of the BIPV/T-VCS coupling and developed numerical models to simulate the thermal performance of the ventilated concrete slab and BIPV/T roof. The 3-D control volume explicit finite difference thermal model developed to simulate the ventilated concrete slab performance was simplified to a 9-layer model. One of Chen's suggestions for future studies (Y. Chen, 2009, p. 112) was the development of a further simplified model that could reduce the computational efforts required to minimal levels.

1.3.2 Energy Analysis of Ecoterra™ (Doiron, 2011)

Doiron et al. (2011) completed a whole-system energy analysis of the Ecoterra™ house using monitored data. He completed his master thesis on this topic (Doiron, 2011). He estimated the annual energy consumption of the house at 10 300 kWh. This includes about 3000kWh due to the addition by the occupants of an electric garage heater and other items such as extra lighting. If this amount is excluded, it represents only 19% of the Canadian average for single-family detached homes. His discussion about the house end-use energy breakdown (Figure 1.5) helped identify the major lessons learned throughout the duration of this project, from the design stage to commissioning.

Making use of the ventilated concrete slab monitored data, he estimated approximately that 1545 kWh of solar thermal energy was collected at the roof and that only 329.8 kWh was stored in the ventilated slab concrete over the one-year study period. It was noted that the amount of thermal energy collected could be substantially increased by using higher roof slopes (around 45 degrees), possibly with a glazed section. The potential for energy storage improvement is also evident and he listed several avenues for future studies aiming to increase the fraction of solar energy stored. Namely, he

suggested examining advanced charging strategies to improve the solar energy storage in the VCS.

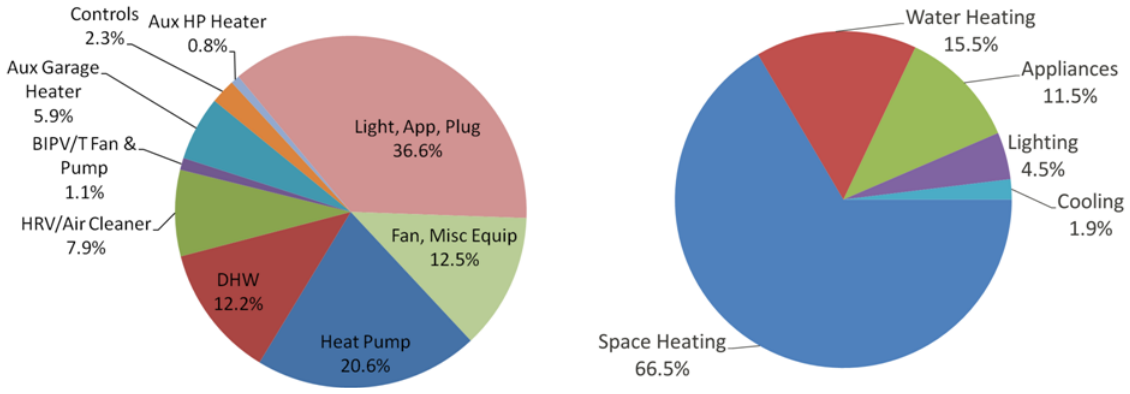

(a) Ecoterra™ (b) National Average Single Family Detached Home

Figure 1.5: Annual energy consumption by end-use: (a) Ecoterra™ house (b) Canadian average. (Source: Doiron, 2011, p. 70)

1.4 Motivation

Comfort conditions in high performance buildings must remain adequate even if design requirements include reducing the annual energy consumption. Moreover, managing the building loads and its interaction with the grid are key elements in their design process. Similarly, efforts should be made to adequately couple the energy loads with the renewable gains. Therefore, during design, thermal performance simulations should be completed with these aspects in mind. But, the level of complexity of detailed simulation programs does not guaranty the accuracy of the results obtained and their use for routine building design analysis is cumbersome

Therefore this thesis is a contribution to solving this problem by presenting a methodology to develop appropriate simplified linear models that will improve our

knowledge of thermal energy storage systems so that active solar thermal storage is optimized.

The following justifies the development of a methodology to identify a statistical data-driven model of an active/passive solar thermal storage system using system identification techniques as an important research topic.

1.4.1 Comparison between Modeled and Actual Energy Use at the Ecoterra™ House

The actual energy consumption of the Ecoterra™ house was compared against the modeled values determined prior to construction and occupation. The production of electricity from the PV collectors was 2570 kWh, only 75% of the projected value. It is known that a good part of the energy production shortage is due to a higher than expected snow cover of the PV arrays during the winter months. The less than optimal BIPV/T roof pitch (30 degrees – chosen due to prefabrication constraints) is among the variables influencing this accumulation. Thus, designing a similar house with a more optimized BIPV/T system having collectors sloped at 40 to 50 degrees would significantly enhance the house energy production (both electricity and useful heat), and improving its operation would allow to store higher amount of solar heat into the ventilated concrete slab.

1.4.2 Reduction and Displacement of the Peak Demand

The house peak loads are an aspect as important as its net annual energy consumption. At the national level, this demand determines the total electricity capacity required to satisfy peak demands. Therefore, load management and interaction of the

house with the electric grid are an important part of the design process of smart net-zero energy houses, and particular attention should be given to the coupling of the energy loads and renewable gains. Solar thermal storage is an important means to address this issue. It allows the house mechanical equipment size to be reduced at the design stage and the energy demand peaks to be lowered and shifted.

This justifies improving our knowledge about solar thermal storage in order to develop efficient control strategies to store more solar gains, to reduce peak loads, to control the solar energy storage and its passive discharge, and to manage the house energy demands. In addition, thermal storage can be used to improve thermal comfort by reducing room temperature swings in solar houses.

1.4.3 Simplified Energy Models for Buildings

Thermal performance evaluations are a key aspect of building engineering and are now a part of the standard process in the building design phase. The complexity of the available detailed simulation tools has increased tremendously during recent years. However, their use for routine building design analysis is cumbersome, namely because of the large number of parameters they require. An alternative approach to assess the building thermal performance is to focus on carefully selected interactions of the building with its envelope, HVAC systems and controls. This approach reduces the number of parameters included in the model. These simplified building thermal models are therefore adequate, potentially accurate and require low computational efforts when used in thermal studies.

Another avenue leading to modeling simplifications is the assumption of linearity. No dynamic system is perfectly linear, however it is worth assuming this simplification when non-linearities can be isolated and reduced to minimal levels.

1.4.4 Data-Driven Models

Artificial intelligence algorithms have been the main tools used to create data-driven models of systems for which no physical parameters were known beforehand (black-box). Recently, a few researchers have worked with statistically estimated black-box (BB) building models. Candanedo et al. (2011) were among the few who used this system identification approach to create this type of thermal building models. They used a simplified linear model to evaluate model predictive control strategies in the case of a residential high solar gain thermal zone. The results of their investigation demonstrated that simplified data-driven models have the potential to ease control strategy evaluations for solar houses and help optimize the thermal mass capacity to collect and store solar energy.

However, there has been little research on the use of statistically identified models for retrofit design analysis of thermal building components focused on keeping the number of parameters low. Even less work has been done on the identification of linear parametric models with monitored data dedicated to the evaluation of various design options for solar buildings systems.

1.5 OBJECTIVES

1.5.1 Main Objective

The main objective of this thesis is to develop a methodology to create a statistical data-driven model of an active/passive storage system using system identification techniques. Two strongly coupled solar systems of the Ecoterra™ house will be studied: the coupling of a ventilated concrete slab to a BIPV/T roof will be the demonstration and validation example. This model should have the potential to be used as a thermal evaluation tool for retrofit solar system evaluations, should be linear, and should have a limited number of parameters. Based on previous work by researchers in our group and others (Athienitis, et al., 1990; T. Y. Chen, 2002; J. A. Candanedo & Athienitis, 2011), it is expected that models up to 5^{th} order can generally expect most of the thermal dynamics of solar houses.

1.5.2 Specific Objectives

The objectives of this thesis are:

- To develop a methodology to identify a data-driven model of a ventilated concrete slab located in the basement of a single-family residential building.
    - This model shall be developed and validated with monitored data logged by the sensors distributed across the Ecoterra™ house and already available in the central database.
    - This model should be statistically identified, have a reduced number of parameters, and be linear in order to simplify future thermal evaluation and control studies.

- To evaluate the effect of data accuracy on the model performances and identified amplitude of its parameters.
- This model should allow the thermal assessment of the VCS performance when it is coupled to different variations of the actual BIPV/T roof of the Ecoterra™ house in order to build control strategies and to optimize its energy storage capacity.

1.6 Thesis Outline

The following summarizes the content of each chapter in this thesis:

- Chapter 1: *INTRODUCTION*. Presents the Ecoterra™ house project and its systems that are closely related to this thesis. Describes the previous research work from which this thesis emerged and the thermal modeling topics that justified the approach chosen for this thesis. Presents the objectives of this thesis and its outline.
- Chapter 2: *LITERATURE REVIEW*. Presents a review of the fundamental theory behind the subjects of thermal modeling of building systems, system identification model simplification, and thermally-activated building systems along with what other researchers have done in these areas.
- Chapter 3: *SYSTEM IDENTIFICATION OF THE VENTILATED CONCRETE SLAB USING MONITORING DATA*. Presents the ventilated concrete slab physical description and its transformation into a simple linear input/output dynamic system. Description of the methodology developed to obtain its mathematical description using monitored data. It describes the strategies applied

to transform data time series in system inputs and output. The last section presents the various validations and tests required to qualify the model as acceptable.

- Chapter 4: *PHYSICAL VALIDATION OF THE VENTILATED CONCRETE SLAB PARAMETRIC MODEL*. Presentation of a second validation of the ventilated concrete slab mathematical model. This time it is completed considering the physical nature of the system rather than simply looking at mathematical validation results. A look at the effects of the measurement device accuracy on the identified model parameters is included.
- Chapter 5: *SIMULATION STUDIES USING THE VENTILATED CONCRETE SLAB MODEL*. The linear parametric model of the ventilated concrete slab is used as tool to perform a BIPV/T roof redesign simulations for potential future residential projects like the Ecoterra™ house. A comparison based on the amount of heat collected and possible VCS active storage capacity of improved BIPV/T roof designs is also included.
- Chapter 6: *CONCLUSION*. Includes conclusions, a summary of the main contributions of the work and ideas for future research.

2 LITERATURE REVIEW

This chapter reviews the relevant literature related to building energy models and their use as guiding tools in the process of understanding the thermal interactions between building components. This review will also provide an overview of the research published on the topic of thermally-activated building floors, with specific attention dedicated to ventilated concrete slabs, used as energy storage and space conditioning devices.

2.1 Thermal Models of Building Systems

Creating models is a fundamental step in research. Models became key tools for engineers because they help in acquiring a better knowledge of the system under study. Models are often used to answer a specific optimization problem. In building engineering, these models are used to reduce the building operation costs, to improve mechanical equipment performance, to reduce the amount of energy consumed, or to improve building occupant comfort.

2.1.1 Generic Components of a Model

A model is made of three components; its input(s), its structure and its output(s). The inputs can be divided into controllable and uncontrollable items. In the building science context, an example of controllable input would be the auxiliary heat supply to the building. In the same context, uncontrollable inputs are often called disturbances and are most often related to weather. The outputs are the reactions of the system to the application of inputs. The structure of the model is made of all the parameters and/or properties that together provide an approximation of the system under study.

2.1.2 Modelling Problem

The modeling route to choose depends on which pair of model components is known before starting the modeling process. The ASHRAE Handbook: Fundamentals (American Society of Heating, Refrigerating and Air-Conditioning Engineers [ASHRAE], 2005, Chapter 32) mentions that every modeling approach falls either in the "Forward" or "Inverse" modeling category.

The separation between "forward" and "inverse" modelling categories needs to be qualified because modelling approaches are often an amalgam of these two. However, their distinct characteristics form the boundaries of the modelling spectrum.

The forward modeling approach is used when all the properties and parameters of the system are known or attributed an estimated value and are available to identify its response to predefined forces or inputs.

The inverse modeling approach is used when the structure of the system is totally or partially unknown. This approach is based on experiments. In most cases, researchers create inverse models of already built systems. In the state of the art literature on building science, these models are often identified as "empirical" or "data-driven" models.

2.1.2.1 Forward Modeling Approach

Forward modeling techniques are mainly used at the building design stage and have the advantage of being based on principles widely accepted by the research community. Forward modeling techniques tend to become progressively more complex as the computational power increases. Detailed building simulation programs are the best

example of forward modelling. These programs are still the main tools used during the early stages of design.

However, their use for routine building design still has some challenges. The large number of parameters required by most forward models has motivated researchers to develop alternative approaches to model building thermal dynamic systems. Unsuitable assumptions made to overcome this difficulty can reduce significantly the confidence level of the model. For this reason, Wang and Xu (2006b) developed a genetic algorithm tool to identify the lumped parameters of a building thermal network model from operation data. This methodology was developed to overcome the difficulty of obtaining the real physical capacitance properties for the building internal mass. They stated that, "The process of collecting a physical description is time consuming and often is not cost effective, or may even be impossible for some cases" (Wang & Xu, 2006b, p. 1928). Recently, Candanedo and Athienitis (2011) modeled a solar house with z-transfer functions. These transfer functions were identified using data generated by a detailed energy simulation program. Their results demonstrate that selecting the appropriate level of modeling for building design is crucial.

Even if their level of detail and modeling capacities are high, detailed energy simulation programs can be too complex for design analysis. Crawley et al. (2008), in their report comparing the capabilities of different building energy simulation programs, suggested that the adopted tools should support the designer's needs without involving excessive simulation efforts.

Their ability to guide designers through the building design process and the choice of mechanical systems and equipment has also been questioned. Recently, O'Brien (2011) developed a methodology for the design of solar residential buildings. His motivation was that although the modeling power of the building energy simulation tools was continuously increasing, they were cumbersome for design. They did not guide clearly the user towards energy improvements and did not allow controlling the level of details to fit the specific design stage requirements.

2.1.2.2 Inverse Modeling Approach

ASHRAE suggests that the inverse modeling approach has the capacity to produce more accurate predictions of the system behaviour (2005). This approach does not require the risk of making erroneous simplifying assumptions and it takes into account the current state of deterioration of the structures because inverse models are usually created with monitored data.

Bekey (1970) presented a survey of identification techniques dedicated to dynamic systems using computer techniques in which he described the three types of inverse modeling problems. The first type is the "design" problem. It requires identifying the system description by fitting a specific physical relationship as closely as possible. The solution of the design problem is not unique. The second type of inverse problem, the "control" problem, includes all situations where the system description and its response are known. This problem requires identifying subsequently which input caused this response.

The trickiest inverse problem is the one for which inputs and their corresponding outputs are given and the mathematical description of system needs to be identified. Bekey (1970) categorized this problem as the "identification" or "modeling" problem. It is this identification problem that can be further separated into "black box" or "gray box". The amount of *a priori* information about the process dictates this additional categorization.

"Black-box" or "total ignorance" models are those for which the identification problem must be solved without any insight into the physical properties or prior knowledge of the process under study. They are data-driven models that mathematically connect the system input(s) to its output(s) without including any physical meanings in the equation parameters. "Black-box" models are built using data gathered from the system responses to disturbances and/or controlled inputs.

"Gray-box" models are determined using some of the available knowledge about the nature of the process and can be considered a combination of the forward and the inverse modeling approaches. However, the specific values of the system parameters remain to be identified using the measured input and output data. The model calibration study carried out by Monfet (2009) et al. is a good example of "gray-box" modelling using monitored data. They calibrated a building energy model of a large institutional building, created using a detailed building simulation tool, by comparing monitored data.

2.1.3 System Identification Techniques

The Swedish professor Lienard Ljung, a pioneer in the field of system identification (SI) research describes SI as: "[...] the art and science of building

mathematical models of dynamic systems from observed input-output data. It can be seen as the interface between the real world of applications and the mathematical world of control theory and model abstractions."(Lennart Ljung, 2010, p. 1).

Identifying inverse models is an essential task in science and engineering research. It would be presumptuous to claim that a single true model description of a system can be determined. Yet, it is reasonable to aim for obtaining a system description that explains, with an acceptable accuracy, the behaviour of a process in response to inputs.

Åström and Eykhoff (1971), in their early review of system identification developments, identified one root of the human interest for this field of research as the "Definite needs by engineers […] to obtain a better knowledge about their plants for improved control" (p. 123). Because computational capacities have increased, the possibilities for system identification have grown exponentially since the early surveys of Åström and Eykhoff (1971) and Bekey (1970). Still, improving controls, design or thermal comfort drive building engineers to make use of, study, and assess system identification techniques.

The following example can illustrate the concept of system identification. An air supply fan is an excellent example of a dynamic system. The current volumetric flow rate of the air at its exit not only depends on the actual electrical current (amps) input but also on its previous values (Figure 2.1).

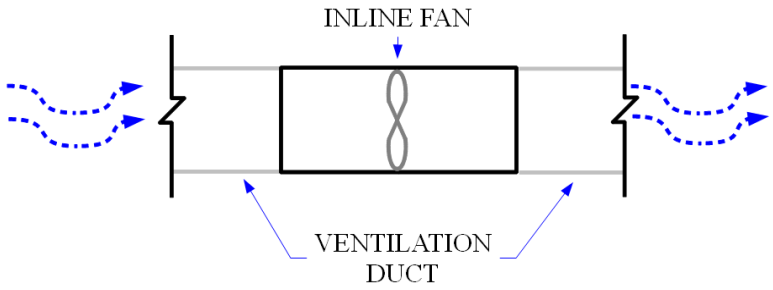

Figure 2.1: An inline fan

This system is symbolically depicted in Figure 2.2. The input is the electrical current and the output is the air volumetric flow rate. Figure 2.3 presents an example of recorded data sets that could be used to identify a model for this system.

Figure 2.2: The inline fan system: u: input; y:output.

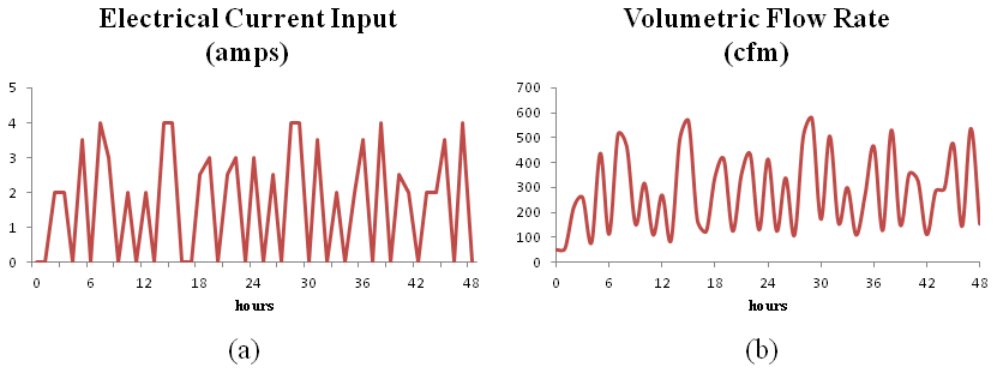

Figure 2.3: (a) Electrical current u, (b) volumetric flow rate y.

Statistical regression and artificial intelligence techniques are the two families of system identification approaches. Therefore, both techniques could be applied in order to identify a model for the previous example of inline air supply fan system. Figure 2.4 illustrates examples of resulting model structures for the two approaches.

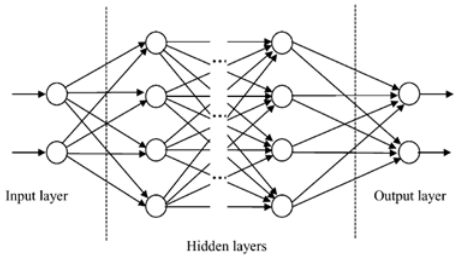

(a)

$$y(t) - 1.50y(t-1) + 0.70y(t-2) - 0.10y(t-3) = 0.04u(t-2) + 0.06u(t-3) + 0.03u(t-4) + e(t) + 0.54t(t-1)$$

(b)

Figure 2.4: (a) Schematic diagram of an artificial intelligence model. (Source: Kalogirou, 2001, p. 378). (b) Example of statistical regression model.

Before presenting the relevant literature related to the use of two techniques in building engineering, the linearity of a system must be explained.

2.1.3.1 Linearity of a System

A system can be qualified as linear if a specific linear combination of inputs acting on the system produces the same linear combination of output responses. The linear description of the properties of a physical system is a mathematical idealization. However, linear models of dynamic systems are useful tools that suit the practical needs of building thermal evaluations. Most of the time building systems are not perfectly linear, but they can be linearized around the operating region for this idealization to be acceptable.

2.1.3.2 Artificial Intelligence Building Models

The artificial intelligence (AI) approaches to model building systems for energy management includes mainly artificial neural networks (ANN). ANNs imitate the learning approach of the human brain by learning processes and recognizing patterns instead of using a mathematical description. In this manner, they are able to replicate the patterns of data time series.

AI models have been widely used for building thermal studies as the available volume of logged sensor data has been increasing. They emerged as a powerful technique to handle black-box system identification problems such as on-line model identification models and retrofit building studies. However, they provide a model totally deprived of any physical meaning.

Kalogirou (2000, 2001) considers ANNs an advantageous technology for building models. He presented ANN modeling techniques as being:

- Fault tolerant in a way that they are able to handle noisy and/or incomplete measured data.
- Good predictors even if they were created with data from systems having many inter-related parameters. This latter characteristic makes them particularly suitable for passive solar building energy analysis.
- Capable of dealing with problems for which humans take decisions based on their intuitions.

In Kalogirou's opinion, their main advantage over statistical regression models is that they are able to deal with non-linear systems having parameters shifting with time because of the alteration of their properties.

Others have suggested that artificial neural networks are limited by their tendency to "overfit" the data (Holcomb et al., 2009; Dodier & Henze, 2004). "Overfitting" occurs when the model, in addition to fitting the system signals, fits the noise included in the data. The flexible structure of ANNs is to blame. ANNs are also often requiring long periods of data to identify a reliable input-output relationship.

2.1.3.3 Statistically Estimated Building Models

Providing a mathematical description to an inverse model is possible. There exist techniques to identify the best parameters for a selected statistical model form with empirical data. Statistical regression methods are a way to identify these parameters. The performance of a model is judged by its capacity to predict outputs when inputs are applied. Specifically, statistical regression methods are used to minimize a prediction error. The prediction-error identification methods form a family of approaches which include linear regression and least-square criterion techniques.

The same input is applied to a model and to the unknown system. The difference between the output of the unknown system and the prediction made by the model is used to identify the model parameters. This procedure is repeated until an acceptance criterion is met.

Statistical modeling techniques were kept in the shadow of artificial intelligence algorithms in recent building research. However, the quest for simplified and accurate building models is an incentive to keep the statistical modeling techniques an option to consider when conducting building thermal studies. They have significant capabilities that justify their usage for empirical building models such as the physical meaning of their parameters and the limited computer power they necessitate. Furthermore, Wen and Smith (2003) demonstrated their potential to handle non-linear systems as time-varying linear processes.

It is usually assumed that statistical identification approaches will fail when dealing with non-linear system. However, the results of the ASHRAE Great Energy

Predictor Shootout II (Haberl & Thamilseran, 1998) have demonstrated that an ensemble of statistical models carefully put together can predict as accurately the energy consumption of buildings as ANNs can. Katipamula (1996) deemed that an arrangement of statistically identified models can make accurate energy predictions for commercial scale buildings known to represent complex inter-dependant systems. He used a multiple linear regression model to predict the energy use of small commercial buildings. His choice is justified because the energy consumption of large commercial buildings is a complex ensemble of relations between climatic conditions, HVAC equipment, building use, building materials and control strategies. This modeling entry was the only non-neural network of the second Shootout and it managed to achieve the second place in the overall event ranking.

An important part of the energy exchanges in solar buildings is made by radiation and solar heat sources are not exciting the building uniformly. T.Y. Chen (2002) developed an alternative methodology to overcome this difficulty while still making use of statistical SI techniques. As the solar radiation is not a consistent heat source, he used two models to boost the radiant floor heating system accuracy. T.Y. Chen and Athienitis (2003) investigated the practical issues related to the statistical parameter estimation of building thermal process models. They concluded that the recursive least-square identification techniques are effective and efficient. However, they are inappropriate for thermal systems with large non-linearities such as those including phase change materials (PCM). They also pointed out that these techniques generally require shorter periods of data to identify the model parameters and their performance can be guaranteed if the issues listed below are reduced to their minimum levels:

- A preliminary evaluation of the thermal process studied should be performed to identify all influential and uncontrollable inputs having an impact on the output(s).
- Special attention should be brought to non-persistent exciting inputs such as solar gains and large unmodelled disturbances. They are critical when recursive least-square estimation is used to identify models because they produce drastic environmental changes and can lead to physically meaningless models.
- Supervisory rules deduced from physical principles should be used to perform robust parameter estimation.
- For systems with low non-linearities and slowly changing environmental influencing variables, the degree of non-linearity of the inputs should be reduced by reducing the prediction range to shorter sub-ranges.
- Using first principles, a preliminary analysis of the thermal system should be done. The structure of the model and its order should be selected accordingly.

Statistical techniques also allow including physical information into their mathematical structure (Dewson et al., 1993). This latter characteristic makes statistically identified models particularly trustworthy when they are compared to ANN models. The models can include some of the thermal process information in their structure and become robust gray-box models.

Statistical techniques also have the merit of necessitating less computational power for model identification and can model a system with fewer parameters than connectionist approaches. Zouak and Mechaqurane (2004) compared the ability of a neural network based model and a linear statistically identified model to predict the

indoor temperature of a residential building. The number of parameters (weights in the case of ANNs) of the neural network model remained very large (30) compared to the model identified using statistical techniques (10). This increased complexity is an obstacle when simple models are desired.

2.1.4 The Quest for Simplified Models

Simplified models are highly desirable in building applications. They have many advantages whether they are used for building research or applications. Even if computational power and modelling tool capabilities are constantly increasing, there is continuous attention directed towards simple models.

Lachal et al. (1992) deemed that sophisticated methods cannot reproduce well all the interactions of large and complex building systems. Their opinion was that simple models with few parameters are preferable because they are:

- Economical in terms of computational time, researcher's time and money.
- Perfectly suited for control applications.
- Comprehensible for all building management professionals.
- Facilitating the synthesis of large building studies and the inter-disciplinary communications.

As Lachal et al. mentioned, simple models are not just an oversimplification of a system: they are an acutely understood selection of relevant system information. They stated that the development and application of simple models require "a deep understanding of all phenomena involved, a coherent choice of significant parameters and

variables, and much care and thinking when analyzing and interpreting the data" (p.1151).

The two approaches to simplify the modeling procedure presented in this review are: decreasing the number of parameters of the model, and limiting the amount of *a priori* knowledge required for modeling.

2.1.4.1 Limiting the Number of Parameters

Several researchers demonstrated that models having a small number of parameters can accurately model the behaviour of buildings, on a small scale as well as on a large scale.

Dewson et al. (1993) attempted to use a set of 5 parameters in a resistive-capacitive network (3R2C) to capture the essential behaviour of a small single-story solar test cell. Their technique was able to predict the temperature of the internal node of the test cell with an RMS difference (between measurements and model predictions) of around 1°C during three experiments.

A decade later, Wang and Xu (2006a) proved that simplified energy models can predict in a robust and accurate way the thermal behaviour of building at a much larger scale. They modeled a 50 storey commercial building using only a trio of lumped parameter models, i.e. two 3R2C circuits and one 2R2C circuit. The test results, from a real commercial building, showed that for all different operation conditions the model emulated the actual cooling load with a 10 % average error.

Wang and Xu also reported that models having a small number of parameters are easier to calibrate than detailed physical models. Kummert et al. (2006) experienced this issue when they completed a heating controller study for passive solar buildings. A first unsuccessful attempt to tune a TRNSYS model with experimental data from a test facility proved that the number of parameters these tools require is often cumbersome. However, their subsequent results obtained with a linear state-space model suggested that simple models can help reach high levels of accuracy and that their reduced number of parameters makes them appropriate for identification techniques.

2.1.4.2 Using On-site Data to Create Simplified Models

Inverse models created on-line with building data are a promising technology for smart-buildings. On-line diagnosis (Kumar et al., 2001; Peitsman & Soethout, 1997), continuous energy monitoring (Wen & Smith, 2003; Yang et al., 2005) and model-based supervisory control (T. Y. Chen, 2001) are among the various possible applications. The need for real-time building management information supply has encouraged researchers to develop techniques to model their thermal behaviour using shorter periods of data and requiring limited computational efforts.

Braun and Chaturvedi (2002) developed an approach to model the building sensible load with limited up-front building information and short periods of training data. Their model required only two weeks of training data and was able to predict hourly cooling loads within about 9% for test data from a Chicago building over a four-week period.

2.2 Thermally-Activated Building Floors

The main topic of this thesis is a ventilated concrete slab located in the basement of a solar house. In addition to storage, this slab serves heating purposes when radiant and free convective energy is released from its surface. The following section will present significant precedents related to the use of thermal mass as an energy storage and radiant floor heating device.

2.2.1 Using the Building Thermal Mass to Heat and Cool

The effective use of thermal mass has received a lot of attention recently as much research is done to reduce the energy consumption of buildings and make use of renewable energy sources. The expression "thermally-activated building systems" (TABS) is employed to designate any system for which the building structure is integrated in the overall energy management strategy. The structure serves as energy storage medium and its thermal behaviour participates in the space conditioning of the indoor environment. Henze et al. (2008) suggested a precise definition for TABS: "[They are] construction elements thermally-activated by water or air driven systems that operate with small differences between room air and HVAC system temperatures allowing the use of low temperature heat sources and sinks." TABS help flatten the peak loads and bring important energy reductions. They are building structures that delay and attenuate the effects of external climatic variables on the indoor environment. Numerous research studies have proved that storing thermal energy in the building fabric is an efficient way to benefit from appropriate external climatic conditions even if they do not match in time the internal load conditions they will eventually alleviate. They are an integral part of low energy building management strategies and can serve as a heating or a cooling device.

Various building components such as walls, floors, ceilings and partitions can be used to store energy. The following paragraphs will focus on methods making use of concrete floor slabs to heat and cool the indoor climate which can be named “concrete core conditioning systems”.

2.2.1.1 Concrete Thermal Mass as a Terminal Heating Device

Concrete slabs heated with embedded pipes through which warm water circulates, or with embedded electric heating wires are the main systems using thermal mass to serve the dual purpose of energy storage and heating the ambient space. Although it is an ancient technique, the number of commercial and residential buildings equipped with radiant floor heating and cooling systems has increased significantly in the last twenty years.

The thermal comfort benefits of radiant floor heating systems are considerable. Olesen (2002) and Myren and Holmberg (2008) presented a list of features reducing the occupant’s perception of thermal discomfort. Predominantly, these systems eliminate the occurrence of uncomfortable drafts and are known to produce a minimum vertical air temperature difference. These authors also mentioned that RFH systems prevent cold corners, reduce the chances of condensation and mold growth, and result in less dust transportation than convective systems, not to mention that they do not require ducts and are totally quiet.

Furthermore, the same level of operative temperature can be reached by an RFH system at a lower air temperature when it is compared to a fully convective heating

system. From an energy standpoint, the lower required air temperature represents significant savings.

The characteristics of thermal mass heating systems are perfectly suited for passive solar buildings. According to Athienitis and Santamouris (2002), the primary requirement when designing a passive solar house is to prevent overheating and target high energy savings. The thermal mass has the capacity to smooth the high frequency variations of the influencing weather inputs by acting as a low pass thermal filter. It also has the potential to reduce the heating energy consumed for space conditioning. Moreover, because radiant heating systems use a low temperature heat transportation medium, distribution losses are reduced and the energy efficiency is increased on the heat generation side. These characteristics make RFH particularly well adapted for solar collectors and heat pumps.

Using concrete thermal mass as a thermal storage device helps accommodating the time mismatch between the solar peak energy generation and the peak household energy loads. Furthermore, it can be used to store the solar gains and consequently solve the problem of solar energy intermittency. Strategies are therefore needed to plan, store and use the generated energy from the sun while moderating the indoor temperature fluctuations in order to respect occupant comfort conditions. Olesen (2002) presented several studies proving that, despite their high thermal mass, RFH systems are not prone to overheating and creating uncomfortable situations. Radiant floor heating systems and their thermal mass have a “self-control” property inherent to their low-temperature heating nature. Because the temperature difference between the floor and the room air is

small, a little increase in room temperature due to the internal load from occupants will instantly bring a reduction in the heat output from the heated floor.

2.2.1.2 Concrete Thermal Mass as a Cooling Device

The hollow core slab in which air passes through the channels is the main thermal mass system used as a cooling device. As the air is pushed through the hollow cores, the turbulent flow increases the convective energy exchange with the thermal mass. Having a large area, the surface of the concrete slab becomes an energy sink for the building enclosure by proving effective natural convection and radiative cooling.

The TermoDeck® system is of this type (Figure 2.5). The hollow core slab is integrated in the ventilation system. At night, the concrete slab is pre-cooled with the inlet of outdoor air. This allows the large thermal mass of the floor (and ceiling) to subsequently absorb heat during the day. It has been demonstrated that this type of systems offers considerable energy and comfort advantages (Corgnati & Kindinis, 2007; Barton et al., 2002; Henze et al., 2008).

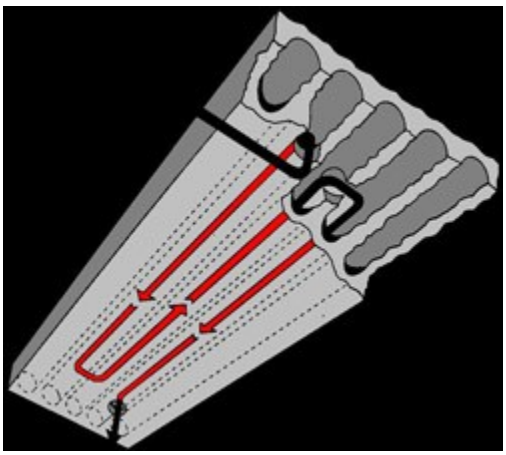

Figure 2.5: TermoDeck system. (Source: http://www.termodeck.com/how.html)

2.2.2 Modeling Thermally-Activated Building Systems

When using or designing thermally-activated thermal mass as space conditioning devices, the creation of temperature control and thermal storage strategies is difficult because of the inherent inertia of the energy release from the concrete thermal mass. The combination of active charging by an auxiliary heating device and passive charging by the radiation of the sun adds up to this complex task. This challenge has prompted many researchers to develop various models using different numerical techniques to understand thermally-activated building systems and further depict their thermal behaviour.

Radiant floor heating systems were modeled in several ways. Analytical models have been used to evaluate different control strategies and study the transient behaviour of its heat transfer (Athienitis, 1997; Athienitis & Chen, 2000). Other researchers conducted RFH studies using finite element models. These models were mainly used to study the influence of physical design parameters on the thermal performance of radiant floor heating systems (Weitzmann et al., 2005; Sattari & Farhanieh, 2006).

It is mainly the study of predictive control strategies that motivated the creation and use of radiant floor data-driven statistically estimated transfer function models. T.Y Chen (2002) used a model of this type within an improved algorithm for generalized predictive control (GPC). This data model was subsequently used to compare the thermal performances of the RFH system when it is controlled by the GPC, on/off and PI controllers. More recently, Candanedo and Athienitis (2011) used also a transfer function data-driven model to study the application of the predictive control methodology at

different levels in a passive solar house. It was applied to, among other things, the control of a RFH system.

The transient heat transfer through the concrete of the ventilated slab and their thermal performance was studied by many researchers. Most of them solved their analytical thermal models numerically by using the finite difference methods with a two-dimensional heat transfer scheme (Zmeureanu & Fazio, 1988; Barton et al., 2002). Lumped parameters (Ren & Wright, 1998) and CFD models (Winwood et al., 1994) have also been employed in the past. Ventilated concrete slabs have also been modeled by conduction transfer functions (Chae & Strand, 2013).

Y. Chen (2009) also studied the Ecoterra™ ventilated concrete slab. In his master's thesis, he contributed in developing the design of this innovative type of ventilated concrete slab installed in the basement of the Ecoterra™ house. He assessed the performance of the BIPV/T-VCS coupling and also developed a numerical model to simulate the thermal performance of the ventilated concrete slab. However, he chose to model the three-dimensional heat transfer within the slab concrete core.

He started by using monitored data to identify the heat transfer coefficient between the steel deck and the ventilation air in the slab. The cross sectional area of each channel is 77 cm^2. Each deck has an approximate length of 10.3m. The data used were from 9 locations on the VCS. At each location, he retrieved the soil temperature just under the insulation, the middle cavity air temperature in the channels, the middle layer concrete temperature and the top layer temperature (surface temperature) data. His

findings were that this heat transfer coefficient, $h_{c.vcs}$ could be approximated with this linear correlation function of the air velocity v_{air} in the channels (m/s):

$$h_{c,\text{vcs}} = 3.94 v_{air} + 5.45 \tag{2.1}$$

However, this correlation is highly dependent on the accuracy of the sensors involved in his experiment and on Chen's assumption that the incoming BIPV/T air flow is evenly distributed in the 19 embedded channels of the slab.

He then used his own 3-D control volume explicit finite difference thermal model to simulate the ventilated concrete slab thermal performance. His work evolved from a regular discretization model having a large number of control volumes to one where the slab was divided into only 9 layers in which the accuracy remained adequate.

He compared the simulation results of concrete core temperatures with monitored sensor data, for different layers of the slab, i.e. top, middle and bottom surfaces. Although the simulation matched closely the measured temperatures, neglecting the effect of the absorbed transmitted solar radiation is one of the suspected causes of discrepancy between the simulated and monitored temperature data.

2.3 Conclusion

The numerical model Chen created to assess the thermal performance of the ventilated concrete slab built in the Ecoterra™ house considered only the active charging of the slab by the forced BIPV/T hot air. Yet, the slab is exposed to large amounts of direct solar radiation, especially during shoulder seasons. For that reason, further investigation is required to obtain better knowledge of this solar system to avoid

exceeding thermal comfort limits and improve its thermal performance. This thesis will analyze the determinant combined effect of forced ventilation warm air in the slab core and absorbed solar radiation.

The literature review showed that ventilated concrete slabs are an efficient system to reduce and delay peak building loads and to improve thermal comfort. Significant research efforts have been made on concrete core conditioning systems used as devices to reduce the cooling load in commercial buildings. Concrete radiant floor are undoubtedly efficient and comfortable heating devices. Thus, further advancements are certainly required to enhance our knowledge of ventilated active/passive energy storage devices in small-scale residential buildings in order to optimize the storage of active solar gains.

Buildings are complex systems in which energy components, occupants and building structures mutually interact. In order to reduce their energy footprints, their inter-relations must be well understood. This review underscored the potential of statistical data-driven system identification techniques to accurately and robustly dissect the thermal behaviour of these building systems. Considering the technical advantages of simple building thermal modeling, this thesis will present a way to characterize the thermal behaviour of an active/passive solar thermal storage system with a simple linear statistical model built with monitored sensor data.

3 SYSTEM IDENTIFICATION OF THE VENTILATED CONCRETE SLAB USING MONITORING DATA

This chapter describes how a mathematical description of the thermal behaviour of the ventilated concrete slab was obtained using a statistical black-box system identification approach. First, from a thermal point of view, the physical description of the room where the slab is located is presented. Second, the decomposition of the slab thermal charging and discharging system into a simple linear multiple-input/single-output description is explained and justified. Subsequently, the development of identification time-series is presented and the procedure used to obtain a mathematical description of the system is detailed. Finally, an analysis of the transfer functions obtained is presented.

3.1 Description of the Room Thermal Zone (South Basement)

3.1.1 Ventilated Concrete Slab Thermal Zone

The ventilated slab is one the sub-systems of the Ecoterra™ house that are connected to the BIPV/T roof. It was integrated in the design of the house to increase the amount of solar energy stored and it is located in the basement of the house. This basement space is divided in two sections (a north and a south section) by portions of 250 mm thick concrete wall. The ventilated concrete slab covers a 3.5 m by 10.5 m floor area in the south section of the basement. The area covered by the embedded ventilation channels and the inlet and outlet manifolds is 3.05 m by 10.36 m. The VCS consists of 19 ventilation channels formed by a steel deck seated on a metal mesh over which approximately 125 mm of concrete was poured, making a thermal mass volume of 5 m^3.

The metal mesh was included in the structure to increase the convective heat transfer coefficient of each air channel.

The staircase to the main level of the house is located in this portion of the basement. Figure 3.1 shows the divisions of the basement and the location of the ventilated concrete slab in the south portion.

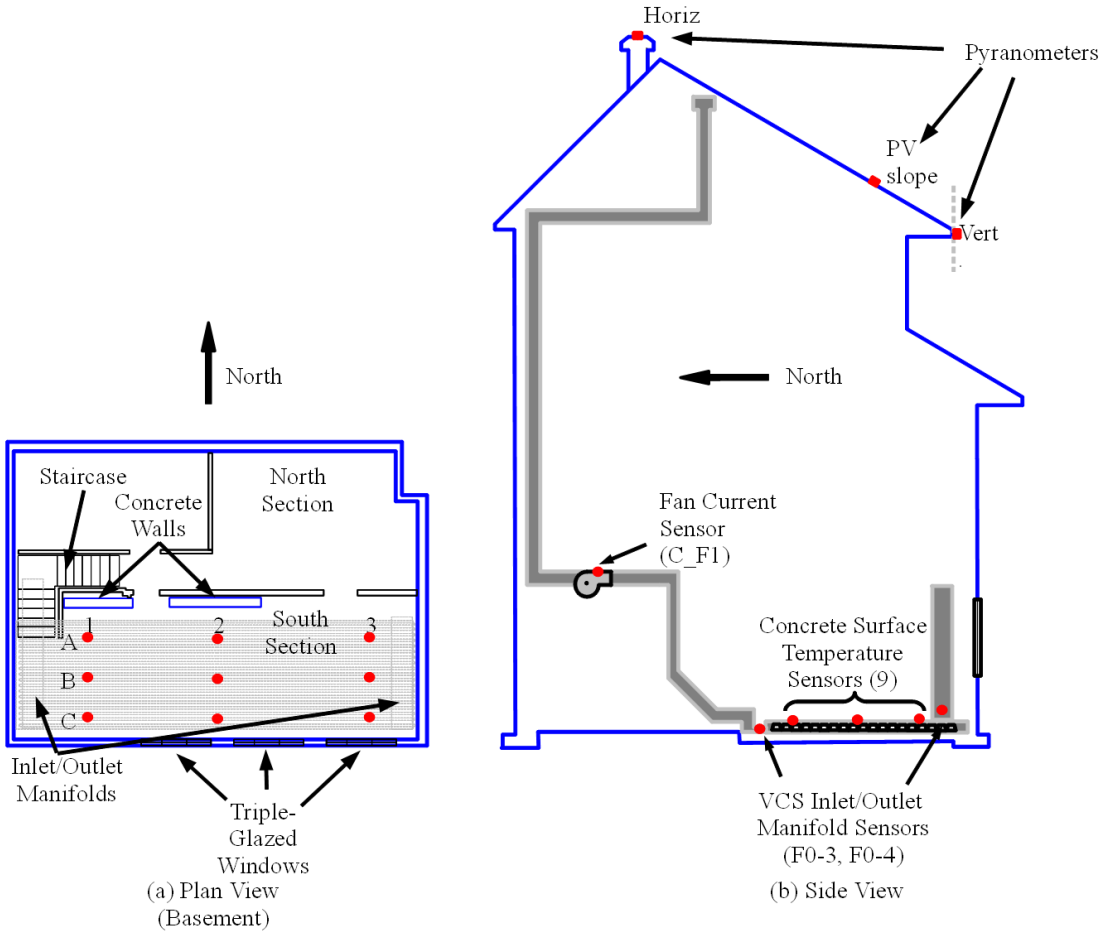

Figure 3.1: (a) Basement floor plan with location of the nine ventilated concrete slab surface temperature sensors. (b) Side view of the Ecoterra™ house with location of sensors.

The ventilated concrete slab was placed directly on grade. A cross section of the slab helps visualize its installation and construction characteristics. The insulation under the basement slab is approximately RSI 1.3 (R7.8). At the time when the sensor data used

in this study were recorded, no floor cover was installed and the house was not yet occupied.

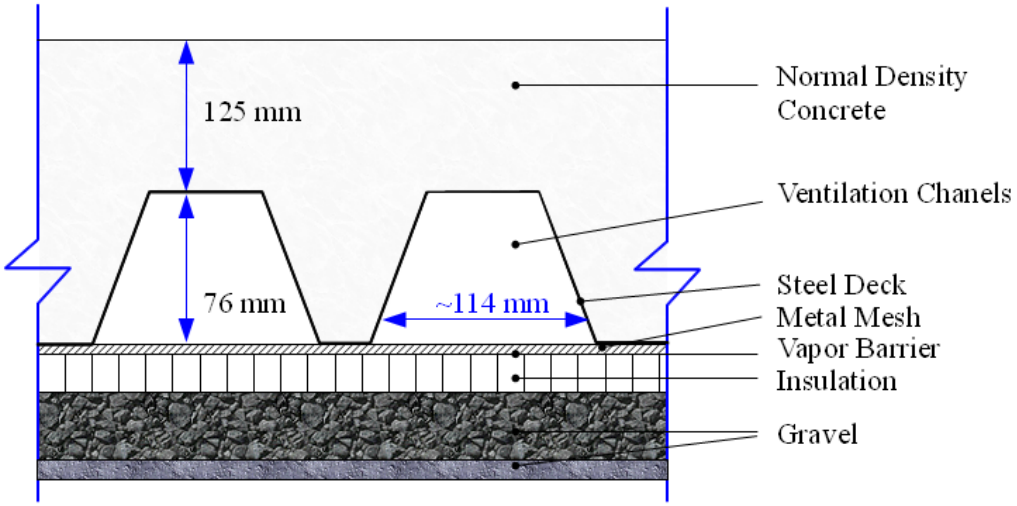

Figure 3.2: Cross section of the ventilated concrete slab. Simplified schematic inspired from Y. Chen (2009, p. 92).

The insulation of the above-grade portion of the basement walls is approximated to RSI 2.5 (R 14.2), and the below-grade portion to RSI 5.7 (R 32.3). Three large windows are located on the south wall of the room. These windows are triple-glazed, iron-coated and have cavities filled with argon. Each window has a 1.8 m^2 glazing area. Their effective thermal resistance is about RSI 0.85 (R 5) and they have an approximate solar heat gain coefficient of 0.5. After the construction, the air-tightness of the house was measured at 0.85 air changes per hour at 50 Pascal.

3.1.1.1 Heat Transfer in the Ventilated Concrete Slab

The ventilated concrete slab is a system in which the heat transfer is time-dependant. It should therefore be treated as a transient problem. This is due to its ever changing boundary conditions. It is a complex system for which heat transfer phenomena

occur by different modes, i.e. conduction, radiation (short wave and long wave), natural convection, and forced convection.

Figure 3.3 shows a cross-section simplification of the ventilated slab. It represents the type of simplification that would facilitate an eventual 2-D or 3-D finite difference thermal modeling of the slab. For simplification purposes, the corresponding information was split between the two channel cavities illustrated, but similar convective heat transfer phenomena occur in each channel cavities.

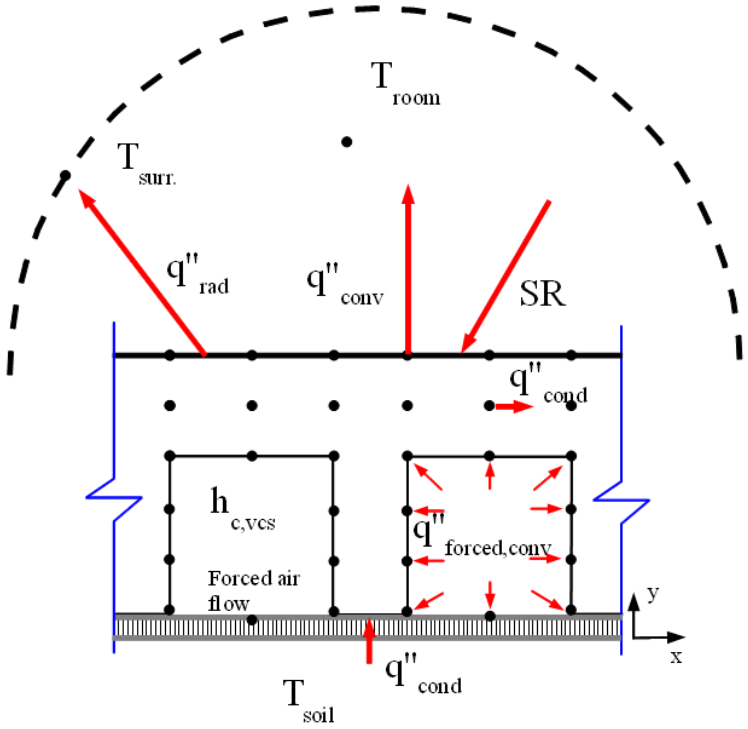

Figure 3.3: 2-D schematic representation of the heat exchange mechanisms within the VCS, boundary conditions, and nodal network discretization.

The boundary conditions of the VCS system are created by the room air, the temperature of surrounding surfaces in the basement south room, the ground soil temperature, the air flow temperature within the channels, and the corresponding flow rate. The slab surface also absorbs transmitted short-wave solar radiation (SR). On its

perimeter sides, the VCS is directly in contact with the concrete footing and the portions of 250 mm thick concrete wall. Therefore, these elements represent the surrounding boundary conditions of the VCS thermal system.

At its surface, the VCS exchanges energy by long-wave radiation with the surrounding surfaces of the enclosure. A natural convective energy exchange also takes places with the basement room air. The radiative heat transfer ($q''_{rad,surf}$) and convective heat transfer ($q''_{conv,surf}$) processes at the VCS surface can be expressed by:

$$q''_{rad,surf} = \varepsilon\sigma(\mathrm{T}^4_{VCS,surf} - \mathrm{T}^4_{surr}) \tag{3.1}$$

$$q''_{conv,surf} = h_{c,surf}(\mathrm{T}_{VCS,surf} - \mathrm{T}_{room}) \tag{3.2}$$

where ε is the emissivity of the VCS surface, σ the Stephan-Boltzmann constant ($\sigma = 5.67\times10^{-8}\, W/m^2K^4$), $\mathrm{T}_{VCS,surf}$ the VCS surface temperature, T_{surr} the temperature of the surrounding surfaces, T_{room} the temperature of the room air, and $h_{c,surf}$ the convective heat transfer coefficient at the concrete surface.

Within the concrete, the heat is transmitted by conduction. The transient three-dimensional heat conduction is presented by (3.3) where α is the thermal diffusivity. The boundary condition at the bottom of the slab is expressed by $T(y=0) = T_{soil}$.

$$\frac{1}{\alpha}\frac{\partial T}{\partial t} = \frac{\partial^2 T}{\partial x^2} + \frac{\partial^2 T}{\partial y^2} + \frac{\partial^2 T}{\partial z^2} \tag{3.3}$$

As the VCS is a transient system with a complex geometry, the solution to this thermal problem would require discretizing the slab in a three-dimensional network of

nodes. Equation (3.4) is the explicit finite difference equation for the concrete nodes used in the previous study of the VCS by Y. Chen et al. (2010). In this equation $\Delta T^{i}_{x,y,z}$ is the temperature gradient between the current node at *x,y,z* and the adjacent node along the direction and $U^{i}_{x,y,z}$ is the conductance between these two nodes, $T^{c.r}_{x,y,z}$ is the effective solar-air temperature, and $h^{c,r}_{x,y,z}$ the combined heat transfer coefficient for the radiation and convection occurring at the VCS surface. It follows that, for the concrete internal nodes, the last terms of (3.4) are neglected.

$$\frac{\left(T^{t+\Delta t}_{x,y,z} - T^{t}_{x,y,z}\right)\cdot C_{x,y,z}}{\Delta t} = \sum_{i} \Delta T^{i}_{x,y,z} \cdot U^{i}_{x,y,z} + (T^{c.r}_{x,y,z} - T^{t}_{x,y,z})\cdot \mathrm{A}_{x,y,z}\cdot h^{c,r}_{x,y,z} \qquad (3.4)$$

The energy exchange between the concrete and the air stream within the VCS channels occurs by forced convection because of the BIPV/T–VCS mechanical ventilation. The solution to this part of the VCS thermal energy problem requires determining if the flow is turbulent or laminar. This information will then allow selecting the adequate correlations to calculate the Nusselt number (Nu) leading to the identification of the convective heat transfer coefficient between the interior surfaces of the channels and the travelling air. In cases of forced convection, it is most of the time a function of Re (Reynolds number) and Pr (Prandtl number). It must be mentioned that radiative heat exchanges between the inner surfaces of the channels also occur.

3.1.1.2 Active Charging

Active charging refers to a phenomenon for which the state of a thermal energy storage medium is modified by a controlled intervention. Hence, the ventilated slab is

actively charged when the heated air from the BIPV/T roof, which is exposed to the radiation of the sun, is blown through its channels. Its active charging is controlled by the supervisory control system of the house. When the BIPV/T fan is running, the heated roof air can be diverted towards the slab in order to store this collected solar thermal energy. Controls ensure that an adequate temperature difference exists between the roof cavity air and the slab. Once the air has travelled through the channels embedded in the slab, it is exhausted outdoors.

3.1.1.3 Passive Charging/Discharging

Passive charging refers to the natural capacity of a thermal energy storage medium to accumulate and slowly release energy to the indoor space by natural convection and longwave radiation. Therefore, the solar radiation entering the basement room and hitting the concrete surface of the ventilated slab allows this zone of the house to passively benefit from solar energy. Three large south-facing windows allow solar radiation to enter the living space of the basement south room.

3.1.2 Energy Flows during Solar Dominated Period

The thermal behaviour of Ecoterra™'s ventilated concrete slab was studied during the usual heating season in Quebec. More specifically, solar dominated periods were chosen for this study. A solar dominated period is defined as a period during which the passive and active solar gains are sufficiently high to maintain the indoor air temperature in the Ecoterra™ house above the setpoint. Therefore, during these periods the house does not receive any auxiliary heat input from its ground source heat pump.

Solar dominated periods are critical because they correspond to periods during which the combination of auxiliary heat input to the room and solar thermal charging of the slab is likely to produce overheating situations. During these periods, the ventilated concrete slab is exposed to large amounts of direct solar radiation and the BIPV/T roof transforms efficiently the solar radiation into thermal energy. High floor surface temperatures as well as high living space air temperatures can potentially result in thermal comfort problematic situations. Moreover, during solar dominated periods the ventilated concrete slab is used at its full potential. It therefore represents an ideal series of days to characterize its response to the combined effects of active and passive solar charging.

Doiron (2011) presented a schematic representation of the energy flows in Ecoterra™. All significant possible energy gains and their transmission into the house are described. As depicted in Figure 3.4, the effective energy flows during the solar dominated periods selected are considerably simplified.

Crossed-out on Figure 3.4 are the energy transmission paths that can be neglected for the solar dominated periods selected for this study (two series of days in March 2009). Dampers were set so that the roof-warmed air was redirected through the ventilated concrete slab channels and, as explained earlier, the ground source heat pump did not supply any heat to the indoor living space. Because the house was not occupied during the periods studied, internal gains are considered negligible and the house passive solar gains were not controlled by awnings.

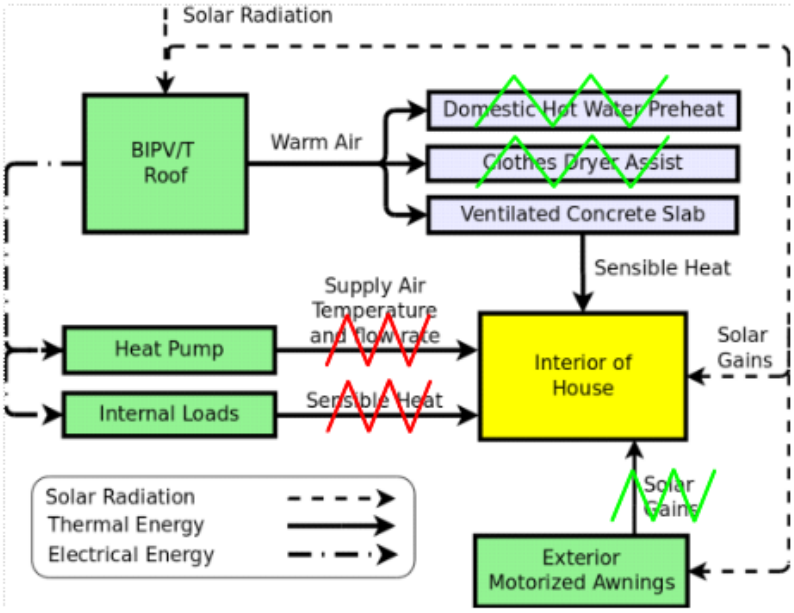

Figure 3.4: System energy flows during solar dominated periods, modified figure from Doiron (2011, p. 57).

The solar dominated periods were identified by analyzing the Ecoterra™ south basement room air temperature sensor data. High frequency fluctuations (less than 2 hours) indicate that the geothermal system is inputting heat to the house. In order to be qualified as a solar dominated period, the data should be free of any high fluctuations during day time.

3.2 Ventilated Concrete Slab Dynamic Modelling

The main focus of this thesis is the ventilated concrete slab. A methodology was developed in order to better understand and model the thermal behaviour of the ventilated concrete slab. Specifically, research efforts were focused to describe, using a mathematical model, how the active and passive charging of the ventilated concrete slab were influencing its surface temperature.

Therefore the ventilated concrete slab represents the dynamic system studied. Because of its inherent thermal capacity, it is evident that the current thermal response of the slab depends on the current and past values of its energy stimuli. With a simple model, we can predict its future response with weather forecasts as inputs.

A system is an entity which is subject to the influence of different variables acting together and which reacts by outputting a unique response (described by one or more variables). System identification methods were developed to build mathematical descriptions of dynamic phenomena. In other words, a model is a mathematical description of a dynamic system. Once identified, these models are useful tools for simulation, prediction and control of output variables of any type. Even if a model is reliable, it remains an estimation of the true phenomena.

3.2.1 Ventilated Concrete Slab System

An analysis of the ventilated concrete slab energy inputs and thermal zone energy flows allowed identifying three inputs influencing possibly the slab surface temperature output (y) during the solar dominated periods in a significant way.

The first input is the heat absorbed by the VCS (u_1) when hot air is injected through its embedded channels. This hot air is drawn through the insulated manifold of the roof after it has traveled along its channels and been heated by the sun under the metal roof layer. Therefore, this active charging input can be identified as the only controlled input of the system because it is the only one that can be manipulated by the house control system.

Solar gains through the basement south windows correspond to the second significant input (u_2) influencing the VCS surface temperature. Passive charging of the slab can be also qualified as a measured disturbance because the basement window did not have any controllable shading device.

The third input selected for the identification of the system was the exterior ambient temperature (u_3). This input can also be qualified has a measured disturbance. Even though the house is highly insulated, it was assumed that the exterior temperature had an indirect impact on the slab surface temperature.

A number of assumptions were established before starting the system identification procedure in order to clarify the dynamics of the system studied and restrict the modeling task to a clear thermal scheme. First, it was assumed that the south basement room air temperature was not influencing significantly the VCS surface temperature during solar dominated periods. It was assumed that the convective heat transfer was mainly occurring from the slab surface to the room air, and that the corresponding heat transfer coefficient and the difference of temperature between the room air and the concrete surface temperature remained relatively constant.

Secondly, the influence of ground temperature was also neglected. It was assumed that since this temperature is varying with a low frequency (one year), it had no significant influence on the daily fluctuations of the slab surface temperature.

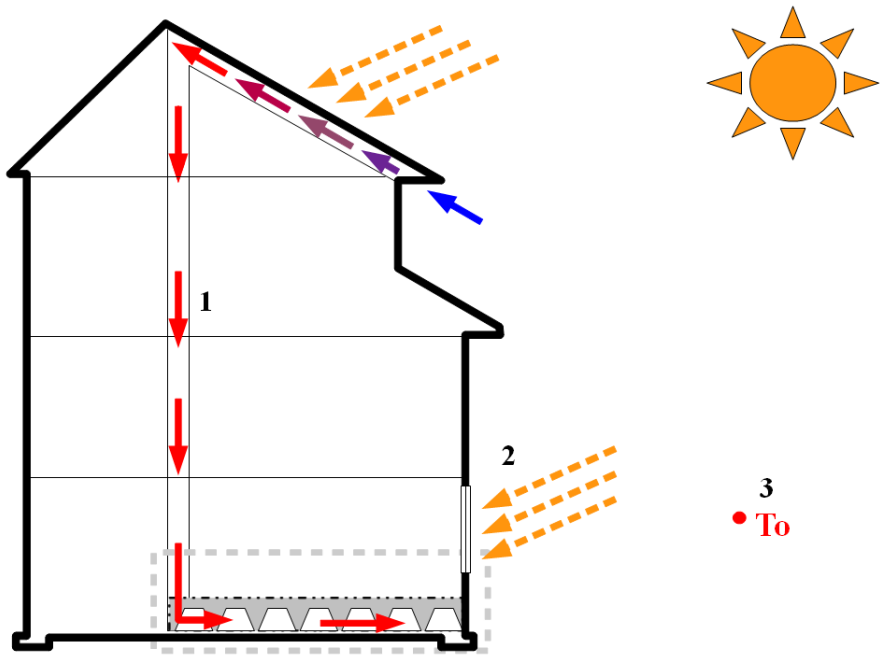

Figure 3.5: Ventilated concrete slab system and influencing inputs.

Figure 3.5 represents the ventilated concrete slab as a device to store and use solar heat in the Ecoterra™ house and Figure 3.6 symbolically depicts this system.

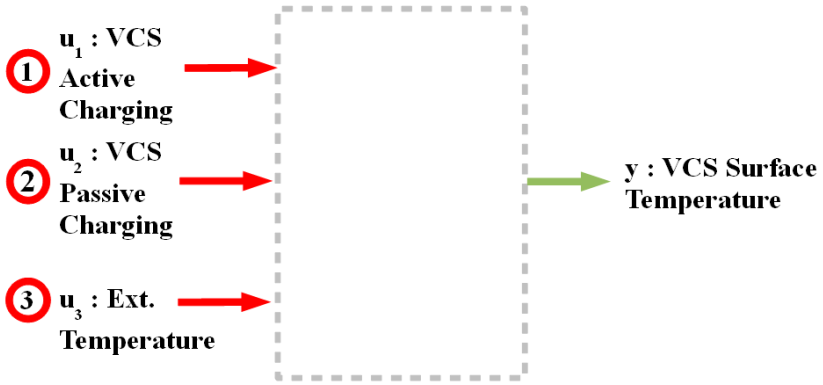

Figure 3.6: VCS system

The following paragraphs will describe how a mathematical model of this system was inferred from observed data using a statistical system identification technique.

3.2.2 Continuous-time and Discrete-time Representation of Transfer functions

As shown on Figure 2.2, typical dynamic systems are represented by an input signal $u(t)$ and an output signal $y(t)$. Linear, time-invariant, causal[2] systems are completely characterized by their impulse response $g(\tau)$.

$$y(t) = \int_{\tau=0}^{\infty} g(\tau)u(t-\tau)dt \tag{3.5}$$

Since most relationships between the system inputs and outputs are expressed in terms of differential equations and solved using Laplace transforms, equation (3.5) can be re-written using the s notation

$$Y(s) = G_c(s)U(s) \tag{3.6}$$

where $G_c(s)$ represents the impulse response function in the Laplace form. It also represents the ratio of the input and output Laplace transforms, $\frac{Y(s)}{U(s)}$.

However, typical real life physical experiments, as it is the case with the Ecoterra™ house, require dealing with observations of inputs and outputs in discrete time. Therefore, the inputs and outputs are observed at sampling instants:

$$t_k = kT, k = 1, 2, ... \tag{3.7}$$

[2] A system is linear if it responds to a linear combination of inputs by the same linear combination of outputs. A system is time-invariant if its response to the input does not depend on absolute time. A system is causal if its response at time t depends on the input up to that time only.

where T denotes the sampling interval of the data acquisition system. The continuous-time transfer function can be transformed so that the notation is switched from the continuous-time to the discrete-time.

$$G_c(s) \rightarrow G_T(z) \tag{3.8}$$

$G_T(z)$ is the discrete-time transfer function of the system, i.e. a ratio of the z-transforms, $\frac{Y(z)}{U(z)}$. Hence, the system identification procedure described in this thesis is the methodology applied to find the polynomials that create the most suitable z-transform description for the ventilated concrete slab dynamic system of the Ecoterra™ house.

3.2.3 System Identification Procedure

3.2.3.1 Experimental Set-up

The system identification approach chosen to model the ventilated concrete slab system is directly based on monitored data. The input and output signals of the VCS system were recorded by multiple sensors installed throughout the Ecoterra™ house. It is the analysis of these data that will lead to a mathematical description of the system.

The collected data were carefully analyzed in order to identify the best monitoring periods for a solar dominated system identification study. The reason for this is that the data used were not recorded during a specifically designed experiment but during the normal operation of the energy systems of the house.

Over 150 sensors are installed in the Ecoterra™ house. They monitor energy consumption, temperatures and outdoor conditions. These sensors were installed by the

three parties involved in the Ecoterra™ project: SBRN, Hydro-Quebec, and CMHC. Each party had its own data acquisition system. However, all recorded data are stored in a common data-base and queries can be done via the web. For this thesis, data recorded by the SRBN and Hydro-Quebec were used. The SBRN sensor data were recorded by an Agilent data acquisition device every three minutes. Each data logged is a three-minute average. Hydro-Quebec used a sampling frequency of 20 seconds and the output data is an average value for a 2-minute period. Since data comes from multiple sources with varying sampling intervals, outputs from the database are interpolated to one-minute intervals.

Because they used different data logging devices, SBRN and HQ data stored in the Ecoterra™ database had a slight mismatch in time. The data processing scripts written by Doiron (2011) allowed synchronizing the logged information in order to work with data having similar timestamps.

Figure 3.1 shows the position of all the sensors related to this thesis. The signals used to estimate and validate the VCS surface system model were created with data recorded by the 9 VCS surface temperature sensors, by the two thermocouples recording the air temperature at the inlet and outlet VCS manifold, by the fan current monitor, and by the three pyranometers located on the roof top.

Estimation Data for Active Charging Input

The active charging input signals were created by manipulating the data extracted from the data-base. Data recorded by three different sensors were used to create the u_1 signals: the fan current data logged by one of Hydro-Quebec sensors (C_F1) recording

amp measurements, and the temperature data logged by two SBRN thermocouples at the inlet and outlet VCS manifolds (Figure 3.1).

First, the correlation presented by Doiron (2011, p. 48) was used to obtain the volumetric flow rate in cubic feet per minute using HQ current logged data:

$$\dot{V} = 96.195I^{1.0979} \tag{3.9}$$

where $\dot{V}$ is the volumetric flow rate in CFM and I is the fan current input in amps.

Subsequently, applying the first law of thermodynamics allowed estimating the active energy input to the slab thermal mass. The concrete of the slab and its channels were identified as the control volume for this calculation. At each time step, the average air temperature between the inlet and outlet manifold was used to select the thermophysical properties of air at atmospheric pressure such as its specific heat and its density. u_1 is therefore the rate at which energy is actively transferred into the concrete in Watts and it is calculated as follows:

$$\dot{Q}_{act} = \dot{m} C_p \Delta T \tag{3.10}$$

where $\dot{m}$ is the mass flow rate of the warm air [kg/s], C_p is the specific heat [J/kg·°C] and ΔT the air temperature difference between the VCS inlet and outlet manifolds [°C].

Data Estimation for VCS Passive Charging Input

The passive charging input signals were obtained using the measurements of the vertical pyranometer located on the south-facing façade of the Ecoterra™ house. This sensor measures the global solar radiation received on the south vertical plane.

First, the portion of direct and diffuse solar radiation was calculated at each time step. Considering the day number (n), the geographic coordinates of the house (45° North), and the south façade surface angles ($\beta = 90°$, $\psi = 0°$), the portions of direct and diffuse daylight on the window surface were estimated as well as the incidence angle of the solar radiation (θ).

The Clearness Index model was used to identify the beam and diffuse fraction of global solar radiation on the window surfaces. The appropriate monthly clearness indexes (K_T) for Montreal was selected among the data contained in Table 3.1.

Month	Kt	Month	Kt	Month	Kt
January	0.45	May	0.49	September	0.49
February	0.51	June	0.49	October	0.41
March	0.50	July	0.52	November	0.35
April	0.48	August	0.49	December	0.38

Table 3.1: Montly K_T indexes for Montreal, Canada.

The hourly clearness index (k_t) was calculated using the formula presented by equation (3.11). The a and b coefficients were calculated using the correlations established by Collares-Pereira and Rabl (Duffie & Beckman, 1980, p. 89):

$$k_t = \left(a + b\cos\left(\omega t\right)\right) \cdot K_T \tag{3.11}$$

$$a = 0.4090 + 0.5016\sin(h_s - 60) \tag{3.12}$$

$$b = 0.6609 - 0.4767 sin(h_s - 60) \tag{3.13}$$

where ω is the Earth's spin rate [°/hr], t the current time [hr] and hs the sunset hour angle [°].

The hourly diffuse clearness index (k_d) was calculated from Orgill and Hollands correlation (Duffie & Beckman, 1980, p. 81):

$$k_d = \begin{cases} 1.0 - 0.249 k_t & for\ k_t < 0 \\ 1.577 - 1.84 k_t & for\ 0.5 < k_t < 0.75 \\ 0.177 & for\ k_t > 0.75 \end{cases} \tag{3.14}$$

and the beam clearness index (k_b) can be established by:

$$k_b = k_t - k_d \tag{3.15}$$

This set of clearness indexes known, estimates of the incident beam solar radiation (I_b), incident sky diffuse solar radiation (I_{ds}), and ground reflected diffuse solar radiation (I_{dg}) are calculated as follows:

$$I_o = 1353\left(1 + 0.033 cos\frac{360 \cdot n}{365}\right) \tag{3.16}$$

$$I_b = I_o k_b cos\theta \tag{3.17}$$

$$I_{ds} = I_o sin\alpha \cdot k_d \cdot \frac{(1 + cos\beta)}{2} \tag{3.18}$$

$$I_{dg} = I_o sin\alpha \cdot (k_d + k_b) \cdot \frac{(1 - cos\beta)}{2} \tag{3.19}$$

where I_o is the extraterrestrial normal solar radiation [W/m^2]. The readings of the south façade pyranometer were then split into direct and diffuse solar radiation portions (F_{dir}, F_{diff}) according to the following ratios:

$$F_{dir} = \frac{I_b}{I_b + I_{ds} + I_{dg}} \tag{3.20}$$

$$F_{diff} = 1 - F_{dir} \tag{3.21}$$

Second, the solar gains through the south windows of the basement were calculated considering the effective transmittance of the windows. It was calculated using the Edwards induction method for triple glazed windows. The extinction coefficient of each layer of glass (k) was approximated to 10 (1/m) and the refraction index (n_g) to 1.52. A 0.95 transmittance for the low emissivity coatings was assumed in order to take into consideration their optical effect on the entering solar radiation. The diffuse portion of daylight was also considered in the calculation of solar gains entering the room through the windows. The effective diffuse solar transmittance of the glazing system (τ_{diff}) was estimated at 0.2432.

Therefore the system's passive solar charging input u_2 was calculated as the sum of direct ($u_{2,dir}$) and diffuse ($u_{2,diff}$) solar gains entering the south basement room through the three windows.

$$u_{2,dir} = F_{dir} \cdot t_{eff} \cdot G \cdot A_w \tag{3.22}$$

$$u_{2,diff} = F_{diff} \cdot t_{diff} \cdot G \cdot A_w \tag{3.23}$$

$$u_2 = u_{2,dir} + u_{2,diff} \tag{3.24}$$

where τ_{eff} is the effective window transmittance for the portion of direct solar irradiance, A_w, the total glazing area of the three windows [m^2] and G the pyranometer reading [W/m^2].

Data Estimation for Surface Temperature

The output of the VCS system is its surface temperature. Nine sensors record the surface temperature of the slab. They are evenly distributed on the slab surface as shown in Figure 3.1. The data used as the system output is the calculated average of the nine thermocouple surface sensors' reading.

Estimation and Validation Data Sets

The following data from two distinct solar dominated periods were used to create the VCS surface temperature model. Data set 1 corresponds to a five-day monitoring period that started on March 13th 2009. Data set 2 corresponds to a six-day monitoring period that started on March 20th 2009. Figure 3.7 and Figure 3.8 show the input and output signals.

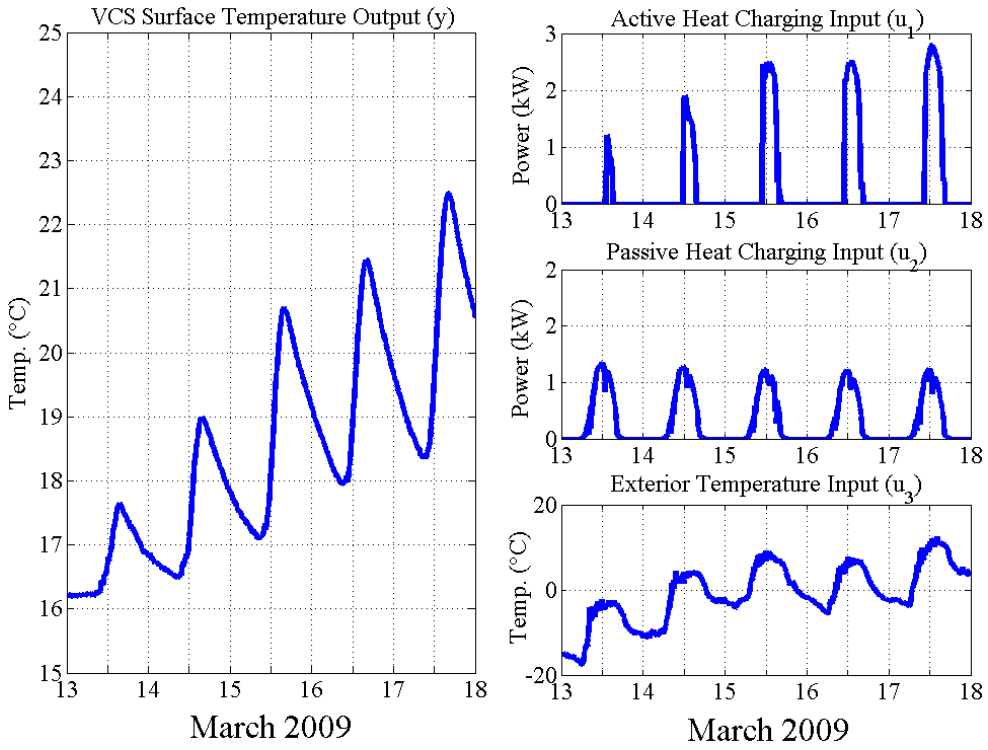

Figure 3.7: Input and output signals used to estimate the VCS surface temperature model. They correspond to Data set 1.

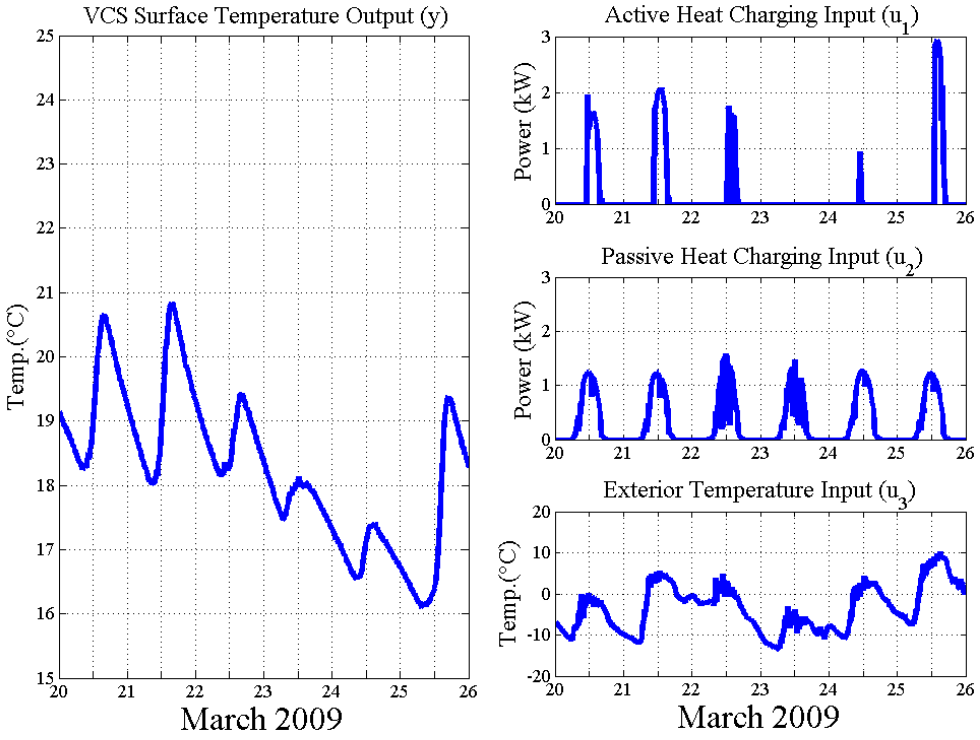

Figure 3.8: Input and output signals used to validate the VCS surface temperature model. They correspond to Data set 2.

3.2.3.2 The Model Set

The identification of the VCS model was, for the large part, an iterative procedure. The process can however be presented as an identification loop. Figure 3.9 represents this system identification iterative loop. The models resulting from the first iterations did not meet the performance criterion established for the model validation. For simplification reasons, the system identification results presented in the following sections are from the final round of identification.

For this thesis, the model identification was completed without restricting the values of the parameters or integrating any physical insight to the model structure. These choices have been made to demonstrate the strength of the model obtained despite the simplicity of the system identification approach used.

A class of models was first selected and the search for the most suitable VCS surface temperature model was restricted to this family. Moreover, the family of model structures was selected according to modeling preferences, i.e. linearity and reduced number of parameters. The linearity of a model is assumed when the model's response to a linear combination of inputs matches the same linear arrangement of outputs. Although the ventilated concrete slab is most likely not a perfectly linear system, it is assumed that in this case linearity dominates the non-linear thermal effects. This assumption is an idealization of reality, but the model validation will confirm that the chosen model describes adequately the VCS properties for the purpose of surface temperature estimation and prediction.

Subsequently, the system was assumed to be time-invariant and non-anticipative. Therefore, the system's response to inputs does not depend on the absolute time and it only depends on the inputs up to and including the current time instant.

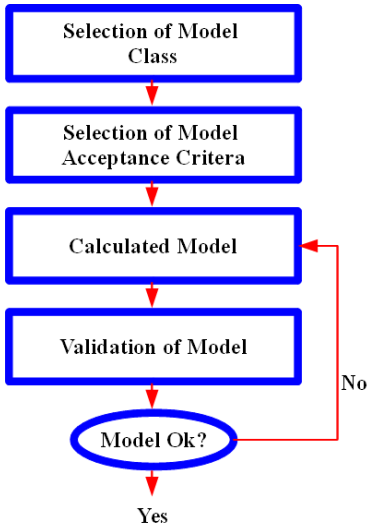

Figure 3.9: Iterative system identification loop.

For a specific linear system, the relationship between input(s) u and output(s) y can be expressed by a simple linear difference equation (L. Ljung, 2009). In equation 3.25, e(t) is the white noise term. It can be measurement noise or inputs influencing the system in an unpredictable way. In the case of the VCS, it was assumed that e(t) represents the measurement noise, i.e. errors linked to the data acquisition performance.

$$\begin{aligned} &y(t) + a_1 y(t-1) + \ldots + a_{n_a} y(t-n_a) \\ &= b_1 u(t-1) + \ldots + b_{n_b} u(t-n_b) + e(t) \end{aligned} \tag{3.25}$$

Polynomials A(q) and B(q) correspond therefore to:

$$\begin{aligned} A(q) &= 1 + a_1 q^{-1} + \ldots + a_{n_a} q^{-n_a} \\ B(q) &= 1 + b_1 q^{-1} + \ldots + b_{n_b} q^{-n_b} \end{aligned} \tag{3.26}$$

where q^{-1} is the backward shift operator used to condense the polynomial notations. Hence, the model of the system can be presented as:

$$A(q)y(t) = B(q)u(t) + e(t) \tag{3.27}$$

For discrete-time polynomial models, z is used instead of q. The z operator will be used later in this chapter.

This simple mathematical representation of the model is also called an auto-regressive model with exogenous input (ARX). It is this family of linear parametric models that was chosen in order to find the best model for the VCS surface temperature system.

In the case of the VCS surface temperature system, the model to identify had three inputs, i.e. the active energy charging u_1, the passive energy charging u_2 and the exterior temperature u_3. As a result, the ARX model structure is slightly augmented to accommodate this multiple-input/single-output (MISO) system.

$$A(q)y(t) = B_1(q)u_1(t) + B_2(q)u_2(t) + B_3(q)u_3(t) + e(t) \tag{3.28}$$

The structure of the ARX model to identify can be schematized by Figure 3.10 where $\frac{B_1}{A}$, $\frac{B_2}{A}$, $\frac{B_3}{A}$ and $\frac{1}{A}$ represent the four transfer functions of the model. These transfer functions are ratios of polynomials for each input. One transfer function is also attributed to the white noise term.

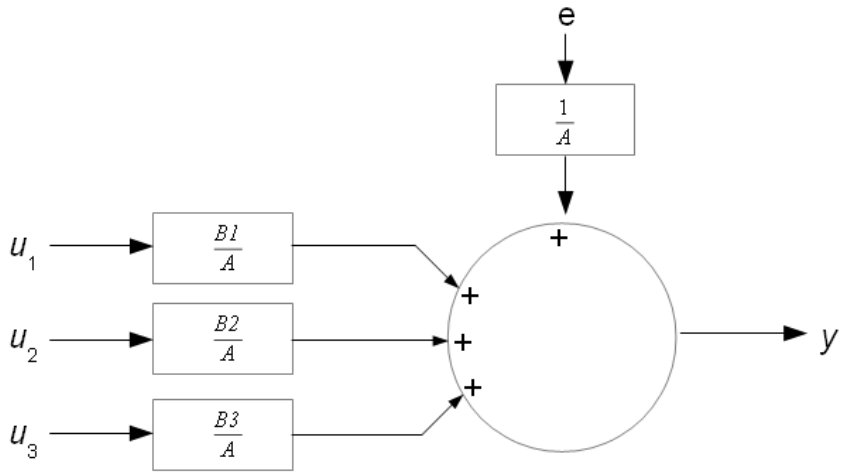

Figure 3.10: Transfer function representation of ARX polymonial model.

The estimation procedure involves identifying the group of parameters that will together form the most suitable model for VCS surface temperature prediction. $\theta_{a,b}$ denotes the group of parameters to be determined:

$$\theta_{a,b} = [a_1 \ldots a_{n_a} \quad b1_1 \ldots b1_{n_{b1}} \quad b2_1 \ldots b2_{n_{b2}} \quad b3_1 \ldots b3_{n_{b3}}]^T \tag{3.29}$$

The identification of the coefficient values of each polynomial is the complex task in the system identification procedure. In the current study, these parameters were not identified by manipulating the physical laws governing the system, but by using a parametric identification technique. Parametric identification techniques are methods based on the resolution of a minimisation problem. In this case, the coefficients of the polynomials (A, B_1, B_2 and B_3) were found using the least-squares optimization method.

3.2.3.3 Model Acceptance Criteria

A satisfactory model is one that respects a list of criteria that together justify the quality of the model. The fit of the model with the validation data, the residual quality and the stability of the model are the most important criteria to meet.

The fit is a scalar measurement of how well the selected model explains the data. Its evaluation is the first step towards the acceptation of the VCS model. This fit is calculated as the percentage of the output variations from the monitored data. For the evaluation performed for this thesis, it was defined as:

$$FIT = \left(1 - \frac{\left(\sum_{n=1}^{N} \left(y(n) - \hat{y}(n) \right)^2 \right)^{1/2}}{\left(\sum_{n=1}^{N} \left(y(n) - \bar{y} \right)^2 \right)^{1/2}} \right) \cdot 100\% \qquad (3.30)$$

where y is the measured validation output data, ŷ is the calculated model output and is the arithmetic mean of the model output. N is the total number of measurements in the validation data set.

The analysis of the model residuals is essential in order to assess the model quality. The residuals are the part of the data that the model is not able to reproduce, i.e. not explained by the model. A good quality model has “white” residuals, i.e. residuals that do not contain any traces of past inputs. The ARX model form restricts the modeling of the noise component because the noise model (1/A) is linked to the deterministic part of the model (B/A). Weak results in the residual analysis may indicate that the ARX form should be abandoned for another family of models. A different form of model may be more suitable and may allow modeling the noise component with more flexibility, i.e with additional polynomial(s).

The model stability is an additional criterion to consider when a model is validated. The analysis of the poles and zeros provides the required insight to assess the model stability.

For this thesis, additional efforts were also made in order to obtain a simple model. Therefore, the order of the model was a criterion considered during the model identification process. High-order models were rejected because they require more computational power and bring large parameter uncertainties.

3.2.3.4 Model Estimation and Model Validation

The System Identification Toolbox of MATLAB was used to build the various mathematical models analyzed in this thesis. This tool uses the inputs and output data from dynamic systems to create models. Since sampled inputs and outputs are discrete signals, the time-domain options for linear systems were used for this thesis.

For practical reasons, the data used for identification and validation were for one-hour time steps. High sampling frequencies are often problematic because they complicate the parameter identification process and they contain irrelevant information that can mislead the model estimation process. It was assumed that decimation reduced the irrelevant portion of the data without decreasing the fit to the process dynamics. This hypothesis is made because the thermal response of the slab is slow due to its high thermal inertia. In order to validate this assumption, the output of the selected model will be compared to the original system output logged at each 5-minute interval.

The validation step is the decisive test in the system identification process. Using an independent data set to validate the model created during the iterative estimation process is the preferable method. This approach is known as cross-validation. Therefore, validating the model with data set 2 allowed verifying that the model created was not overfitting the estimation data (data set 1) with artifacts.

At first, the number of poles and the number of zeros for each input were set to 3. When a polynomial model is re-arranged into the transfer function form, poles are the values of z that make the denominator of a transfer function equal to 0. The ratio of the numerator and denominator polynomials has to be re-written so that the highest order terms are unity and that the polynomials are factorized. Zeros are the values of z that make the numerator of a transfer function equal to 0 in that case. The following example presents the concept of poles and zeros for discrete (z) polynomial transfer functions. Consider that one of the MISO dynamic system transfer function is:

$$\frac{C(z)}{D(z)} = \frac{1 + 0.8z^{-1} + 0.12z^{-2}}{1 + 0.92z^{-1} + 0.95z^{-2} + 0.15z^{-3}} \tag{3.31}$$

This ratio of polynomials can be re-written in terms of z instead of z^{-1}.

$$\frac{C(z)}{D(z)} = \frac{z^2 + 0.8z + 0.12}{z^3 + 0.92z^2 + 0.95z + 0.15} \tag{3.32}$$

The denominator and numerator can then be factored. Therefore, -0.6 and -0.2 are the zeros of the transfer function, and -0.3,-0.5 and -1 are its poles.

$$\frac{C(z)}{D(z)} = \frac{(z + 0.6)(Z + 0.2)}{(z + 0.3)(z + 0.5)(z + 1)} \tag{3.33}$$

The physical nature of the VCS surface temperature system indicates that there should be a time delay before the active and passive solar gains affect the surface temperature output. In addition, as a first-guess selection, a 3600 second dead time associated to the exterior temperature input was selected for the SI iterations. Therefore, the delays (n_k) were all set to 1 time step. For each estimation, the model stability,

residuals and fit were monitored until an adequate model was identified. The model order was gradually increased during the iterative selection process.

The trial-and-error estimation process showed that a model made of an 8th order A polynomial and third order polynomials for B_1, B_2 and B_3 respected the fit, stability and residual independence criteria. Its fit was evaluated to 91.6 %. The identified model is presented in the z-transform transfer function form as follows:

$$\frac{B_1(z)}{A(z)} = \frac{0.0002191z^{-1} - 7.094e^{-05}z^{-2} - 2.453e^{-05}z^{-3}}{A(z)} \tag{3.34}$$

$$\frac{B_2(z)}{A(z)} = \frac{0.0002382z^{-1} + 1.607e^{-05}z^{-2} - 6.719e^{-06}z^{-3}}{A(z)} \tag{3.35}$$

$$\frac{B_3(z)}{A(z)} = \frac{0.0116z^{-1} - 0.003392z^{-2} - 0.00788z^{-3}}{A(z)} \tag{3.36}$$

where the polynomial A(z) is:

$$\begin{aligned} A(z) &= 1 - 1.231z^{-1} - 0.005362z^{-2} \\ &+ 0.6118z^{-3} - 0.4557z^{-4} + 0.004525z^{-5} \\ &+ 0.1066z^{-6} + 0.02667z^{-7} - 0.05225z^{-8} \end{aligned} \tag{3.37}$$

On Figure 3.11 and Figure 3.12, a good fit between the recorded validation data and the predicted model output can be observed. Figure 3.12 shows that the difference between the model predicted output and the measured data used for validation is very low. The average absolute value of those residuals is 0.062.

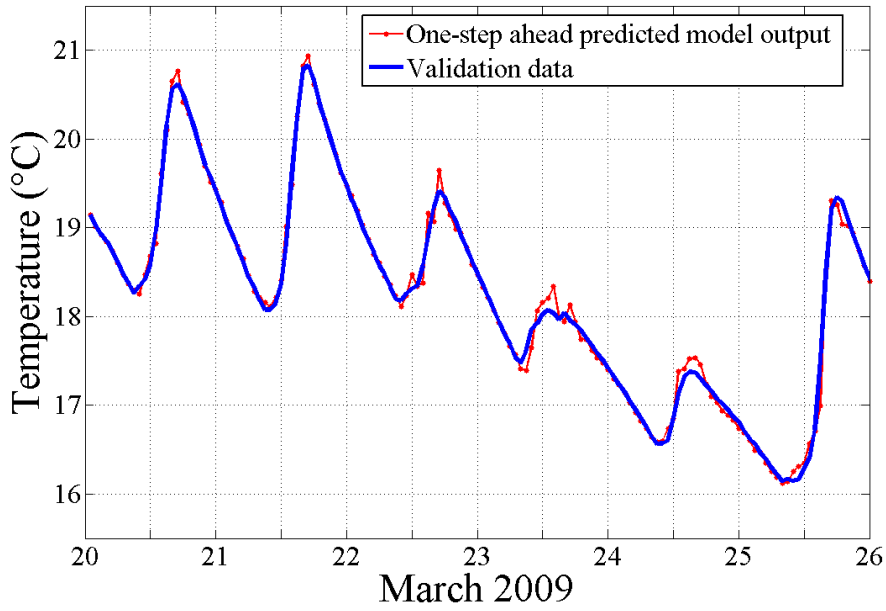

Figure 3.11: Comparison of the response of the parametric model and monitored data used for validation.

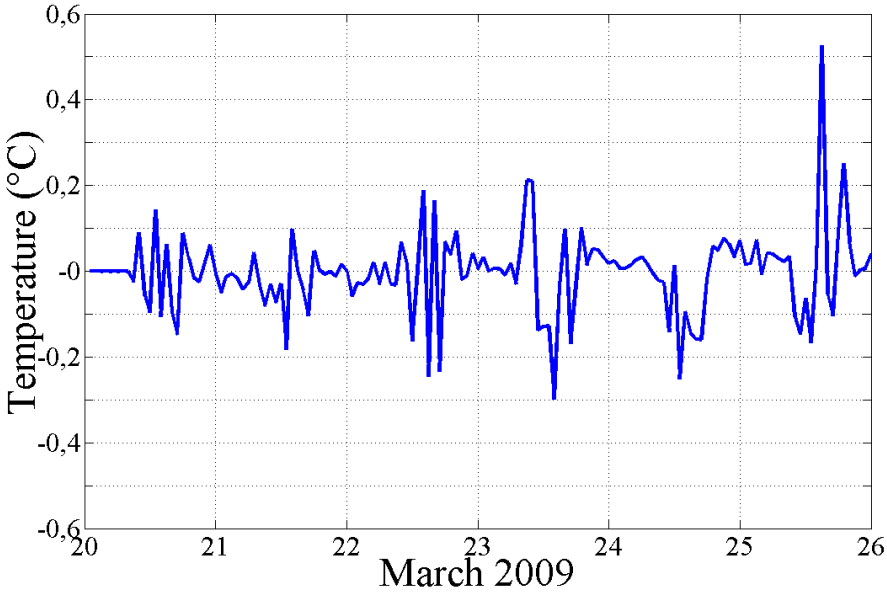

Figure 3.12: Difference between parametric model and monitored validation data.

The analysis of the poles and zeros of each input confirmed stability. As shown in Figure 3.13, the magnitude of each pole is lower than 1 and this confirms the stability of the discrete-time VCS system model.

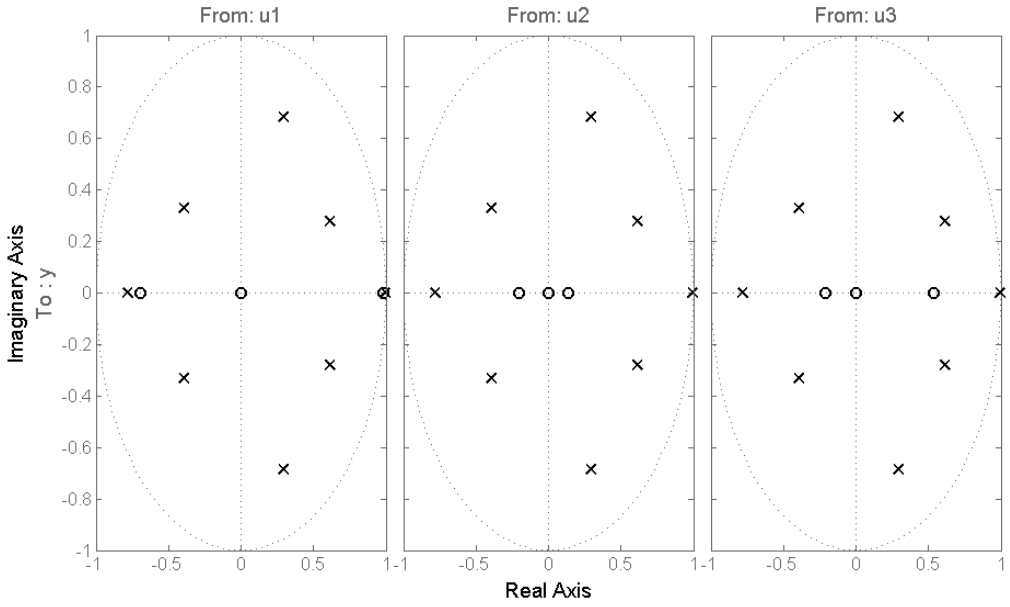

Figure 3.13: Pole(x)-zero map(o) of the VCS surface temperature ARX model.

As shown by the plots of Figure 3.14, the results of the whiteness test proved that the residuals do not include any repeating patterns, i.e they are not auto-correlated. The cross correlation functions between residuals and inputs do not show any significant deviations outside the 99.9% confidence region.

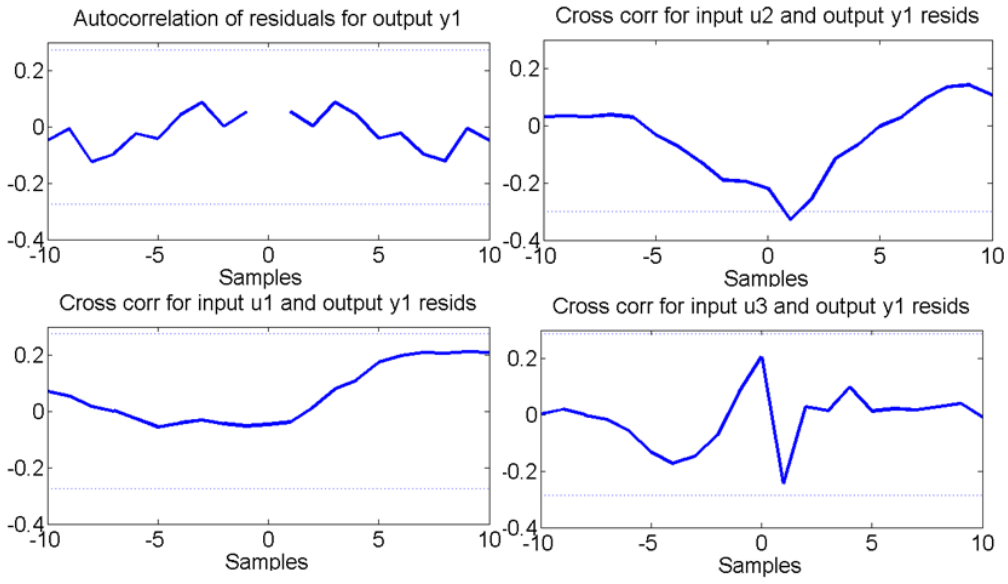

Figure 3.14: Residual analysis plots.

The choice of decimation interval was verified by comparing the model output with the validation measured data before they were decimated from 300 seconds to 3600 seconds time steps. A visual analysis of Figure 3.15 shows that there is neither significant amplitude difference nor phase shift between the two signals. Hence, the decimation of the monitored data to one-hour intervals was a satisfactory assumption.

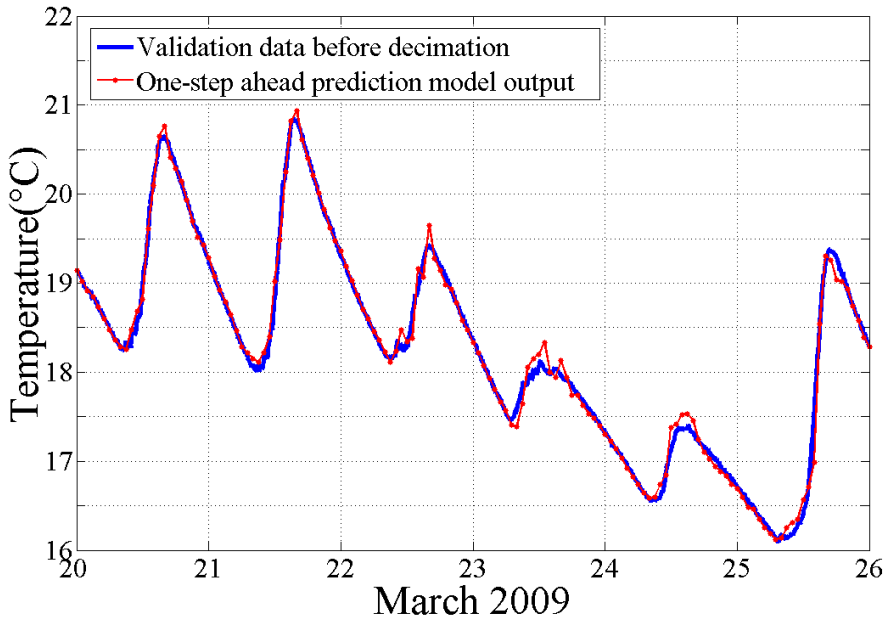

Figure 3.15: Comparison of the parametric model output and pre-decimation monitored data.

3.3 Conclusion

It can therefore be concluded that this model was successfully verified and could be accepted as a reasonable approximation of the true VCS surface temperature system. In addition, it is of an acceptable degree of simplicity with 17 parameters only considering that it is a 3-inputs and 1-output MISO model.

Previous studies have demonstrated that low order models (3^{rd} to 5^{th} order) are able to capture the essential behavior of small buildings enclosures with floors having significant thermal mass (Athienitis et al., 1990; J. A. Candanedo & Athienitis, 2011).

The results of the current are demonstrating it once again. The selected model was made of an 8^{th}-order *A* polynomial and three 3^{rd}-order *B* polynomials. This model respected the fit, stability and residual independence validation criteria.

4 PHYSICAL VALIDATION OF THE VENTILATED CONCRETE SLAB PARAMETRIC MODEL

The mathematical validation of the model was completed in the previous chapter. However, a model can be mathematically acceptable, but possibly lead to physically unrealistic results when its physical application is considered. The latter part is the main purpose of this chapter.

A subsequent practical evaluation confirms the validity of the identified ventilated concrete slab temperature model by analyzing the coupling of the system inputs with its output. Taking into consideration the physical nature of the ventilated concrete slab, the model is validated. A subsequent analysis evaluates the effects of the measurement device accuracy on the identification of the ARX model parameters.

4.1 Relative Weight of Each Influencing Variable

MATLAB SI toolbox provides an automated tool to build parametric models of physical systems and mathematical validation functions. However, the system identification process is highly related to its application. Therefore, an insight into the model characteristics remains a crucial step in order to accept the model as a suitable representation of a physical system.

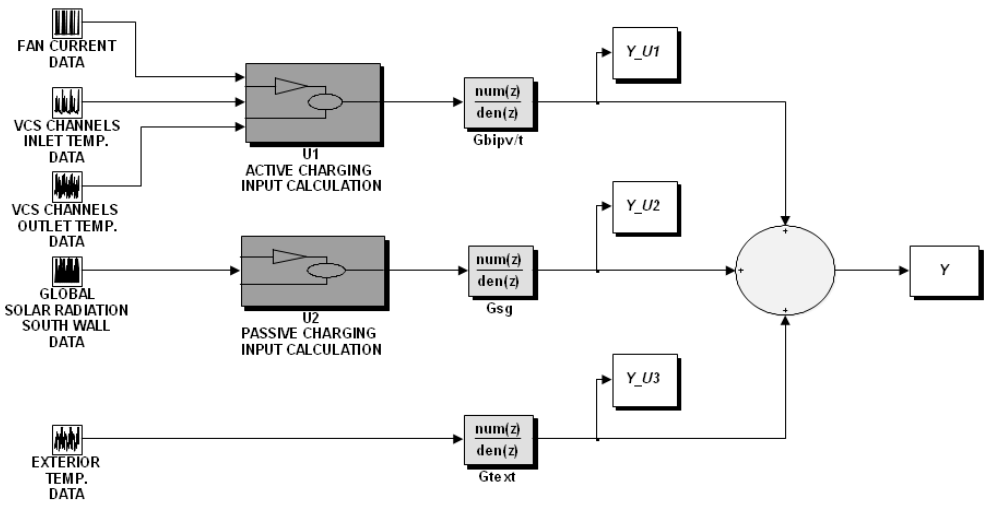

Figure 4.1: Simulink model used for the calculation of the relative weight of each system input on the total VCS surface temperature response.

The ARX parametric model structure allows rearranging the four polynomials of the MISO VCS surface temperature model into three discrete time transfer functions. This transfer function model schematic is shown in Figure 4.2. The MISO transfer function model was used to quantify the relative importance of each of the input variables affecting the surface temperature of the concrete surface. This analysis helps in understanding the relative importance of each input as it affects the surface temperature of the ventilated concrete slab.

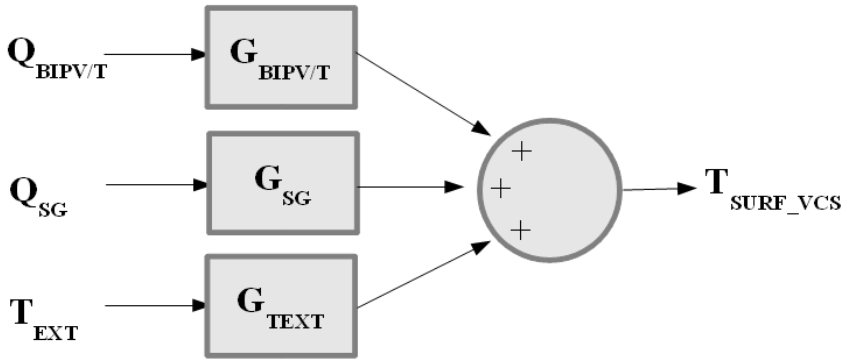

Figure 4.2: Transfer function representation of VCS surface temperature linear parametric model.

The MATLAB/Simulink platform was used to evaluate the relative weight of the three thermal inputs on the surface temperature. The input data from data set 1 was incorporated as signals into the Simulink model (Figure 4.1) and connected to their respective transfer function block. The relative temperature response of the VCS surface to each of the three inputs was calculated by running simulations.

It can be observed that inputs u_1 and u_2 have the most important contributions to the concrete surface temperature rise (Figure 4.3 and Figure 4.4).

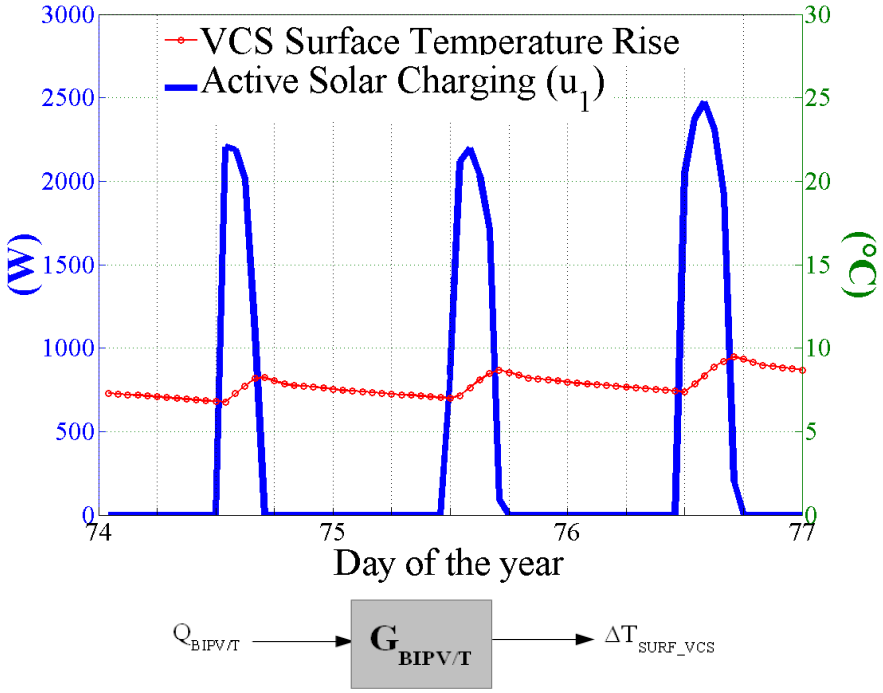

Figure 4.3: Relative weight of u_1 on the surface temperature of the ventilated concrete slab.

Conversely, the exterior temperature input (u_3) has very little impact on the fluctuation and total temperature response of the slab (Figure 4.5). These results indicate that, for solar dominated periods, the ventilated concrete slab surface temperature is heavily dependent on the passive solar gains and the active solar energy input from the BIPV/T roof through the 19 embedded channels. The high insulation value of the house

and its relatively high air-tightness explain the negligible impact of the exterior temperature on the VCS surface temperature.

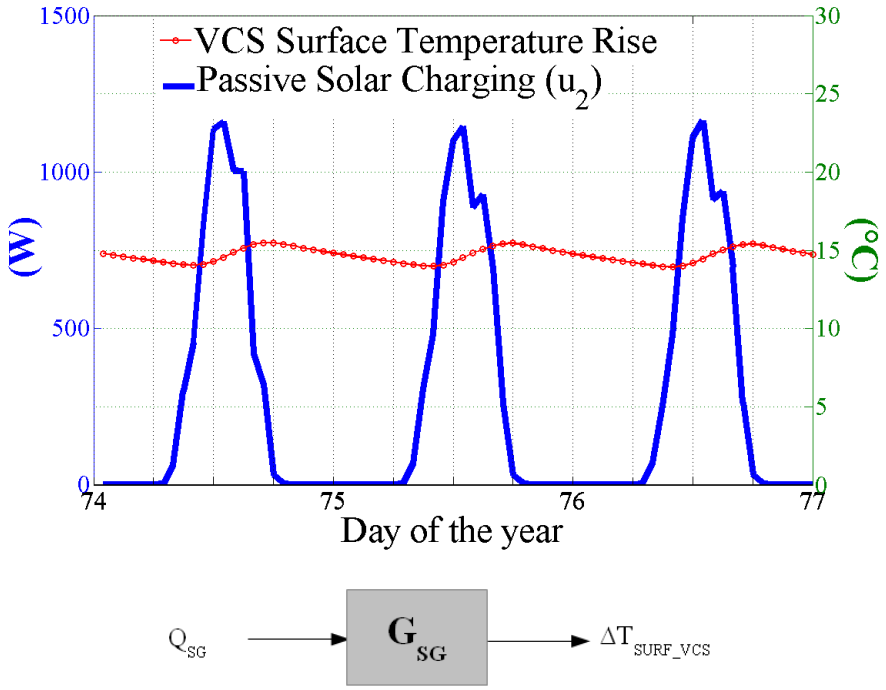

Figure 4.4: Relative weight of u_2 on the surface temperature of the ventilated concrete slab.

Although the data-driven process of system identification was completed without applying any constraints to the polynomial identification, these observations indicate that the VCS parametric model identified has characteristics which are in accordance with the thermal characteristics of the thermal mass storage system.

These results also suggest that the VCS surface temperature model could be further simplified by neglecting the exterior temperature as an input to the dynamic system without jeopardizing the validity of the model.

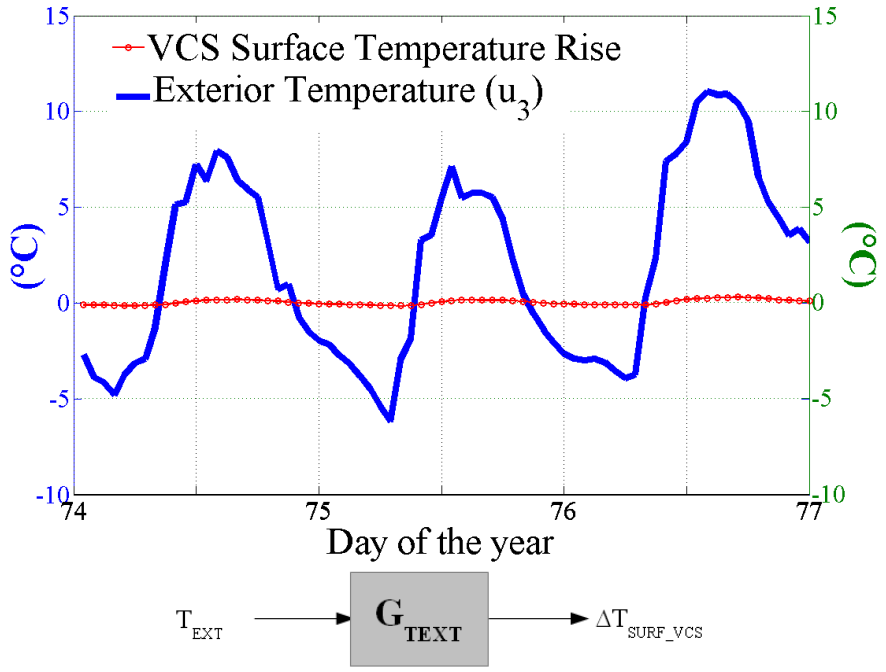

Figure 4.5: Relative weight of u_3 on the surface temperature of the ventilated concrete slab and sensor accuracy analysis.

4.2 Peak Response Delay and Sensitivity Analysis

As observed in Figure 4.6 and Figure 4.7, the delay between the peak solar inputs (active and passive) and their respective peak temperature effect on the surface of the slab are physically consistent. This delay, in the case of the active solar input, is of about 3.0 hours. The corresponding delay for the passive solar gains is of the order of 5.0 hours. These findings are an additional proof that the coupling between the identified model inputs and the VCS surface temperature output is physically relevant and that an in depth analysis of the model characteristics can provide valuable information about the VCS intrinsic thermal dynamic. These conclusions could be made even if the approach chosen for the identification of the parametric model was nearly a "black-box" identification process.

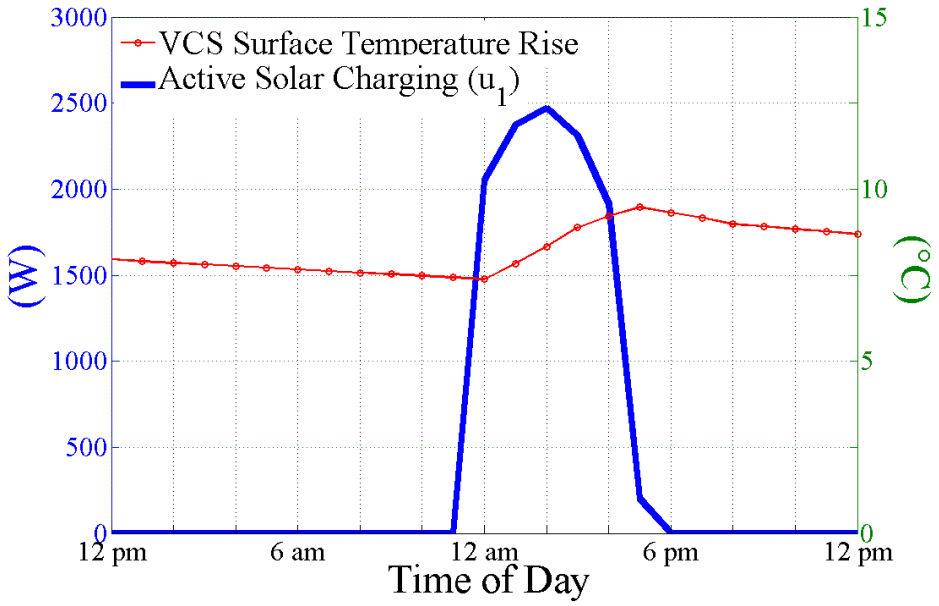

Figure 4.6: Delay between the peak of active solar charging input and its respective peak VCS surface temperature response.

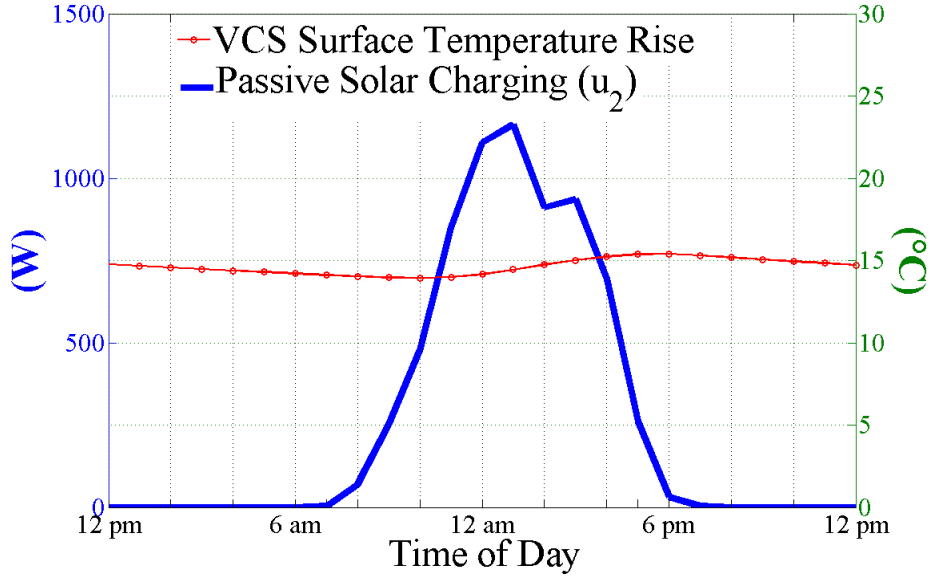

Figure 4.7: Delay between the peak of passive solar charging input and its respective peak VCS surface temperature response.

No model is valid if the data used for its identification is of bad quality. Therefore, data quality is an essential consideration in dynamic system identification applications. The VCS parametric linear model was identified with sensor data from the Ecoterra™ monitoring system and does not incorporate any data correction algorithm.

Nevertheless, the house measurement devices and sensors have their respective error. The following table summarizes the accuracies of the sensors which recorded data used for this thesis.

Measurement device	Accuracy
Type T Thermocouples	±0.5 °C
Pyranometers	± 5.0% of reading
Amp Meters	±0.05% of reading + 0.06

Table 4.1: Measurement devices and their accuracies (Doiron, 2011, p. 53).

An analysis was completed in order to evaluate the effect of the sensor accuracy on the parameters of the ARX VCS surface temperature model. The estimation and validation data used in the system identification procedure presented in the previous chapter were modified in order to simulate the lower and upper bounds of each sensor accuracy range. The random error component of each measurement device was not considered in this analysis. The transformed data sets were then used to estimate two additional parametric linear models. The same model structure was chosen (ARX) while the polynomial orders and input delays were kept (n_a=8, n_{b1}=3, n_{b2}=3, n_{b3}=3, n_k=[1 1 1]) identical. The parameters amplitudes of the two new models were compared to those of the original model.

It can be observed from Figure 4.8 that the amplitudes of the two new model parameters remain similar when they are compared to the parameters of the original VCS surface temperature model.

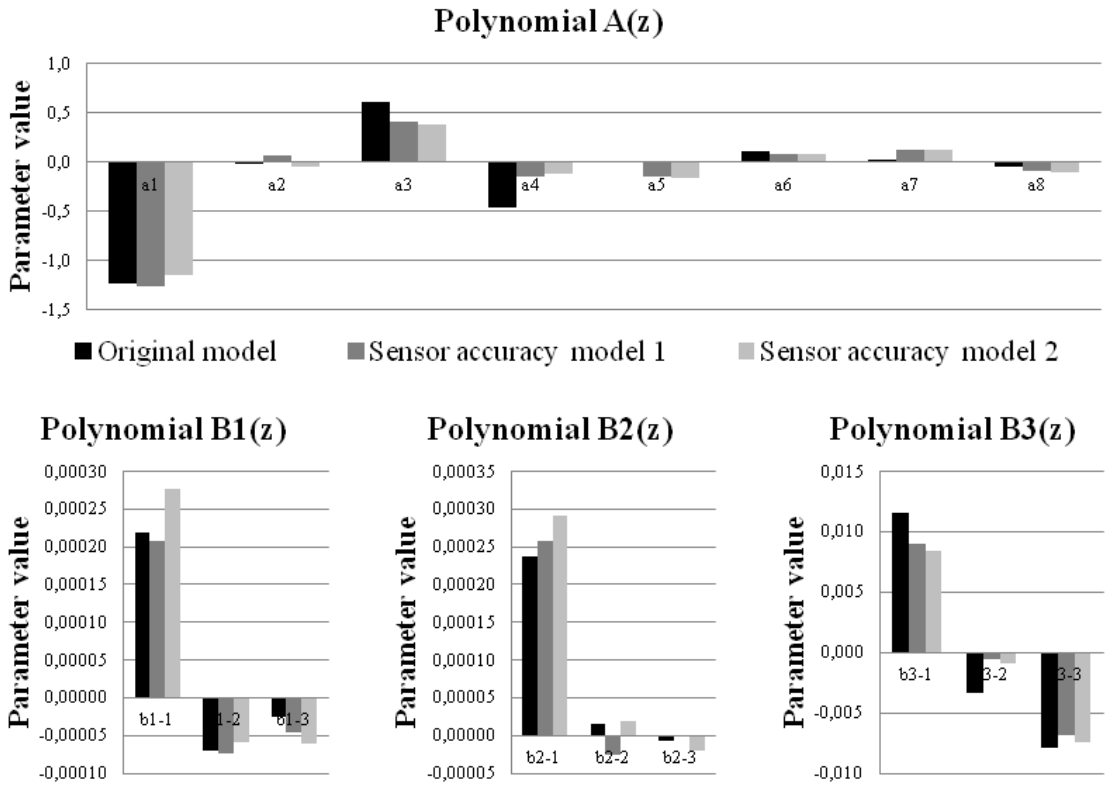

Figure 4.8: Effect of sensor accuracy on the linear model parameter values.

Subsequently, the two new models created for this sensitivity analysis were used to simulate the relative weight of the three model inputs. These results were compared to those presented in the previous section and are shown on figures Figure 4.9 to Figure 4.11. A MATLAB/Simulink procedure similar to the one used in the previous section was used for this evaluation.

It can be observed that the relative weight of each input on the concrete surface temperature is not significantly altered when the input data signals are modified to simulate the effect of the sensor accuracy on the system identification results.

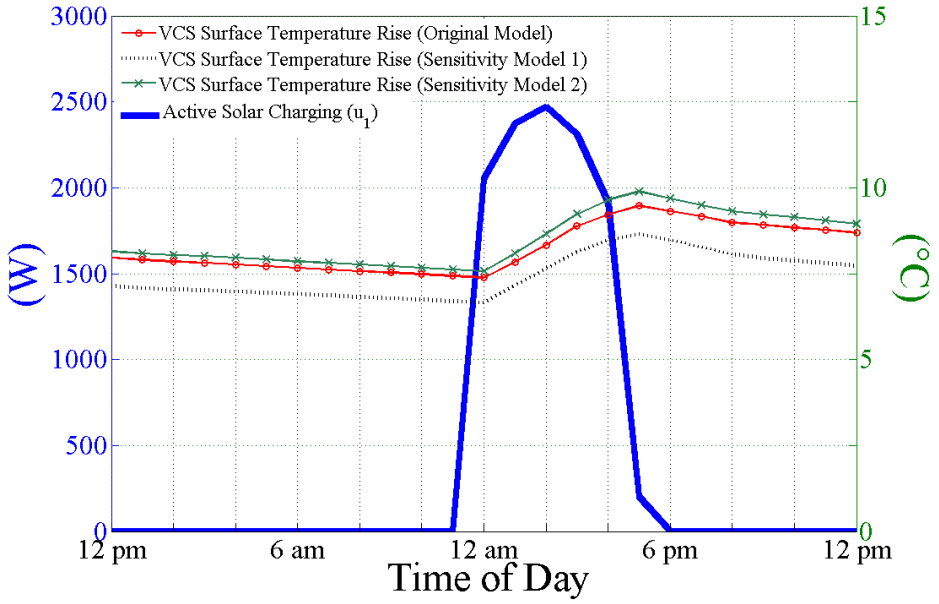

Figure 4.9: Results of the modelling sensitivity analysis for the active solar charging input (u_1).

Although small, the maximal discrepancy (about 2°C of variation with the original model) is observed for the passive solar input. This could be explained by the fact that the pyranometers are the sensors having the largest inaccuracies.

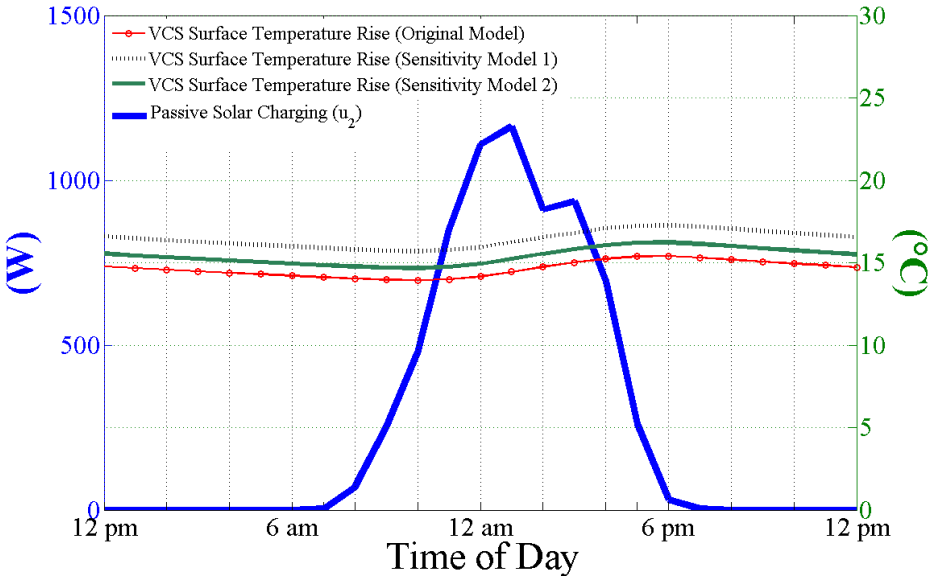

Figure 4.10: Results of the modelling sensitivity analysis for the passive solar charging input (u_2).

Moreover, as it is shown on figures Figure 4.9 to Figure 4.11, the parametric models created to assess the sensitivity of the system identification methodology to the accuracy of the monitoring sensors do not lead to any shifts in the peak concrete temperature fluctuation response. All three parametric models have their outputs in phase.

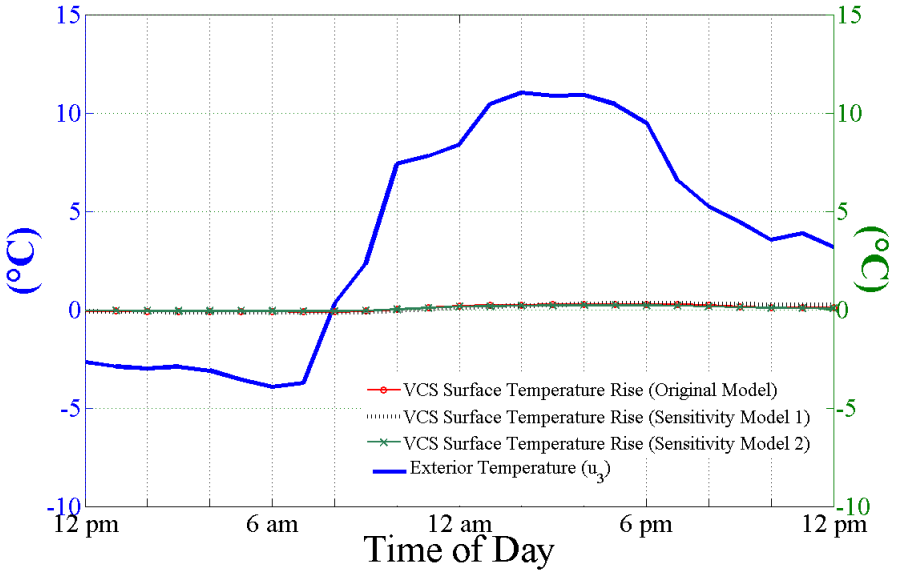

Figure 4.11: Results of the modelling sensitivity analysis for the exterior temperature input (u_3).

It can therefore be concluded that the system identification methodology developed to identify a parametric linear model for the VCS active/passive solar thermal storage system is robust. This, because it is, to a small extent only, sensitive to the input data imperfections related to the sensor accuracies.

4.3 Model Limitations

Although the previous analysis lead to positive conclusions about the linear parametric VCS surface temperature validity, this model still has several limitations that restrict its future usage to specific circumstances. Although simplified data-driven models

can facilitate the evaluation of control strategies and simulations, their use is restricted by the data acquisition context and assumptions made during the model identification procedure.

In the current case, the experiments were non-intrusive, i.e. the data was recorded without applying any constraints to the system. However, limitations related to season, floor coverage, and auxiliary heating device remain. They reduce the range of applicability of the VCS thermal model. An application of the model in inadequate building environment conditions could lead to erroneous predictions and analysis results.

4.3.1 Season Dependency

In the current case, the VCS surface temperature model is season dependant. Therefore, its use must be restricted to high solar radiation periods occurring during winter. Although the distribution of the solar radiation on the VCS surface was not considered during the system identification, it is likely that a significantly different angular incidence of solar radiation on the surface could invalidate the parametric model. It must also be mentioned that a different thermal state of the ground surrounding the foundations of the house could also invalidate the model and consequently limit its use for simulation and predictions.

4.3.2 Floor Coverage

The model was developed with sensor data recorded when the VCS surface was free of any floor cover. Therefore, using the model when carpeting or other floor finishes are installed on top of the concrete surface will result in inaccurate VCS surface temperature predictions. A modification of this kind could greatly influence the energy

flows coming from the VCS channels to its surface and the effect of the incident solar radiation entering through the fenestration.

4.3.3 Auxiliary Heating Operation

As mentioned in the previous chapter, the model was identified using data from a solar dominated period, i.e. a period when no auxiliary heating device was heating the house. As a result, its use would be inadequate in the case where an auxiliary heating device is functioning. In that case, additional variables would be influencing the thermal behaviour of the VCS surface.

4.4 Conclusion

The mathematical validity was confirmed in the previous chapter. The physical validity was established by the analysis presented in this chapter. The results presented in this chapter indicate that the VCS dynamic linear model behaviour is consistent with the physical nature of the ventilated concrete thermal storage system. The minimal impact of the sensor accuracy on the identification results was also demonstrated. There was an indication that the number of inputs could be decreased by neglecting the effect of the exterior temperature on the VCS surface temperature variation. These investigations have proven that system identification procedures, even if they are performed for completely unknown processes, cannot be totally executed by an automatic application and that thinking and insight into the system application characteristics cannot be ignored.

Finally, the limitations of the model were listed and should be taken into consideration if the model is to be integrated in control or design simulation studies.

5 SIMULATION STUDIES USING THE VENTILATED CONCRETE SLAB MODEL

The previous chapters presented how a low order linear parametric model was developed for the ventilated concrete slab of the Ecoterra™ house. The active heat charging input (u_1) from the BIPV/T roof is the most important input to this dynamic system as it is the only input over which operating strategies can be applied to optimize the solar thermal storage.

An evaluation of the discrepancy between the energy modelling and actual consumption of the Ecoterra™ house based on the results presented by Doiron (2011) was completed (see Appendix V). As a result, the BIPV/T roof operation was singled out as one of the main sources of energy production deficiency in the house. Moreover, it was already known that limitations related to prefabrication and transportation of the house sections to the site had resulted in an imperfect BIPV/T roof design.

In this chapter, improved BIPV/T designs were considered to increase the solar heat (and electricity) available from the roof. The linear polynomial model, in its transfer function form, was used to study their possible storage capacity into the ventilated concrete slab. Simulations were carried out for the month of March using measured data. Once again, this period of the year was selected for its cold exterior temperatures and high amounts of solar radiation available.

5.1 BIPV/T Design Alternatives

For this investigation, the design alternatives studied were combinations of roof tilt modifications and additions of a glazing section. By increasing roof slope, the amount

of solar radiation incident during the winter is increased and the addition of a glazed section at the end of the BIPV/T roof increases air outlet temperatures and collected heat. The analysis was limited to these alternatives because they are the most promising in terms of energy performance enhancement of the house. This model is strongly linked to the current physical description of the ventilated concrete slab. Therefore, neither the thickness of the concrete slab, the number of channels embedded in it nor its dimensions can be altered if this model is to be used. However, it demonstrates an important use of the model developed for energy studies without completing whole house simulation, that is to say an important use of transfer function models.

5.1.1 Main Modified Parameters

5.1.1.1 Tilt Angle of the Solar Collectors

The actual tilt angle of the BIPV/T roof on the Ecoterra™ house is 30°. Doiron (2011) examined the possibility of increasing the Ecoterra™ roof slope in order to improve the performance of another similar house project and reach the net-zero energy ultimate objective. This potential modification would allow better solar exposure during winter when the solar altitude is low and energy demands are at their highest levels. He found that the useful thermal output roughly doubles for a 45° configuration. Likewise, a considerable influencing factor on the energy collection performance of a BIPV/T roof is the snow accumulation (Athienitis, 2007), known to be reduced to minimal levels when angles over 40 degrees are used.

For these reasons, increasing the tilt angle of the BIPV/T roof towards its optimal value was an option to explore in order to increase the amount of thermal energy to be injected in the concrete of the ventilated slab during sunny periods of the heating season.

5.1.1.2 Glazing Section

The amount of heat collected by the BIPV/T roof would also increase if a glazing portion covering a layer of absorbing material is added at the top section of the roof cover. Figure 5.1 presents the thermal behaviour of the air as it travels across the PV/T roof channels. Candanedo (2011) carried out detailed simulations to evaluate the solar energy output of BIPV/T roof configurations including PV and glazing sections. He found that this portion of the BIPV/T structure is thermally beneficial and increases the exit air temperature. While most of the solar radiation is transmitted through the glass of the glazing section, it is captured by the bottom absorber plate.

Therefore, a glazing section was also an option incorporated in the BIPV/T roof configurations evaluated.

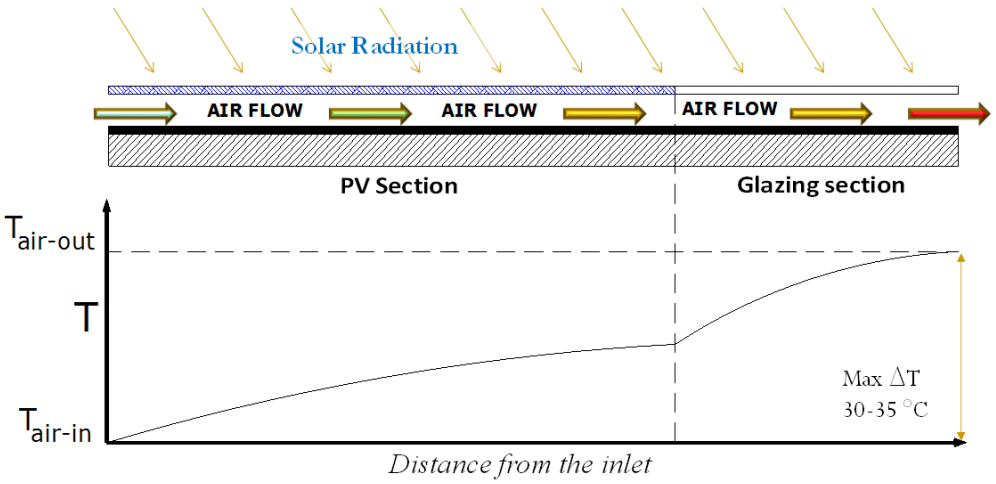

Figure 5.1: Principle of operation of the BIPV/T Roof (Source: J. A. Candanedo, 2011, p. 116).

5.1.2 Evaluated BIPV/T Roof Configurations

BIPV/T roof design alternatives were identified by combining different tilt angles and by optionally adding a glazing section. Four design roof construction options were analyzed and compared to the actual design of the Ecoterra™ BIPV/T roof. The actual roof of the Ecoterra™ house is 10.4m wide and has a total inclined length of 6.2m. The air inlet for each of its channels is not located at the front edge of the roof, making the BIPV/T effective length shorter (5.5m). The height of each air cavity is 0.038m and the BIPV/T roof net cross section, normal to the air path, is 0.332m^2. Figure 5.2 displays the actual BIPV/T roof composition of the Ecoterra™ house and Figure 5.3 presents the four BIPV/T configurations studied.

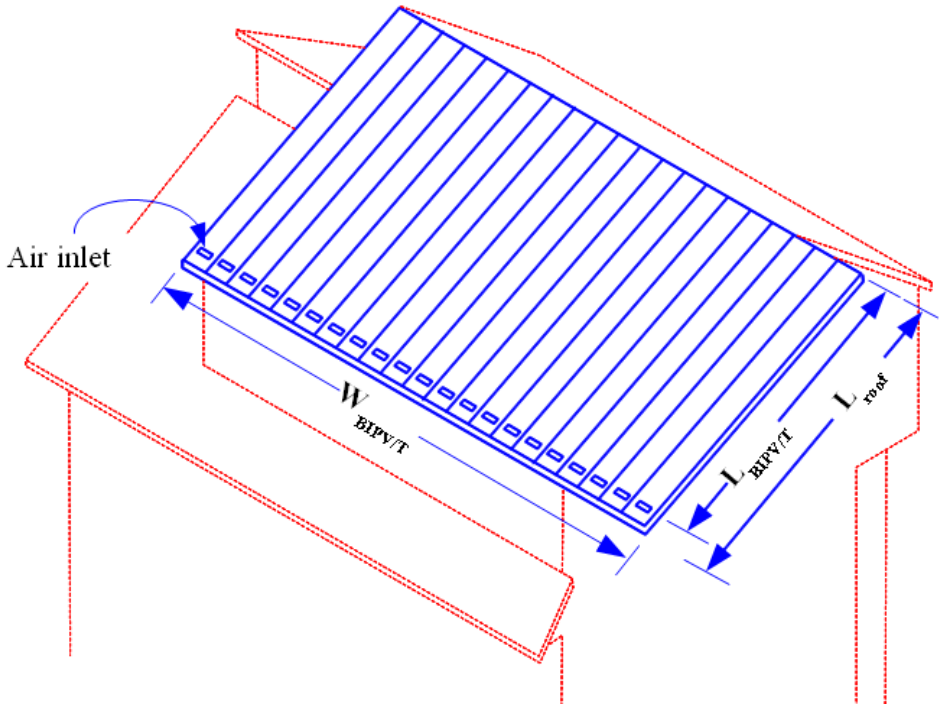

Figure 5.2: Actual Ecoterra™ BIPV/T roof design.

The first alternative analysed (R1) is a roof similar to the actual roof. Its tilt angle is however greater (45°). The total length of the BIPV/T roof is increased in order to keep

the same attic floor area. In this case, it was assumed that the total length (6.73m) is covered with photovoltaic panels.

The second roof (R2) has a similar area exposed to solar radiation. The length of the PV panels was reduced to 5.5 m to include a glazing section having a length of 1.23m at the top. The glazing section has the same inclination as the roof.

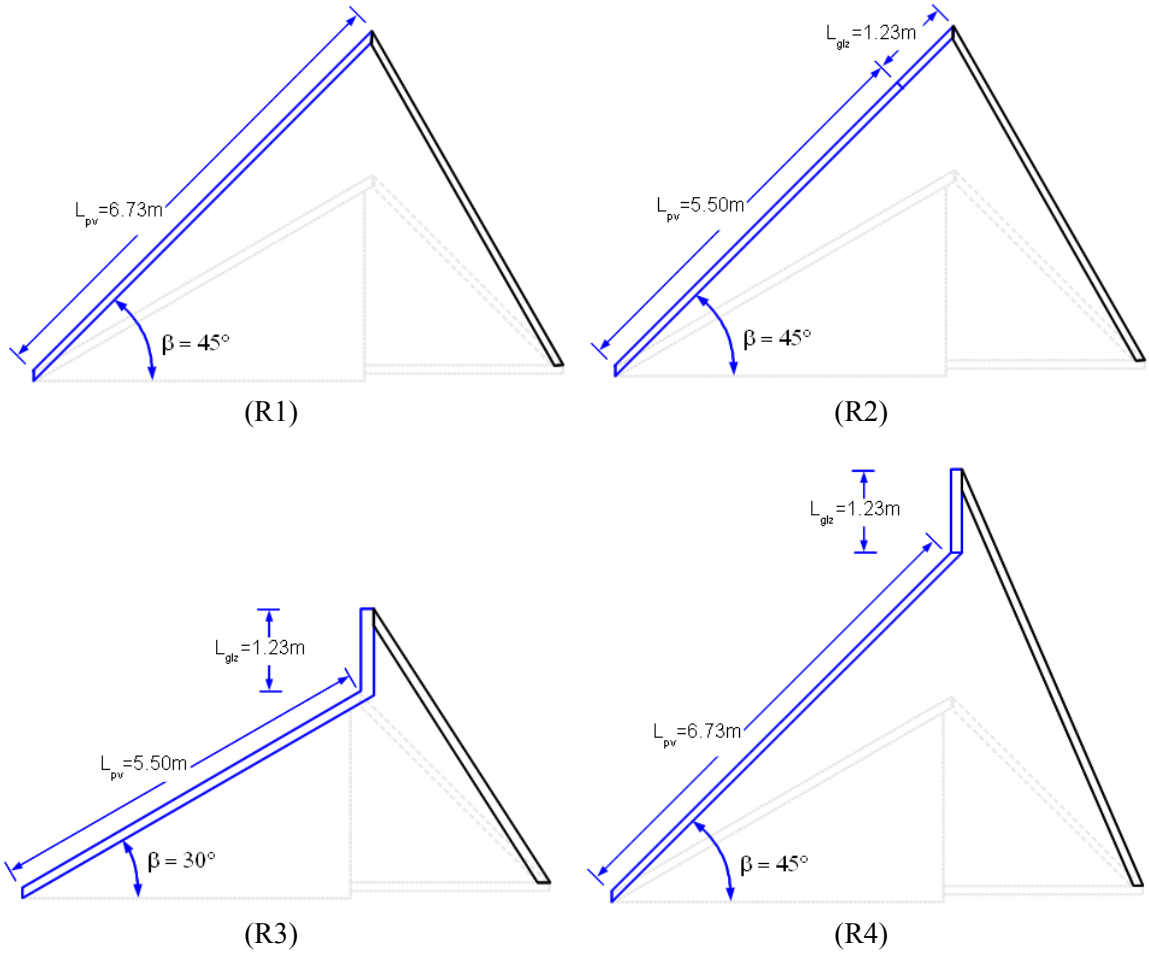

Figure 5.3: Graphical representation of the four BIPV/T roof designs studied.

For the third configuration (R3), the roof tilt angle is 30°. A 1.23m vertical glazing section is added at the top of the 5.5m length of PV. The fourth alternative (R4) also includes a vertical glazing section of 1.23m. However, it is added at the top of the 6.73 m PV-covered section having a 45° tilt angle.

For all BIPV/T options, the width of the BIPV/T roof and the thickness of the air cavity underneath are considered identical to those of the actual roof.

5.2 BIPV/T–VCS Model

5.2.1 Preliminary Calculations and Charging Rules

Considering that the active solar input to the VCS surface temperature linear model is the energy absorbed by the concrete of the slab, several calculations were required in order to translate the BIPV/T roof monitored data into adequate signals for the linear parametric model. First, a numerical model was used to calculate the air temperature at the exit of the channel cavities of the BIPV/T roof. This model was combined with a convective heat transfer coefficient estimation model developed by Chen (2009).

A third numerical model was developed in order to estimate the air temperature at the entry and exit manifolds of the VCS embedded channels. Moreover, a rule-based control scheme was applied to respect the fan activation conditions related to the active thermal charging of the ventilated concrete slab.

5.2.1.1 BIPV/T Exit Air Calculations

A model was used for the calculation of the outlet air temperature at the exit manifold of the BIPV/T roof. It considers several inputs:

- the incident solar radiation on the roof.
- the air flow rate.
- the entry temperature (soffits).

- the exterior temperature.
- the air temperature of the interior space beneath the roof (attic in the current case).

This model, used for open-loop building-integrated photovoltaic/thermal systems, was presented by Candanedo (2011) and was adapted to respect the roof description of Ecoterra™. It allows a steady-state analysis of the roof thermal dynamic phenomena and the thermal capacitance effect of each roof component was neglected. The assumptions set by Candanedo were kept for the current calculations:

- The temperature of each surface inside the control volume was considered uniform.
- The resistance of the PV module and (if applicable) of the glass in the glazing section were considered in the calculations.
- Temperatures were considered equal across the width of each air channels (1-D simulation in the control volume).
- Air leakage or air mixing to the exterior of the air gap was neglected.
- A single uniform value of the convective heat transfer coefficient was used for the top and bottom surfaces of the gap for the section covered with photovoltaic modules only.

Chen (2009, p. 76) created a correlation, based on field testing data, to determine the convective heat transfer coefficient ($h_{c,\ pv/t}$) to be applied at the top and bottom surfaces of each control volume in the BIPV/T roof channels. $v_{air,pv/t}$ is the air velocity (m/s) inside the BIPV/T roof cavity.

$$h_{c,pv/t} = \begin{cases} 10.2 & v_{air.pvt} \le 0.6m/s \\ 12 \cdot v_{air.pvt} + 3 & v_{air.pvt} > 0.6m/s \end{cases} \quad (5.1)$$

Considering this two-stage correlation, $h_{c,pv/t}$ was set to 11 W/m^2·K for the current calculations. This choice is based on the actual equipment operation of the Ecoterra™ house; the air velocity across the roof channels is approximately 0.61 m/s when the fan operates.

The convective coefficient values were modified for the control volume calculations of the glazing section. The previously set value of the interior convective heat transfer coefficient was kept for the top interior surface only. A value 2.5 times higher was used for the bottom surface coefficient to account for the high temperature reached by the low emissivity absorber plate modeled under the glazing (high absorptance). It was assumed that the absorber plate had an emissivity of 0.2.

The model also assumed, as it is the case for the Ecoterra™ house, that the back of the BIPV/T roof had an insulation conductance of a 1 W/(m^2· K).

For each design configuration (R1 to R4), the photovoltaic section was divided in five one-dimensional control volumes in the air stream direction. An energy balance was performed for each control volume. Once the system of equations was solved for the current control volume, the exit air temperature became the entry air temperature of the next control volume. If it existed, a glazing section was thermally modeled in a similar manner at the exit of the PV section. This section was divided into four additional control volumes.

For the simulations, the wind speed was assumed to be 5.5 m/s. This assumption, although realistic for the area, had to be made to account for the absence of accurate on-site sensor measurement for this climatic variable.

5.2.1.2 Slab Charging Control Sequence

In order to ensure that air was injected into the ventilated concrete slab at a useful thermal energy charging temperature, a control algorithm was included to turn on or off the BIPV/T fan. This fan is used to draw air through the cavities of the BIPV/T roof before it can be diverted to the VCS embedded channels.

First, a BIPV/T exit air temperature setpoint was fixed at 15°C. This preliminary condition ensured that the fan operated only if the modeled air temperature at the exit of the BIPV/T roof exceeded this value. The fan operation was also restricted to a certain period of the day, i.e. between 9 am and 5 pm.

Subsequent VCS heat injection conditions were also applied. They were implemented to mimic the similar settings implemented in the actual control system of the Ecoterra™ house (Doiron, 2011, p. 30).

- If an increase in the modeled BIPV/T exit air temperature was detected and it was at least 10°C higher than the slab temperature[3], the fan was turned on and operated at a 425 cfm volumetric flow rate.
- When the air temperature decreased and the temperature difference with the slab became lower than 5°C, the fan was turned off.

[3] Average surface temperature

For the purpose of this study, the temperature difference flags were reduced to maximize the heat injection in the VCS. They are higher in the actual control system because they take into account the noise the fan creates if it starts and stops too frequently and the ducting heat losses between the BIPV/T roof manifold and the basement concrete slab.

5.2.1.3 Ducting Heat Losses

Analysis of the sensor data recorded in the Ecoterra™ house has shown that there are significant heat losses occurring in the ducts between the BIPV/T roof manifold and the ventilated concrete slab located in the basement. For this study, these heat losses were not modeled; perfect duct insulation was assumed as this could be corrected in future similar construction projects.

5.2.1.4 Heat Absorption Calculations

In order to feed the VCS surface temperature linear model with the appropriate inputs, the total air stream energy loss across the VCS slab was calculated. This quantity matches the active heat charging input variable considered in chapters 3 and 4. Each of the 19 VCS channels was separated into 10 control volumes (Figure 5.4).

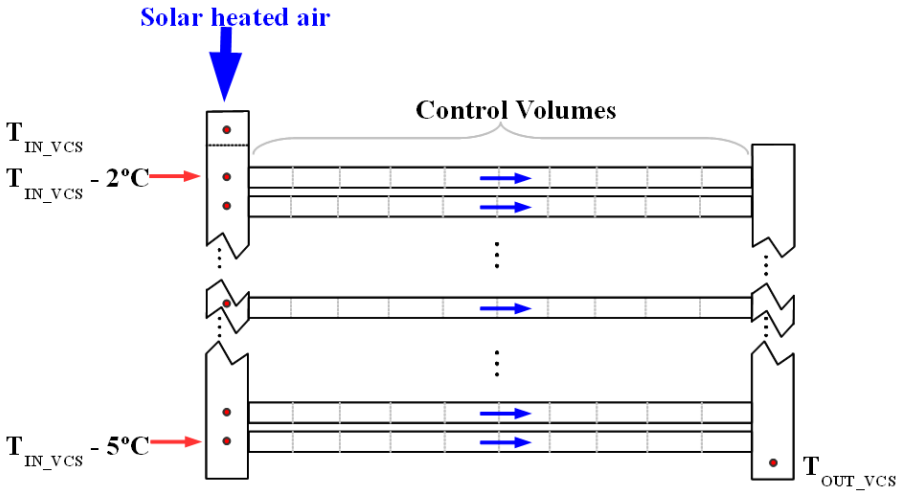

Figure 5.4: VCS channels inlet and outlet temperature calculation.

For each control volume, the following system of equations was solved to evaluate the corresponding exit air temperature. This exit temperature was used as the inlet temperature for the next control volume of the channel.

$$\Delta q_{air} = \Delta q_{air\_to\_slab} + \Delta q_{air\_to\_soil} \tag{5.2}$$

$$\Delta q_{air} = \left(T_{air,o} - T_{air,i}\right) \cdot m \cdot Cp_{air} \tag{5.3}$$

$$q_{air\_to\_slab} = h_{c\_vcs} \cdot A_{chn} \cdot \Delta T_{lm\_slab} \tag{5.4}$$

$$q_{air\_to\_soil} = U_{ins} \cdot A_{soil} \cdot \Delta T_{lm\_soil} \tag{5.5}$$

A_{chn} is the area of the steel deck surrounding the air and A_{soil} is the area of the bottom surface. The log mean temperature difference is defined as:

$$\Delta T_{lm} = \frac{\left(T_s - T_{air,o}\right) - \left(T_s - T_{air,i}\right)}{ln\frac{\left(T_s - T_{air,o}\right)}{\left(T_s - T_{air,i}\right)}} \tag{5.6}$$

where T_s is either the soil or the slab temperature.

The cross-sectional area of each channel is 0.0077m^2 and the conductance of the rigid insulation under the slab ( ) is 0.59 W/(m^2 ·K). The air velocity (m/s) in each channel (V_{air}) was calculated with the correlation presented by Chen (2009, p. 95) using the air flow data at the inlet of the slab. The following equation presents this correlation for International Standard units where Q is the volumetric flow rate in m^3/s.

$$Q = V_{air} \times 0.148 \tag{5.7}$$

The convective heat transfer coefficient inside the channels (h_{c_vcs}) was also determined using a correlation Chen derived from a site test (Y. Chen, 2009, p. 104):

$$h_{c\_vcs} = 3.94 \cdot V_{air} + 5.45 \tag{5.8}$$

The soil temperature was assumed uniform under the ventilated concrete slab. The concrete temperature surrounding the channels was also considered uniform over the slab area. Based on Chen's observations, the temperature difference between the top surface and the layer of the slab at the channel level is negligible (less than 0.5 °C difference). Therefore, the previous time-step temperature calculated with the linear model of the slab was fed as input in order to solve the system of equations and identify the exit temperature of the air stream in each control volume.

The air heat exchange in the entry or exit manifold were not modeled. It was assumed however, based on the analysis of the recorded sensor data, that the inlet air temperature of the first channel was 2°C inferior to the slab air inlet ($T_{in,vcs}$) drawn from the roof manifold and that the inlet temperature difference between the first and last (19th)

channel was 5°C. The VCS outlet air temperature, ($T_{out,vcs}$), was calculated assuming a perfect air mix across the outlet manifold of the channel network embedded in the slab.

Finally, the total heat transfer from the air to the concrete (Δq_{air}) was calculated using:

$$\Delta q_{air} = \dot{m}_{air}\, Cp_{air} (T_{in,vcs} - T_{out,vcs}) \tag{5.9}$$

This value includes the losses to the ground and the losses (absorption) to the concrete of the slab. It corresponds to the active charging input of the VCS surface temperature linear model, i.e. the input of $G_{BIPV/T}$.

5.3 Simulations

The simulations were completed using Simulink as presented in Figure 5.5. The inputs (left) are signals created with Ecoterra™ sensor data for the selected period of days. The main modeling blocks are presented.

The following analyses were completed using monitored data from the month of March 2009. This restriction is forced by the inherent characteristics of the parametric linear model developed for this thesis (Chapter 3). The data from March 4th 2009 was used.

The simulations allowed verifying the heat storage capacity of the ventilated concrete slab when it receives heated air from different BIPV/T roof designs. The baseline BIPV/T roof construction considered for comparison is the actual Ecoterra™ roof having a 30° tilt and fully covered with photovoltaic panels.

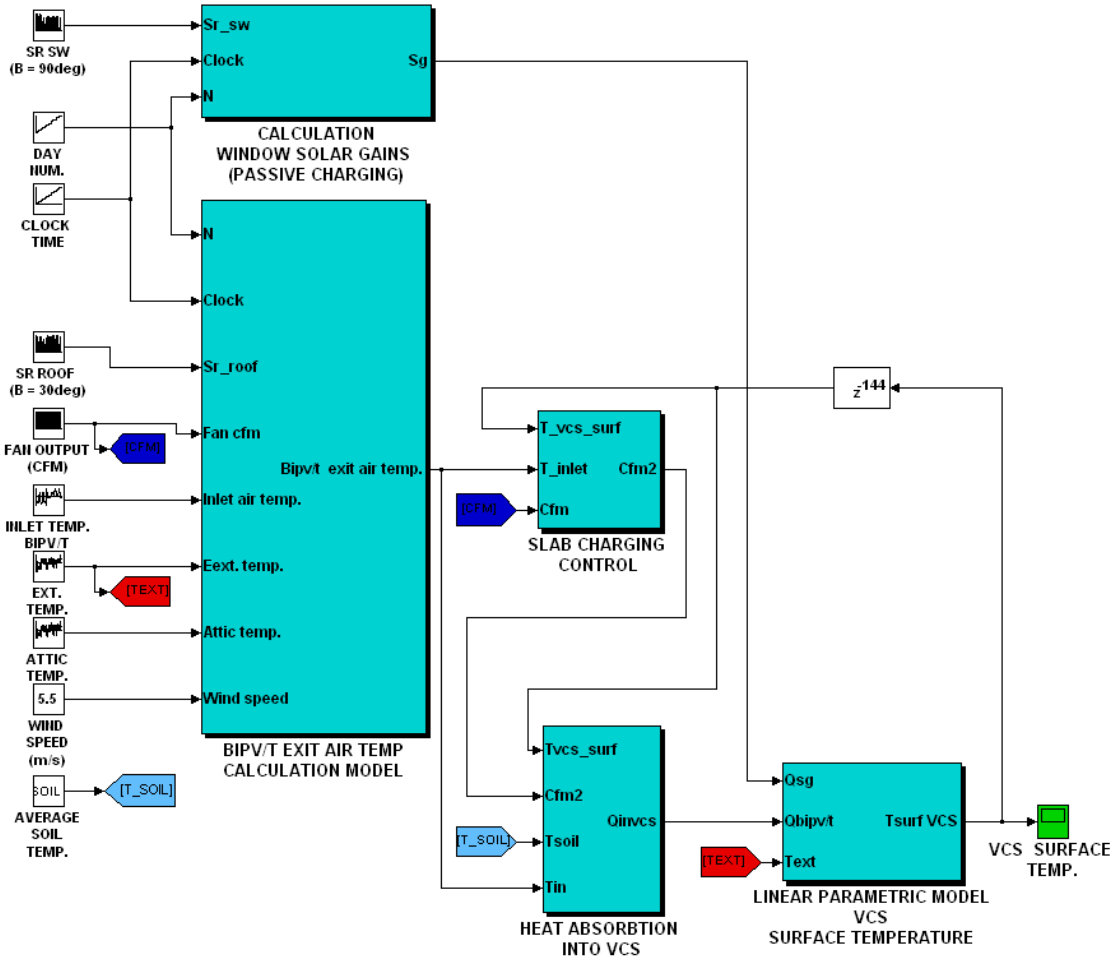

Figure 5.5: Simulink model used for BIPV/T–VCS system configuration evaluations.

5.3.1 BIPV/T Roof Exit Air Temperature

The impact of the roof design on the air temperature at the exit manifold of the BIPV/T roof was studied for one day in March. Figure 5.6 shows the exit air temperature for each BIPV/T roof configuration along with the corresponding global horizontal solar irradiance and exterior temperature for March 4th 2009. Results confirmed that the addition of a glazing section is highly beneficial. The exit air temperature is significantly increased when a glazing section is integrated in the BIPV/T roof construction. The simulation results show that the exit air temperature can be increased by 12°C when a glazing section is added. The vertical inclination of the glazing section has no significant

thermal impact. Moreover, the simple increase of the roof tilt from 30° to 45° does not provide any significant thermal benefits when this end-of-winter sunny period is considered.

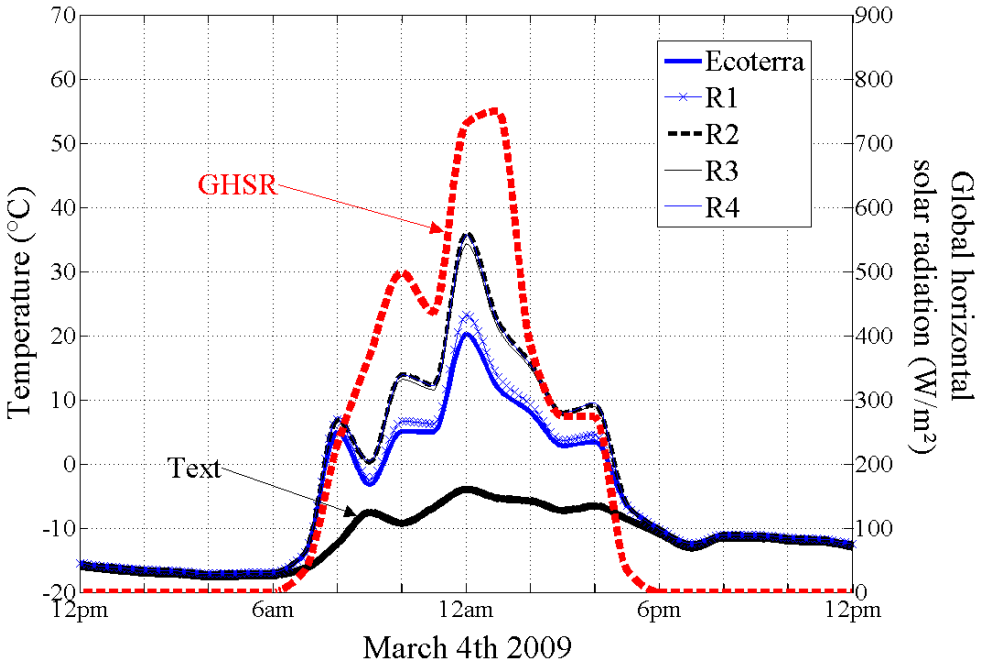

Figure 5.6: Exit air temperature for the each BIPV/T roof configuration, global horizontal solar radiation and exterior temperature.

As designs R2, R3 and R4 provided similar BIPV/T roof exit air temperatures and were those providing the highest temperatures, R4 only was kept as an example for the following analysis.

5.3.2 Ventilated Concrete Slab Heat Absorption

The most important role of the ventilated concrete slab is to store and release thermal energy, at a desirable rate, in order to reduce the need for space heating. Using the BIPV/T simulation outputs, the amount of thermal energy collected by the BIPV/T roof and the electricity generated by the PV panels were calculated for design R4 and the actual Ecoterra™ roof for the day of March 4th 2009. These quantities were calculated

with equation (5.10) and equation (5.11). The efficiency of the photovoltaic panels used for these calculations (PV_{eff}), 5.15%, was chosen according calculations performed by Doiron (2011, p. 92). In this case, it is assumed that the complete effective area of the BIPV/T roof, excluding the glazing section, is covered with PV panels.

$$\dot{Q}_{coll} = \dot{m}_{air}\, c_{p,air} \rho_{air} (T_{outlet,bipv/t} - T_{ext}) \tag{5.10}$$

$$\dot{Q}_{elect} = PV_{eff} G_{tot,roof} \tag{5.11}$$

The u_1 transfer function ($G_{BIPV/T}$) from the VCS polynomial model was used to calculate the amount of energy available for storage and the amount of energy that can actually be stored in the ventilated slab. These two quantities were calculated according to equations (5.12) and (5.13):

$$\dot{Q}_{avail,stor} = \dot{m}_{air} \cdot c_{p,air} \cdot \rho_{air} \cdot (T_{outlet,bipv/t} - T_{VCS.surf}) \tag{5.12}$$

$$Q_{stored,VCS} = \rho_{conc} \cdot V_{tot,conc} \cdot c_{p,conc} \cdot \Delta T_{surf,VCS} \tag{5.13}$$

where $\Delta T_{surf,VCS}$ is the difference between the lowest and peak surface temperatures on the VCS surface temperature fluctuation curve (Figure 5.8) for the active charging input (u_1). This curve was obtained by using the transfer function $G_{BIPV/T}$. The next values were used for the variables of the equations.

	Symbol	Value
Specific heat of air at atmospheric pressure, 300K	$c_{p,air}$	1007 $J/kg \cdot K$
Density of air at atmospheric pressure, 300K	ρ_{air}	1.16 kg/m^3
Specific heat of concrete	$c_{p,conc}$	900 $J/kg \cdot K$
Total volume of concrete in VCS	$V_{tot,conc}$	5 m^3
Density of concrete, 300K	ρ_{conc}	2300 kg/m^3

Table 5.1 : Values and properties used in the BIPV/T and VCS energy calculations.

The results of these calculations for March 4th 2009 are presented on Figure 5.7. It can be observed that the amount of thermal energy collected by BIPV/T design R4 is approximately twice the amount collected by the Ecoterra™ roof. The same observation can be done for the thermal energy available for storage into the VCS.

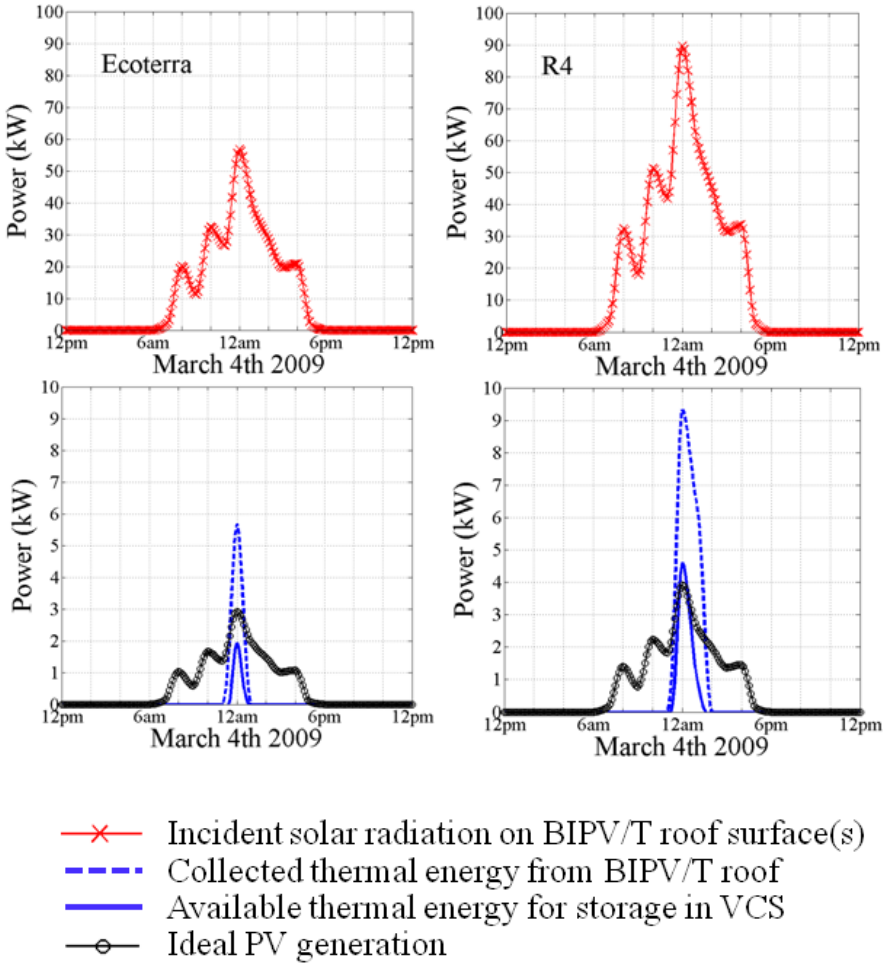

Figure 5.7: Energy graph for the actual BIPV/T roof of the Ecoterra™ house and design R4 (March 4th 2009).

The daily amounts of each of the energy variables presented previously are summarized in Table 5.2. The simulation results showed that it is possible to collect 175% more thermal energy with design R4 when the actual Ecoterra™ BIPV/T roof is used for comparison. Moreover, it allows to store 183% more energy in the slab than the actual BIPV/T roof configuration when its current state of charge is considered.

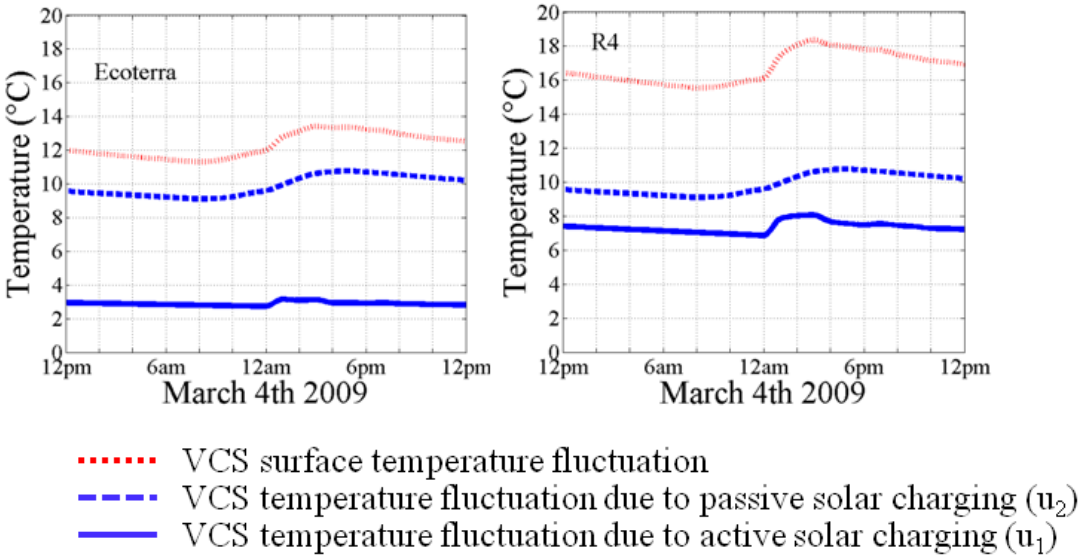

Figure 5.8: Simulated ventilated concrete slab surface temperature fluctuation for the actual BIPV/T roof of the Ecoterra™ house and BIPV/T roof design R4 (March 4th 2009).

	Ecoterra™	BIPV/T Design R4
Incident Solar Radiation on BIPV/T roof surface(s)	257.8 kWh	409.9 kWh
Ideal Electricity Production (PV eff : 5.15 %)	13.3 kWh	17.9 kWh
Thermal Energy Collected	5.7 kWh	15.7 kWh
Thermal Energy Available for Storage	1.9 kWh	5.6 kWh
Energy Stored in the Slab	1.2 kWh	3.4 kWh

Table 5.2: BIPV/T roof energy production and ventilated concrete slab energy storage for the actual Ecoterra™ roof and studied design R4 (March 4th 2009).

Furthermore, the daily heat storage numbers obtained using the VCS polynomial model allowed to determine that the percentage of heat collected from the BIPV/T roof effectively stored in the slab is approximately 22%. This fraction is the same for design R4 and the BIPV/T roof of Ecoterra™. It can also be observed on Figure 5.8 that the passive solar gains (u_2) are responsible for a 2°C surface temperature increase.

5.4 Conclusion

This chapter presented a study in which the ventilated concrete slab surface temperature parametric linear model was used to analyse its thermal performance when it is coupled with different BIPV/T roof designs.

The data recorded by the sensors of the house for one day in March 2009 were used by different calculation sub-models in order to feed the linear parametric model with the correct inputs and subsequently evaluate the VCS surface temperature response to active solar heat injection from different PV/T roof configurations.

It has been verified that the BIPV/T roof designs that include a tilted glazing section are the best configurations for thermal energy collection and storage into the ventilated concrete slab. Simulation results showed that design R4 allowed storing 3.4 kWh of heat into the VCS for the day of March 4th2009. Simulations demonstrated that a much lower amount, 1.2 kWh, could be stored when the actual BIPV/T roof configuration of Ecoterra™ is considered.

It was demonstrated that the linear data-driven model developed for the VCS storage system is a useful and simple tool for thermal evaluations when such system is connected to active solar systems such as a BIPV/T roof. It was also verified that its level of resolution and the assumption of linearity were adequate for residential thermal storage studies.

The speed of the thermal simulations performed using the linear data-driven model developed for the VCS storage system nor the amount of computation time saved with respect to building detailed simulations were studied. However, it was demonstrated

that the transfer functions of the model allow quick and valuable thermal comparisons to assist the decision-making process in the case of redesign studies. It is a more efficient and quicker alternative to whole building detailed simulations, particularly for comparing design and operation options on a relative basis.

6 CONCLUSION

This thesis demonstrates the development of system identification methodology to identify a linear data-driven model for an active/passive solar thermal energy storage system. This system was a ventilated concrete slab (VCS) located in the south portion of the basement of an energy efficient solar house. A statistical regression approach and the System Identification Toolbox of MATLAB were used to obtain the mathematical description (i.e. dynamic model) of the TES system.

The dynamic model has three inputs and one output. The three inputs include the heat absorbed by the VCS mass when solar-heated air (from BIPV/T roof) is flowing through the embedded channels (u_1), the solar gains transmitted through the basement south windows (u_2), and the exterior ambient temperature (u_3). The output of the system is the surface temperature of the slab (y). The most important input on which this study was focused is the solar heat input from the BIPV/T system.

The data recorded by the Ecoterra™ monitoring system was used to create data sets for the system identification process. The parametric model was identified without restricting the parameter values or enforcing any physical information about the nature of system. Linearity and parameter number reduction were the mandatory goals to respect during the system identification process.

Apart from the mathematical validation, a subsequent validation was performed considering the physical nature of the VCS system. A sensitivity analysis was also conducted in order to determine the effect of the accuracies of the monitoring sensors on determining the model parameters. Furthermore, the limitations restricting the use of this

model were addressed. They were the model's season dependency, the addition of floor coverage material on the VCS, and the combined operation of an auxiliary heating device.

Finally, the model was used to evaluate the thermal performance of the VCS when it is coupled with a different BIPV/T roof with different configurations. The evaluated configurations considered the effect of increasing the Ecoterra™ BIPV/T roof tilt to 45° and including an additional glazing section.

Based on the work done for this thesis, important conclusions can be drawn:

1. A methodology was developed to enable the identification of a parametric model of the VCS system with 17 parameters. This model was estimated and validated using monitored data. The statistical regression approach was used to identify this model. Its number of parameters can be considered low as compared to the quantity of parameters required when similar building system models are created with detailed energy simulation tools.
2. The linear parametric data-driven model was confirmed to be an efficient tool to compare design and operation options on a relative basis. Comparative results can be easily obtained with this model when different solar thermal system design options are analysed in the context of redesign studies.
3. The mathematical and physical validations of this model have proven that black-box statistical system identification procedures cannot be totally executed by an automatic application. They require an adequate selection of polynomial model family, order and delay. Furthermore, the insight into the system application characteristics cannot be ignored.

4. The identified parametric model for the VCS surface temperature was linear. The validation process proved that the linear assumption made during the system identification procedure was reasonable. This confirmed that the inherent linear thermal processes of the VCS system are dominant.
5. The relative weight of the three inputs of the VCS system on the surface temperature response was compared. Inputs u_1 and u_2 were confirmed to be the most important contributors to the increase of the concrete surface temperature. It was found that the exterior temperature input (u_3) has very little impact on the fluctuation and total temperature response of the slab. This means that the exterior temperature has a negligible effect on the performance of TES systems in well-insulated energy efficient solar houses having a high air-tightness.
6. Based on the results of the sensitivity analysis, it was determined that the accuracy of the monitoring sensors does not have a significant impact on the value of the identified model parameters or on the simulation results when the model is used to carry out thermal evaluations.
7. Different BIPV/T roof configurations for the Ecoterra™ house were compared based on their active thermal charging capacity when they are coupled to the ventilated concrete slab. The ventilated concrete slab linear parametric model identified in thesis was employed for the thermal simulations. It was found that, for days with cold exterior temperatures and high quantities of solar radiation available, the amount of energy stored in the concrete is significantly augmented when the BIPV/T roof configuration includes a clearly glazed section. On the

other hand, it was found that changing the roof tilt does not significantly increase the amount of energy that can be stored in the VCS during the same period.

8. The system identification procedure was completed using the System Identification Toolbox of MATLAB. The work accomplished in this thesis confirmed that this tool is practical, effective and has the functionalities required to guide the user towards the development of sound data-driven models of thermo-active building systems such as the ventilated concrete slab.

6.1 Summary of Contributions

The main contributions of the work presented in this thesis are summarized as follows:

1. Study of two strongly coupled systems, a solar active system and an active/passive solar thermal storage system, using the linear system theory. Good results were obtained with a relatively simple models and the use of whole building simulation tools was not necessary. The developed model can ease the design of control strategies and the design and operation of integrated solar systems. This developed methodology can be applied to other solar buildings.
2. Mathematical validation of the data-driven model using an independent data set. The validity of the model was confirmed considering the fit of the model output with the validation data and the quality of the residuals. The stability of the model was corroborated while analyzing its poles and zeros.
3. Physical validation of the data-driven model by taking in consideration the inherent nature of the ventilated concrete slab dynamic system. This was completed by analyzing the coupling between the system inputs and their

respective response using the transfer function form of the VCS surface temperature model.

4. Utilization of a data-driven parametric linear model to assess the thermal performance of a ventilated concrete slab system when it is coupled to an active solar system (e.g. BIPV/T roof). The effect of modifying the BIPV/T roof angle and including a glazing section are analyzed and discussed, demonstrating the use of the identified transfer function model of the VCS as a more efficient and quicker alternative to whole building detailed simulations, particularly for comparing design and operation options on a relative basis.
5. Sensitivity analysis in regards to the effects of the measurement device accuracy on the identification of the data-driven ARX model parameters.
6. Identification of the limitations of the model use related to seasons, ventilated concrete slab cover and combined operation of auxiliary heating devices.

6.2 Recommendations for Future Works

Based on the findings of this thesis, some ideas are suggested for future studies as follows.

1. Active solar charging, passive solar charging and exterior temperature were the three significant inputs selected for the identification of a model for the ventilated concrete slab. However, it appeared evident that the exterior temperature has very little impact on its surface temperature. Therefore, future system identification efforts should be conducted in order to verify if this input could be discarded. The influencing inputs would then be restricted to active and passive solar charging.

2. This thesis focused on the thermal behaviour of the ventilated concrete slab during solar dominated periods. An exploration of the system identification possibilities for the remaining part of the heating season would be a challenging study to conduct. It would then be interesting to verify if the assumption of VCS dynamic system linearity would still hold up for other house operation conditions.
3. It would be interesting to evaluate if the active and passive charging inputs could be transformed respectively into a controllable input and a measured disturbance. The BIPV/T fan flow rate could replace the input of active energy injection into the VCS. This would open the door for interesting model predictive control studies allowing the VCS to reach an optimal efficiency while controlling the surface temperature to remain within comfort limits.
4. A sensitivity analysis of the impact of the VCS physical properties on the parameters of the identified model should be conducted using a similar black-box system identification approach. These could include the concrete properties, the slab dimensions, and the ventilation channel configuration (number and form). This would potentially be linked to a system identification study exploring the possibilities of integrating some physical knowledge into the identification procedure. Gray-box models could then be obtained. These potential parametric models would become valuable tools for TES design analysis.
5. The work included in this thesis allowed the identification of a discrete-time mathematical model of an active/passive thermal storage system. The system identification methodology developed could be further improved to study its high

frequency thermal dynamic phenomena through continuous-time modelling and continuous-time simulations.

6. This thesis focused only on the BIPV/T-VCS system of the Ecoterra™ house. However, considering the large quantity of data still available and the robustness of the modeling methodology presented in this thesis, it would be interesting to look at the Ecoterra™ house as a dynamic system by itself. For example, the possibility to create a simple model of the house net energy load response to major climate variables could be investigated. Models of this kind could eventually help utilities to improve their load management strategies.
7. The experimental costs of the data-driven system identification methodology presented were not appreciation criteria for this thesis. However, they will become a decisive factor when it will be applied to real building projects. Therefore, this system identification methodology should be refined in order to allow its use with typically available data in high performance buildings while keeping its accuracy intact.

7 REFERENCES

American Society of Heating, Refrigerating and Air-Conditioning Engineers. *(2005). ASHRAE Handbook Fundamentals.* Atlanta, GA.

Åström, K. J., & Eykhoff, P. (1971). System identification-A survey. *Automatica*, *7*(2), 123–162.

Athienitis, A. K. (1997). Investigation of thermal performance of a passive solar building with floor radiant heating. *Solar Energy*, *61*(5), 337–345.

Athienitis, A. K. (2007). Design of a Solar Home with BIPV-Thermal System and Ground-Source Heat Pump. Presented at the 2 nd Canadian Solar Buildings Conference, Calgary.

Athienitis, A. K., & Chen, Y. (2000). The effect of solar radiation on dynamic thermal performance of floor heating systems. *Solar Energy*, *69*(3), 229–237.

Athienitis, A. K., & Santamouris, M. (2002). *Thermal analysis and design of passive solar buildings* (James & James.). London.

Athienitis, A. K., Stylianou, M., & Shou, J. (1990). A methodology for building thermal dynamics studies and control applications. *ASHRAE Transactions*, *96*(2), 839–848.

Barton, P., Beggs, C. B., & Sleigh, P. A. (2002). A theoretical study of the thermal performance of the TermoDeck hollow core slab system. *Applied Thermal Engineering*, *22*(13), 1485–1499.

Bekey, G. A. (1970). System identification- an introduction and a survey. *Simulation*, *15*(4), 151–166.

Braun, J., & Chaturvedi, N. (2002). An Inverse Gray-Box Model for Transient Building Load Prediction. *HVAC&R Research*, *8*(1), 73–99.

Candanedo, J. A. (2011). *A Study of Predictive Control strategies for Optimally Designed Solar Homes* (Ph.D. Thesis). Concordia University, Montréal.

Candanedo, J. A., Allard, A., & Athienitis, A. K. (2011). Predictive Control of Radiant Floor Heating and Transmitted Irradiance in a Room with High Solar Gains. *ASHRAE Transactions*, *117*(2), 652–665.

Candanedo, J. A., & Athienitis, A. K. (2011). Predictive control of radiant floor heating and solar-source heat pump operation in a solar house. *HVAC&R Research*, *17*(3), 235–256.

Candanedo, L. M. (2010). *Modelling and Evaluation of the Performance of Building Integrated Open Loop Airbased Photovoltaic/Thermal Systems* (Ph.D. Thesis). Concordia University.

Chae, Y. T., & Strand, R. K. (2013). Modeling ventilated slab systems using a hollow core slab: implementation in a whole building energy simulation program. *Energy and Buildings*, *57*, 165–175.

Chen, T. Y. (2001). Real-time predictive supervisory operation of building thermal systems with thermal mass. *Energy and Buildings*, *33*(2), 141–150.

Chen, T. Y. (2002). Application of adaptive predictive control to a floor heating system with a large thermal lag. *Energy and Buildings*, *34*(1), 45–51.

Chen, T. Y., & Athienitis, A. K. (2003). Investigation of practical issues in building thermal parameter estimation. *Building and Environment*, *38*(8), 1027–1038.

Chen, Y. (2009). *Modeling and design of a solar house with focus on a ventilated concrete slab coupled with a building-integrated photovoltaic/thermal system* (Master Thesis). Concordia University, Montreal.

Chen, Y., Athienitis, A. K., & Galal, K. (2010). Modeling, design and thermal performance of a BIPV/T system thermally coupled with a ventilated concrete slab in a low energy solar house: Part 1, BIPV/T system and house energy concept. *Solar Energy*, *84*(11), 1892–1907.

Corgnati, S. P., & Kindinis, A. (2007). Thermal mass activation by hollow core slab coupled with night ventilation to reduce summer cooling loads. *Building and Environment*, *42*(9), 3285–3297.

Crawley, D. B., Hand, J. W., Kummert, M., & Griffith, B. T. (2008). Contrasting the capabilities of building energy performance simulation programs. *Building and Environment*, *43*(4), 661–673.

Dewson, T., Day, B., & Irving, A. D. (1993). Least squares parameter estimation of a reduced order thermal model of an experimental building. *Building and Environment*, *28*(2), 127–137.

Dodier, R. H., & Henze, G. P. (2004). Statistical Analysis of Neural Networks as Applied to Building Energy Prediction. *Journal of Solar Energy Engineering*, *126*(1), 592.

Doiron, M. (2011). *WholeBuilding Energy Analysis and Lessons Learned for a Near NetZero Energy Solar House* (Master Thesis). Concordia University, Montreal.

Doiron, M., O'Brien, W., & Athienitis, A. K. (2011). Energy Performance, Comfort and Lessons Learned From a Near Net-Zero Energy Solar House. *ASHRAE Transactions*, *117*(2), 585–596.

Duffie, J. A., & Beckman, W. A. (1980). *Solar Engineering of Thermal Processes* (Second Edition.). John Wiley & Sons, Inc.

Haberl, J. S., & Thamilseran, S. (1998). The Great Energy Predictor Shootout II - Measuring Retrofit Savings. *ASHRAE Journal*, 49–56.

Henze, G. P., Felsmann, C., Kalz, D. E., & Herkel, S. (2008). Primary energy and comfort performance of ventilation assisted thermo-active building systems in continental climates. *Energy and Buildings*, *40*(2), 99–111.

Holcomb, D., Li, W., & Seshia, S. (2009). *Algorithms for Green Buildings: Learning-Based Techniques for Energy Prediction and Fault Diagnosis* (No. Technical Report No. UCB/EECS-2009-138). University of California at Berkeley.

Kalogirou, S. (2000). Artificial neural networks for the prediction of the energy consumption of a passive solar building. *Energy*, *25*(5), 479–491.

Kalogirou, S. (2001). Artificial neural networks in renewable energy systems applications: a review. *Renewable and Sustainable Energy Reviews*, *5*(4), 373–401.

Katipamula, S. (1996). Great Energy Predictor Shootout II: Modeling Energy Use in Large Commercial Buildings. *ASHRAE Transactions*, *102*, 397–404.

Kumar, S., Sinha, S., Kojima, T., & Yoshida, H. (2001). Development of parameter based fault detection and diagnosis technique for energy efficient building management system. *Energy Conversion and Management*, *42*(7), 833–854.

Kummert, M., André, P., & Argiriou, A. A. (2006). Comparing Control Strategies Using Experimental and Simulation Results: Methodology and Application to Heating Control of Passive Solar Buildings. *HVAC&R Research*, *12*(3a), 715 – 737.

Lachal, B., Weber, W. U., & Guisan, O. (1992). Simplified methods for the thermal analysis of multifamily and administrative buildings, pp. 1151–1159. GA (USA).

Ljung, L. (2009). *System identification: theory for the user* (2nd ed.). Upper Saddle River, NJ: Prentice Hall PTR.

Ljung, Lennart. (2010). Perspectives on system identification. *Annual Reviews in Control*, *34*(1), 1–12.

Monfet, D., Charneux, R., Zmeureanu, R., & Lemire, N. (2009). Calibration of a Building Energy Model Using Measured Data. *ASHRAE Transactions*, *115*(1), 348–359.

Myhren, J., & Holmberg, S. (2008). Flow patterns and thermal comfort in a room with panel, floor and wall heating. *Energy and Buildings*, *40*(4), 524–536.

O'Brien, W. (2011). *Development of a Solar House Design Methodology and its Implementation into a Design Tool* (Ph.D. Thesis). Concordia University, Montreal.

Olesen, B. W. (2002). Radiant Floor heating. In theory and Practice. *ASHRAE Journal*, *44*(7), 19–26.

Peitsman, H. C., & Soethout, L. L. (1997). ARX models and real-time model-based diagnosis. *ASHRAE Transactions*, *103*(1), 657–671.

Ren, M. J., & Wright, J. A. (1998). A ventilated slab thermal storage system model. *Building and Environment*, *33*(1), 43–52.

Sattari, S., & Farhanieh, B. (2006). A parametric study on radiant floor heating system performance. *Renewable Energy*, *31*(10), 1617–1626.

Wang, S., & Xu, . (2006a). Simplified building model for transient thermal performance estimation using GA-based parameter identification. *International Journal of Thermal Sciences*, *45*, 419–432.

Wang, S., & Xu, X. (2006b). Parameter estimation of internal thermal mass of building dynamic models using genetic algorithm. *Energy Conversion and Management*, *47*(13-14), 1927–1941.

Weitzmann, P., Kragh, J., Roots, P., & Svendsen, S. (2005). Modelling floor heating systems using a validated two-dimensional ground-coupled numerical model. *Building and Environment*, *40*(2), 153–163.

Wen, J., & Smith, T. F. (2003). Development and Validation of Online Parameter Estimation for HVAC Systems. *Journal of Solar Energy Engineering*, *125*(3), 324.

Winwood, R., Benstead, R., Edwards, R., & Letherman, K. M. (1994). Building fabric thermal storage: Use of computational fluid dynamics for modelling. *Building Services Engineering Research and Technology*, *15*(3), 171–178.

Yang, J., Rivard, H., & Zmeureanu, R. (2005). On-line building energy prediction using adaptive artificial neural networks. *Energy and Buildings*, *37*(12), 1250–1259.

Zmeureanu, R., & Fazio, P. (1988). Thermal performance of a hollow core concrete floor system for passive cooling. *Building and Environment*, *23*(3), 243–252.

Zouak, M., & Mechaqrane, A. (2004). A comparison of linear and neural network ARX models applied to a prediction of the indoor temperature of a building. *Neural Computing & Applications*, *13*(1), 32–37.

8 APPENDICES

APPENDIX I

Monitored Data from the Ecoterra™ House used in this Thesis

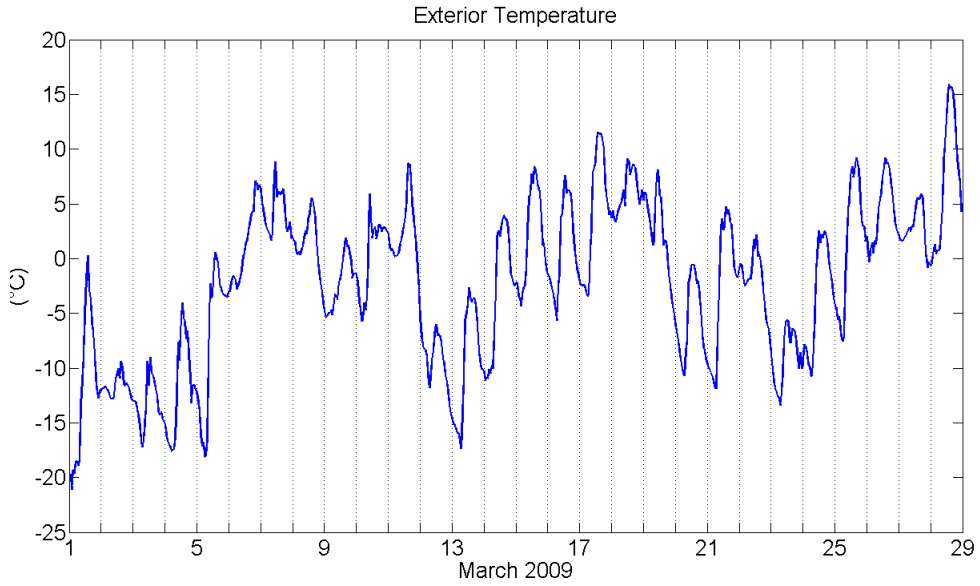

Figure I.1: Exterior temperature data recorded between March 1st 2009 and March 28th 2009.

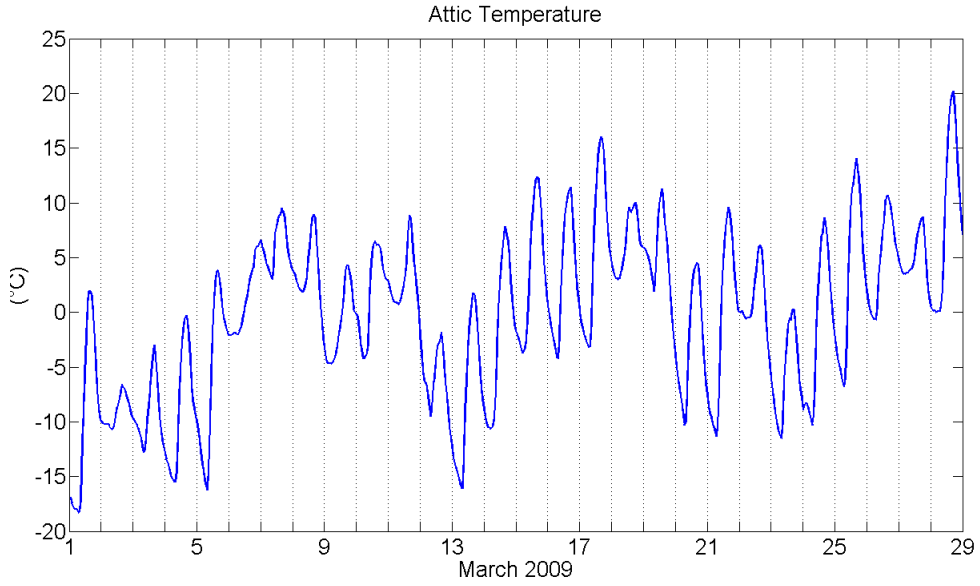

Figure I.2: Attic temperature data recorded between March 1st 2009 and March 28th 2009.

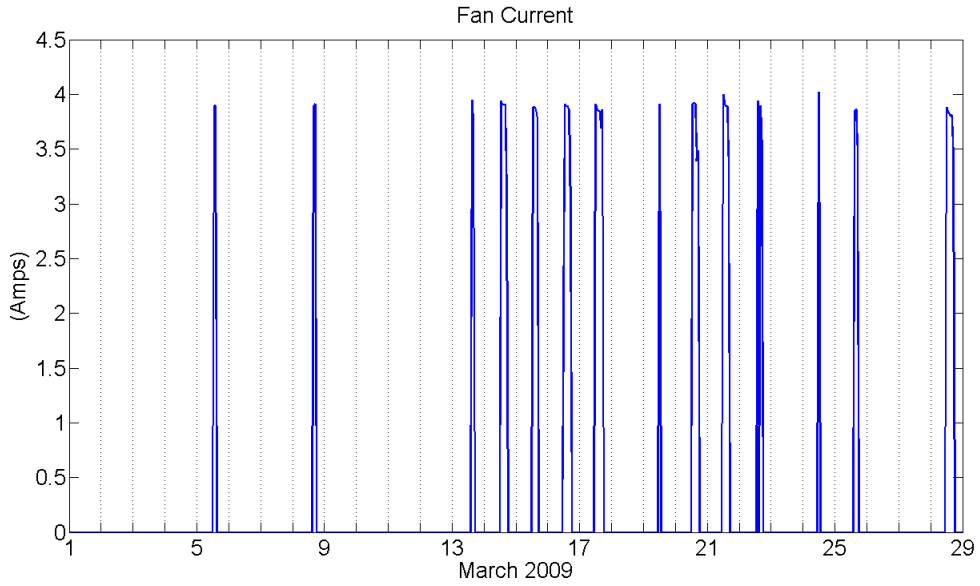

Figure I.3: Fan current data recorded between March 1st 2009 and March 28th 2009.

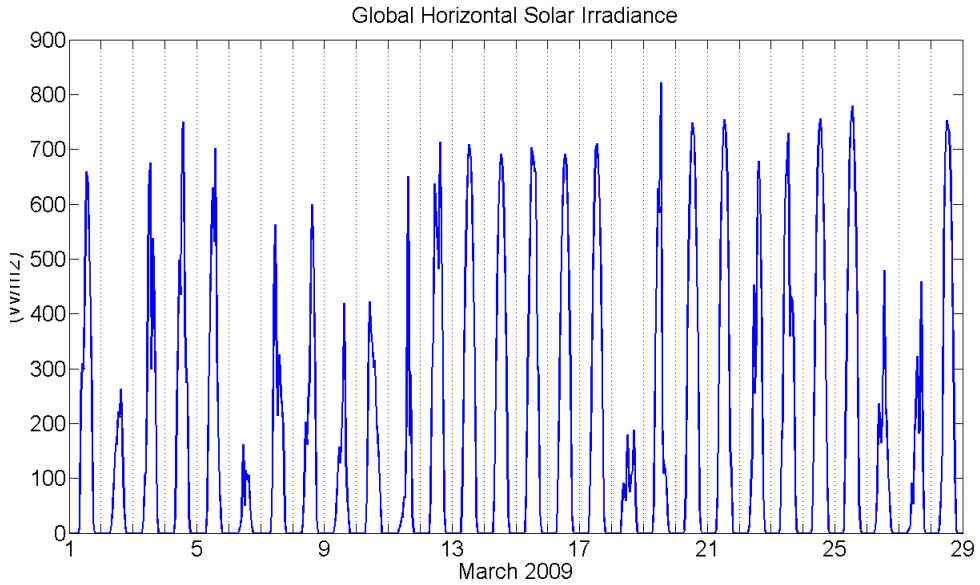

Figure I.4: Global horizontal solar irradiance data recorded between March 1st 2009 and March 28th 2009.

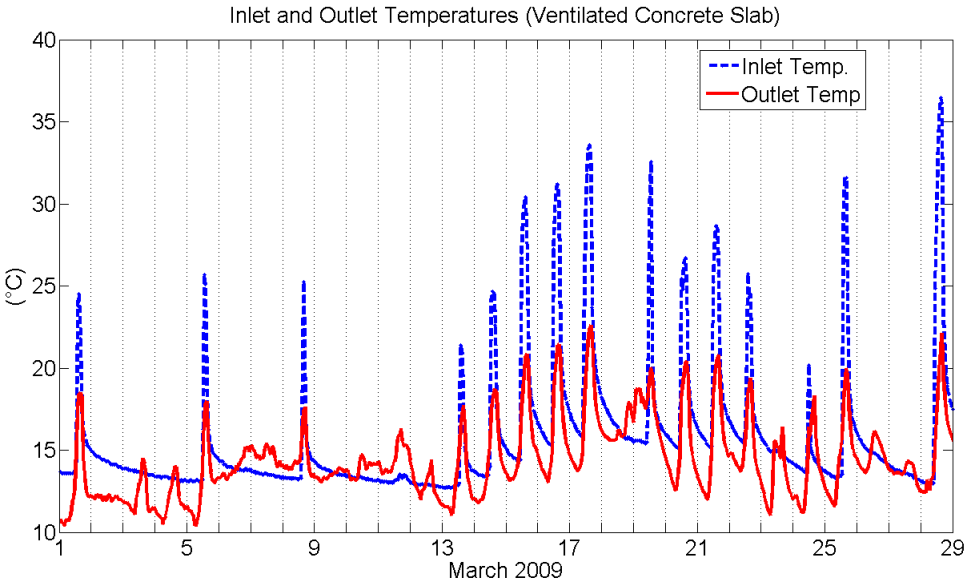

Figure I.5: VCS inlet and outlet temperature data (manifolds) recorded between March 1st 2009 and March 28th 2009.

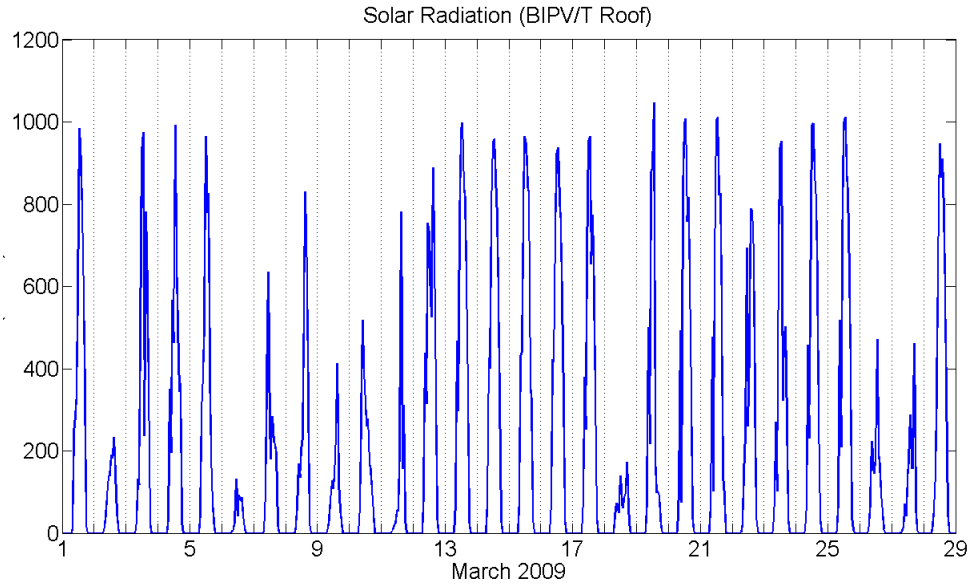

Figure I.6: Roof solar radiation data recorded between March 1st 2009 and March 28th.

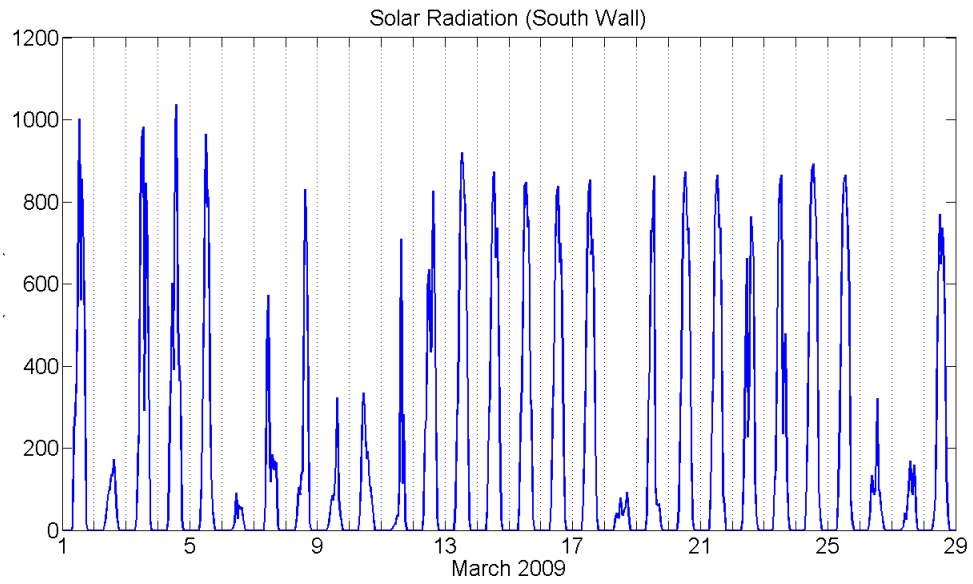

Figure I.7: South wall solar radiation data recorded between March 1st 2009 and March 28th.

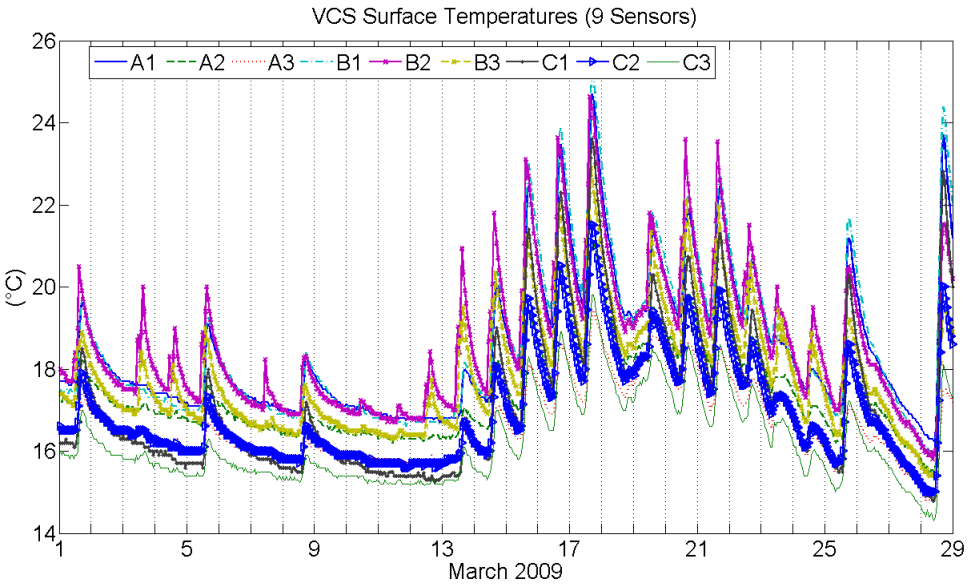

Figure I.8: VCS surface temperature data (9 sensors) recorded between March 1st 2009 and March 28th.

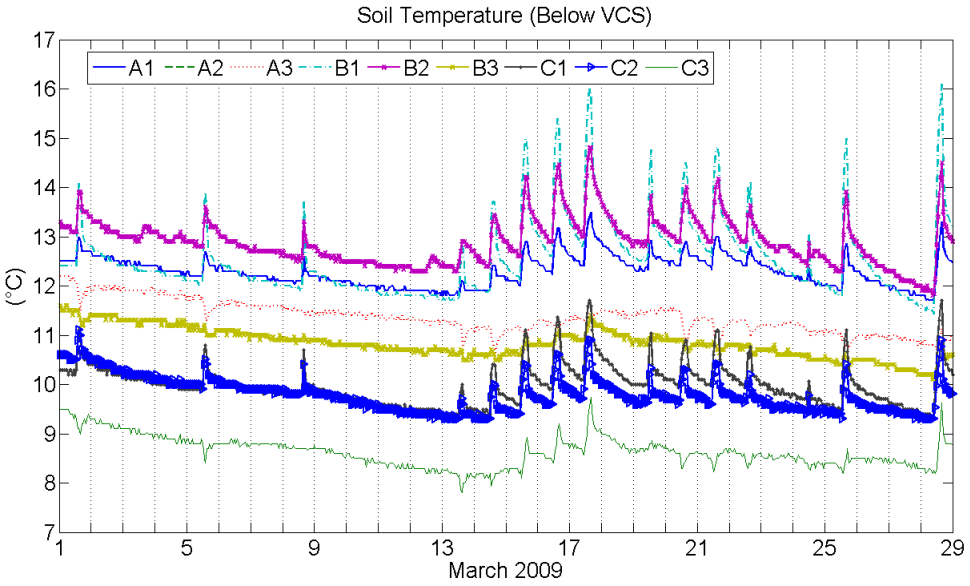

Figure I.9: Ground temperature data (9 sensors) recorded between March 1st 2009 and March 28th.

APPENDIX II

Relevant Ecoterra™ House Drawings

10309

LES MAISONS ALOUETTE HOMES
TEL: (450) 539-3100

Rev:	Date:	Description:	D. V.
	06/11/15	PRELIMINARY PLAN	AL.
	06/12/15	SIGNED PLAN	AL.
	07/06/14	2e SIGNED PLAN	AL.

Representative / Représentant:
ALOUETTE

Project / Projet:
07-0015

Scale / Échelle:
1/4" = 1'-0"

Customer(s) / Client(s):
ECOTERRA ALOUETTE HOUSE

Title / Titre:
FRONT ELEVATION

3
Of / De

FLOOR HEATING SLAB DETAIL

Normal Density plain concrete 4" over steel deck(25 mps with stone 14mm)
Steel Deck (Canam p-2436, galvanized steel)
Ventilation Channel (cavity)
Regular expanded metal
1 7/8" Rigid insulation scealed with acoustique scealan
Polythene
Stone 3/4"

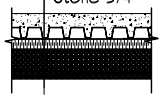

SIDE VIEW FLOOR HEATING

FLOOR HEATING SLAB DETAIL

Normal Density plain concrete 7"
Regular expanded metal
7" x 20" Manifold
Polythene
3" Rigid insulation scealed with acoustique scealant

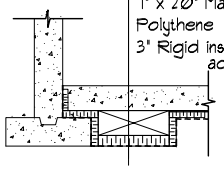

FRONT VIEW FLOOR HEATING

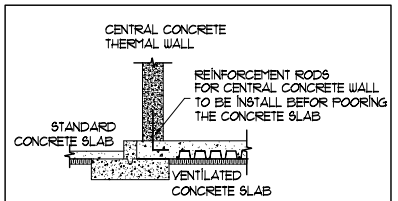

CONCRETE WALL REINFORCEMENT

10309

Rev:	Date:	Description:	D.	V.
	07/07/05	ADD DETAIL REINFORCEMENT CONCRETE WALL	NL	NL
	07/08/13	2nd SIGNED PLAN	AL	NL
	07/08/13	ADD OPENING/CHANGE CONCRETE SLAB ELEV.	AL	AL
	07/08/20	HARDWOOD STAIR	AL	AL

LES MAISONS Alouette HOMES
TEL: (450) 539-3100

Representative / Representant: ALOUETTE
Scale / Echelle: 1/4" = 1'-0"
Project / Projet: 07-0015

Customer(s) / Client(s): ECOTERRA ALOUETTE HOUSE
Title / Titre: FOUNDATION

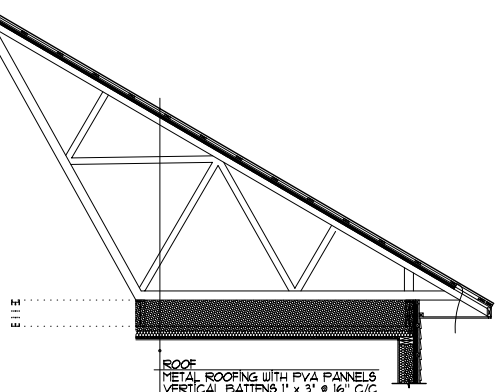

ROOF
METAL ROOFING WITH PVA PANNELS
VERTICAL BATTENS 1" x 3" @ 16" C/C
HORIZONTAL BATTENS 1" x 3" @ 16" C/C
2 TYVEK LAYERS (AIR EMANATIONS PROTECTION)
GRIP GARD APPLIED TO A WIDTH OF 3 FT
ALONG EAVES AND RAKES AND #30 FELT PAPER
APPLIED OVER BALANCE OF SURFACE AREA
15/32" ORIENTED STRAND BOARD (agency certified)
TRUSSES @ 24" c/c
1" BASF WALLTITE FOAM INSULATION (R-6) UNDER OSB
11" BASF ENERTITE INSULATION INSTALLED ON SITE (R-44)
2"x4" FALSE CEILING
2" BASF WALLTITE FOAM INSULATION (R-12)
BATTENS 1" X 3" @ 16" c/c
1/2" GYPSUM

ROOF SECTION (UNDER PVA)

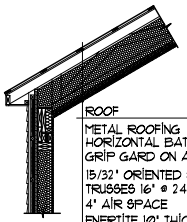

ROOF
METAL ROOFING
HORIZONTAL BATTENS 1" x 3" @ 16" C/C
GRIP GARD ON ALL ROOF, FINISHED ON SITE
15/32" ORIENTED STRAND BOARD (agency certified)
TRUSSES 16" @ 24" c/c
4" AIR SPACE
ENERTITE 10" THICK (R-40)
2" BASF WALLTITE FOAM INSULATION (R12.2)
BATTENS 1" X 3" @ 16" c/c
1/2" GYPSUM

CATHEDRAL DETAIL

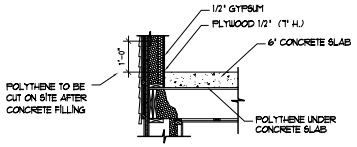

FIRST FLOOR CONCRETE SLAB DETAIL
(FAMILY ROOM)

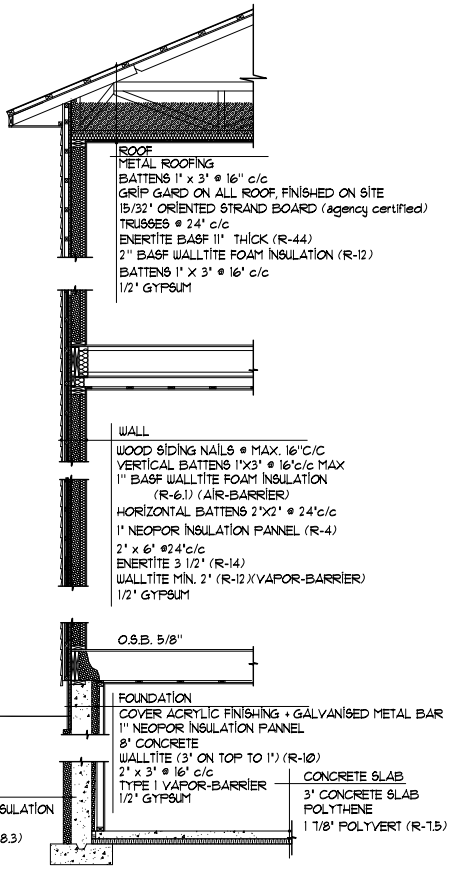

WALL SECTION

FLOOR HEATING SLAB DETAIL
Normal Density plain concrete 4" over
steel deck(25 mpa with stone 14mm)
Steel Deck (Canam p-2436, galvanized steel)
Ventilation Channel (cavity)
Regular expanded metal
1 7/8" Rigid insulation sealed with acoustique sealant
Polythene
Stone 3/4"

SIDE VIEW FLOOR HEATING

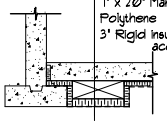

FLOOR HEATING SLAB DETAIL
Normal Density plain concrete 7"
Regular expanded metal
7" x 20" Manifold
Polythene
3" Rigid insulation sealed with
acoustique sealant

FRONT VIEW FLOOR HEATING

10309

Rev:	Date:	Description:	D.	V.
B-A-1	07/08/28	CHANGE FURRING ON EXT. WALLS	NL	
	07/08/13	1" NEOPOR + REMOVE UNIPX ON CONC. WALL	NL	
	2007/08/14	2e SIGNED PLAN	AL	
	2007/10/12	SPECIFIED STYROPORE INSULATION PANNEL	NL	

LES MAISONS ALOUETTE HOMES
TEL: (450) 539-3100

Representative / Representant:
ALOUETTE

Project / Projet:
07-0015

Scale / Echelle:
NO SCALE

Customer(s) / Client(s):
ECOTERRA ALOUETTE HOUSE

Title / Titre:
WALL SECTION & DETAILS

8

13
Of / De:

#10309

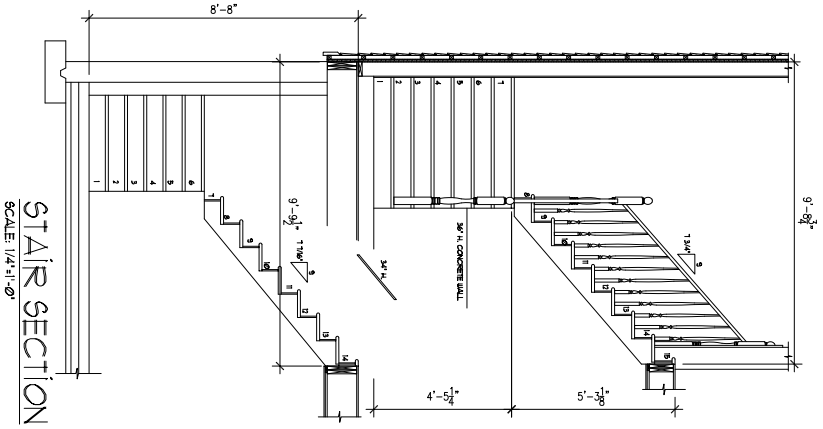

STAIR SECTION
SCALE: 1/4"=1'-0"

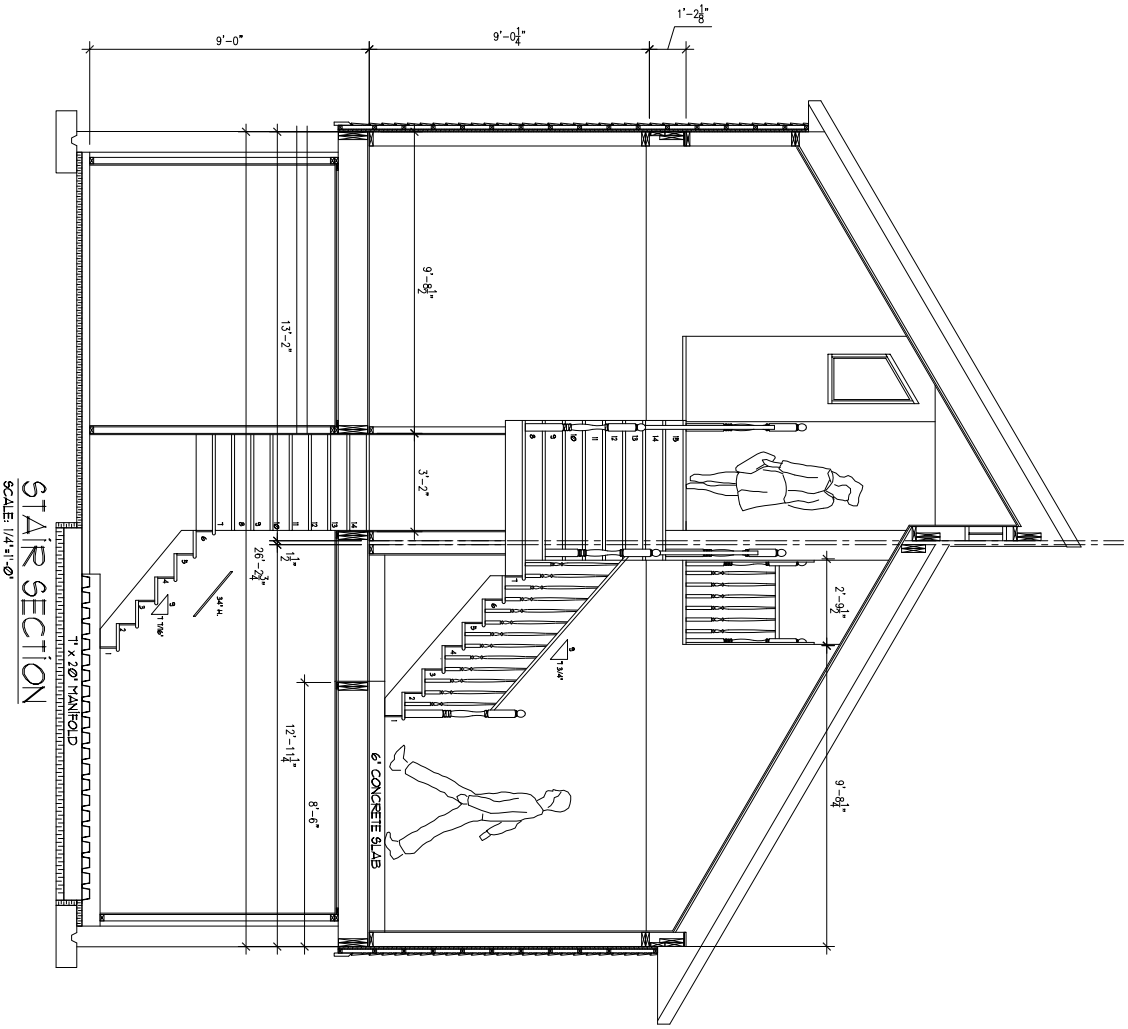

STAIR SECTION
SCALE: 1/4"=1'-0"

9	Customer(s) / Client(s): ECOTERRA ALOUETTE HOUSE	Representative / Representant: ALOUETTE		Rev:	Date:	Description:	D.	V.
	Title / Titre: STAIR SECTIONS	Scale / Echelle: 1/4" = 1'-0"	Project / Projet: 07-0015		07/07/12	ADJUST STAIR SECTION	AL	
13 of Pages					06/12/19	SIGNED PLAN	AL	
					07/06/14	2e SIGNED PLAN	AL	
					07/06/20	ADJUST RISER HEIGHT	AL	

LES MAISONS Almonte HOMES
TEL: (450) 539-3100

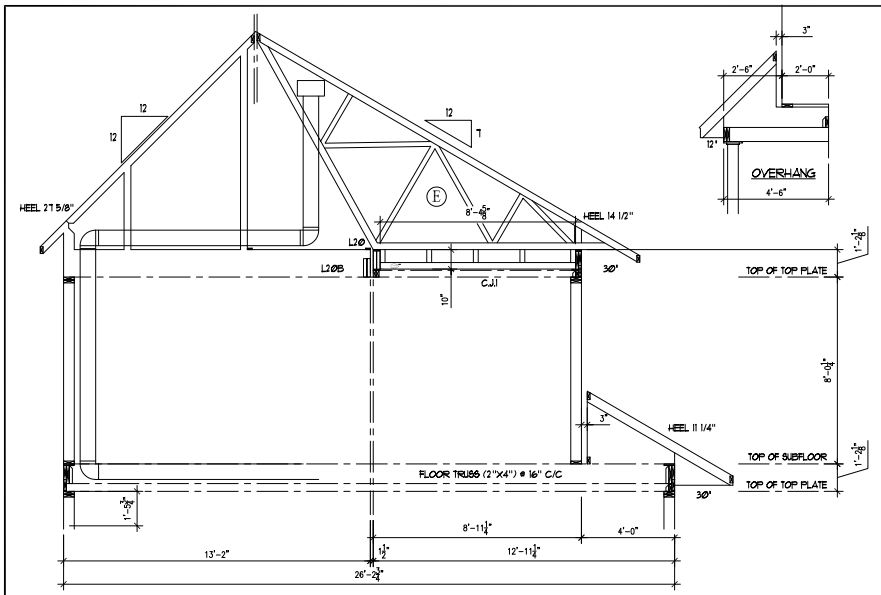

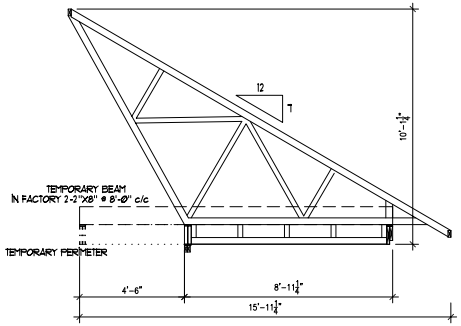

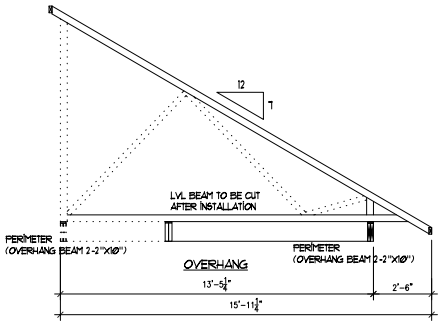

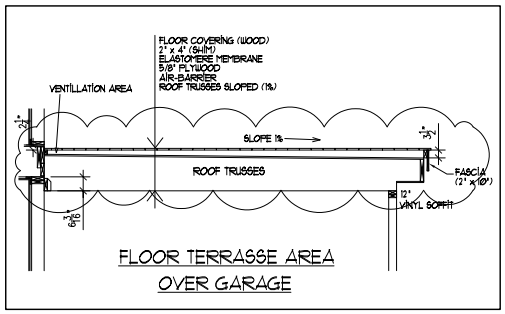

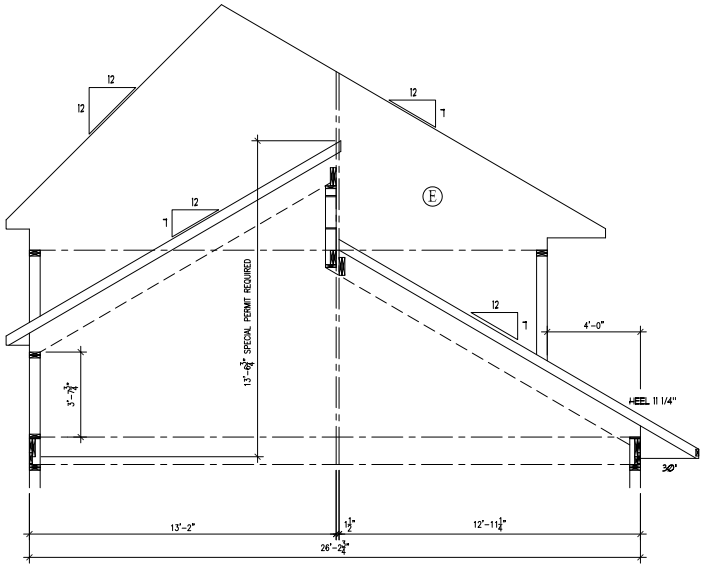

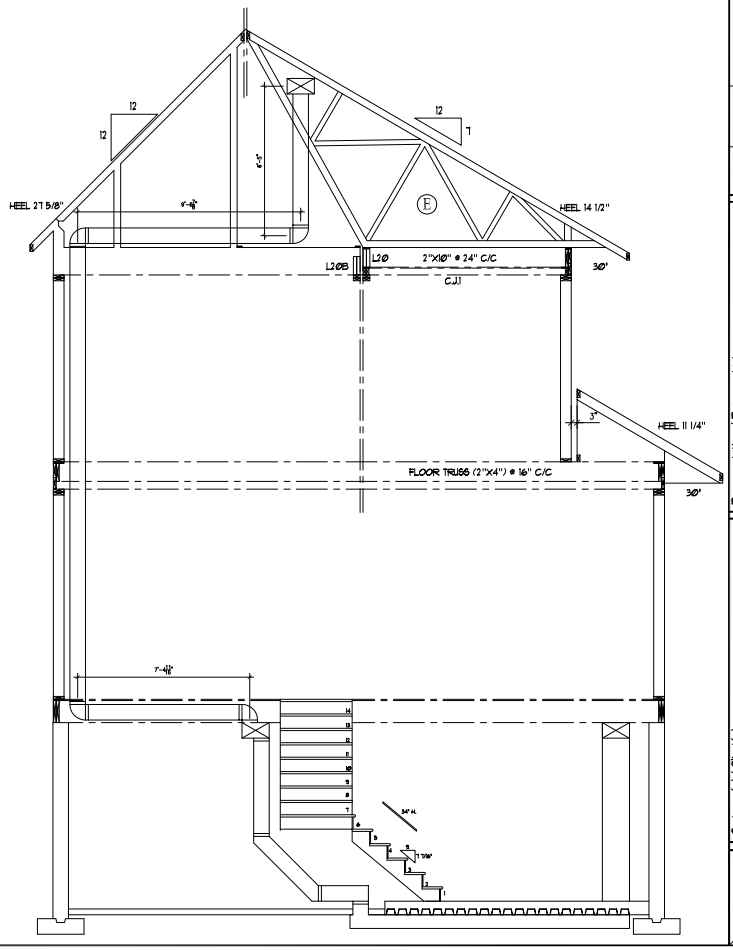

10309

LES MAISONS ALOUETTE HOMES
TEL: (450) 539-3100

Rev:	Date:	Description:	D.	V.
	06/11/15	PRELIMINARY PLAN	AL.	
	06/12/15	SIGNED PLAN	AL.	
	07/06/14	2e SIGNED PLAN	AL.	
	07/06/20	ADJUST RIDER HEIGHT	AL.	

Representative / Représentant:
ALOUETTE

Project / Projet:
07-0015

Scale / Échelle:
1/4" = 1'-0"

Customer(s) / Client(s):
ECOTERRA ALOUETTE HOUSE

Title / Titre:
TRUSSES SECTION & DETAILS

3
OF / De:

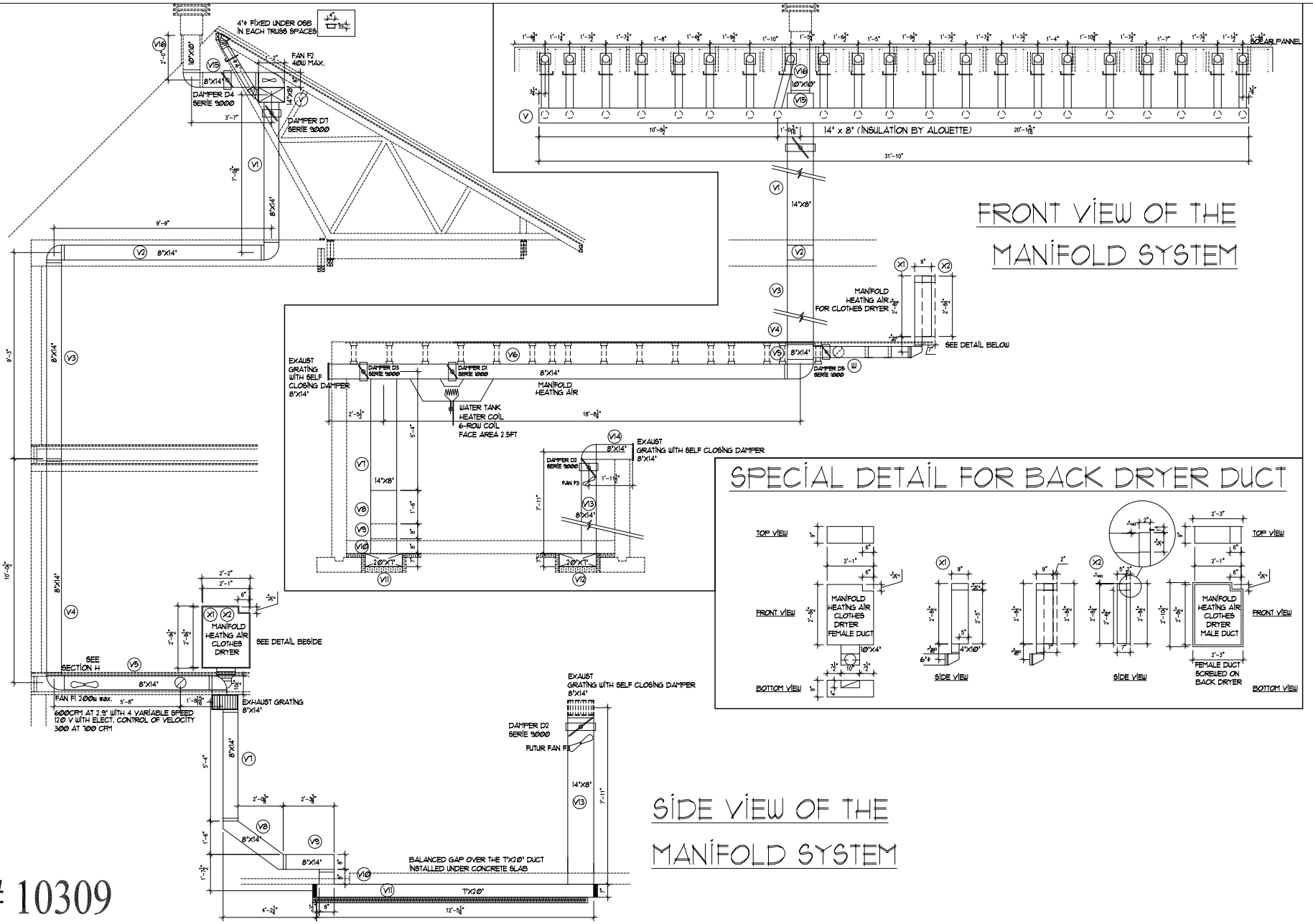

FRONT VIEW OF THE MANIFOLD SYSTEM

SIDE VIEW OF THE MANIFOLD SYSTEM

SPECIAL DETAIL FOR BACK DRYER DUCT

10309

LES MAISONS Alouette HOMES
TEL: (450) 539-3100

Rev:	Date:	Description:	D. V.
	07/06/14	2e SIGNED PLAN	NL
	07/06/18	Change location for side damper	NL
	07/09/05	change 4-row for 6-row coils	NL

Representative / Representant:
ALOUETTE

Project / Projet:
07-0015

Customer(s) / Client(s):
ECOTERRA ALOUETTE HOUSE

Scale / Echelle:
1/4" = 1'-0"

Title / Titre:
MANIFOLD MECANIC DETAIL

M5

1
Of / De

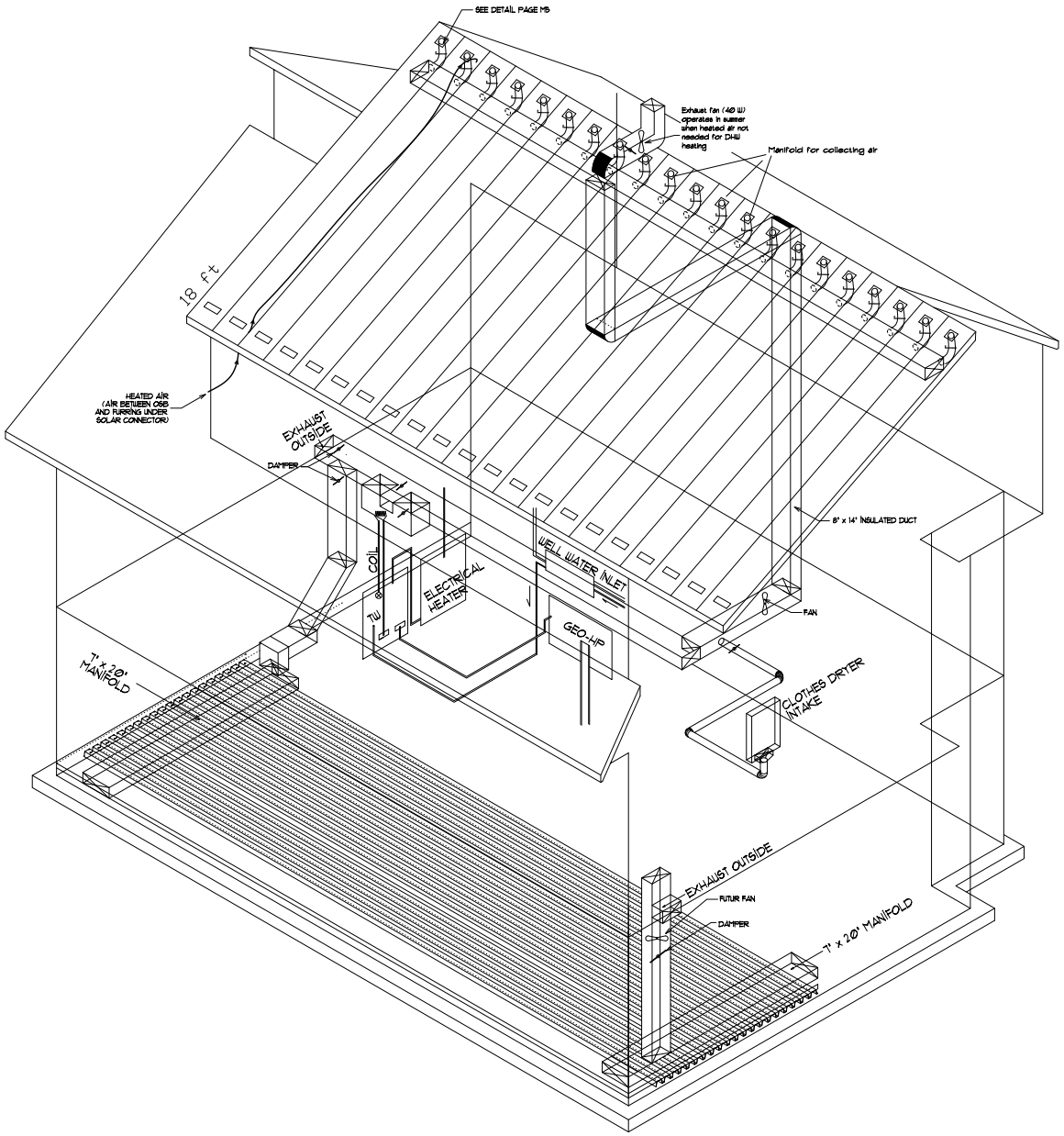

10309

Customer(s) / Client(s):
ECOTERRA ALOUETTE HOUSE

Title / Titre:
3D VIEW OF MANIFOLD AIR DIST.

Representative / Representant:
ALOUETTE

Scale / Echelle:
1/4" = 1'-0"

Project / Projet:
07-0015

Rev:	Date:	Description:	D.	V.
	06/11/15	PRELIMINARY PLAN	AL.	
	06/12/15	SIGNED PLAN	AL.	
	07/06/14	2e SIGNED PLAN	AL.	

LES MAISONS ALOUETTE HOMES
TEL: (450) 539-3100

M1
Of / De:

APPENDIX III

MATLAB M-files

File name : SOL_GAINS.m

```
function SG  = SOL_GAINS(G,theta,Fdir)

%-------------------------------------------------------------------
%%%% IMPORTANT NOTES:
% Function that calculates the solar radiation gains through the
% basement south windows.
% SG: output of the function in W/m2
%-------------------------------------------------------------------

% DESCRIPTION OF INPUTS
% theta: Solar incidence angle on the south windows (degrees)
% G:     Global sol. irr. measured by a sensor on the south wall(W/m2)
% Fdir:  Fraction of direct solar radiation on total solar radiation
%        received on the exterior south wall of the Ecoterra house
%------------

if theta <0.01
    theta = 0.01;
elseif theta > 89.99
    theta = 89.99;
end

% EXTINCTION COEFF. AND REFRACTION INDEX
k = 10.0;        % Good approx. for double strenght glass(1/m)
L = 0.003;       % 3 mm glass
ng= 1.52;

%REFRACTED ANGLE AS A FUNCTION OF INCIDENCE ANGLE
theta_p=asind(sind(theta)/ng);

%-------------------------------------------------
% EDWARDS INDUCTION METHOD FOR TRIPLE GLAZED WINDOWS
%-------------------------------------------------
% A) CALCULATION FOR THE TWO FIRST LAYERS OF GLASS

% ABSORPTION BY GLAZING (1 LAYER)
ta = exp(-k*L/cosd(theta_p)); % Fraction of radiation available after
% each reflection in the glazing

% PERPENDICULAR REFLECTION
rpe = (sind(theta_p-theta)/sind(theta_p + theta))^2;

% PARALLEL REFLECTION
rpa = (tand(theta_p-theta)/tand(theta_p + theta))^2;

% FOR THE PERPENDICULAR COMPONENT OF POLARIZATION (EQUAL FOR GLASS 1
AND 2)
tpe = (ta*(1-rpe)^2)/(1-(rpe*ta)^2);
ppe = rpe*(1+ta*tpe);

% FOR THE PARALLEL COMPONENT OF POLARIZATION (EQUAL FOR GLASS 1 AND 2)
tpa = (ta*(1-rpa)^2)/(1-(rpa*ta)^2);
```

```
ppa = rpa*(1+ta*tpa);

% EFFECTIVE TRANSMITTANCE AND REFLECTANCE OF THE FIRST TWO LAYERS
t12 = 0.5*( (0.95*tpe * tpe)/(1-ppe*ppe) + (0.95*tpa* tpa)/(1-ppa*ppa)
);

      % 0.95 is added to take into account the transmittance of the low-

e

% coating on the inside surface of outside glazing
p12 = 0.5*( (ppe + t12*ppe*tpe/tpe) + (ppa + t12*ppa*tpa/tpa) );

% ABSORPTANCE OF THE TWO FISRT LAYERS (REFL = 1-ABS-TRANSM)
abs12 = 1-p12-t12;

% ITRANSMITTED/INCIDENT (ABSORPTION LOSSES CONSIDERED ONLY)
ta12 = 1 - abs12;

% PARALLEL AND PERPENDICULAR TRANSMITTANCE OF THE 2 FIRST LAYERS

% (theta = 90 and theta = 0)
t12pe = 0.76; p12pe = 0.14;
t12pa = 0.00; p12pa = 0.99;

% B) CALCULATION FOR THE THIRD LAYER OF GLASS

% FOR THE PERPENDICULAR COMPONENT OF POLARIZATION
tpeb = (ta12*(1-rpe)^2)/(1-(rpe*ta12)^2);
ppeb = rpe*(1+ta12*tpe);

% FOR THE PARALLEL COMPONENT OF POLARIZATION
tpab = (ta12*(1-rpa)^2)/(1-(rpa*ta12)^2);
ppab = rpa*(1+ta12*tpa);

% EFFECTIVE TRANSMITTANCE OF THE 3-GLASS SYSTEM
t13 = 0.5*( ( t12pe*(0.95*tpeb) )/(1-p12pe*ppeb)+( t12pa*(0.95*tpab)
)/...
    (1-p12pa*ppab) );
% 0.95 is added to take into account the transmittance
% of the low-e coating on the inside surface of outside glazing

%-------------------------------------------------
% EFFECTIVE SOLAR ENERGY TRANSMITTANCE OF THE WINDOWS
%-------------------------------------------------
% FOR DIRECT IRRADIANCE
Teff = t13;

% FOR DIFFUSE IRRADIANCE
Tdiff = 0.2432;

%-------------------------------------------------
%  SOLAR GAINS INTO THE BASEMENT SOUTH ROOM (W/m^2)
%-------------------------------------------------
% DIRECT SOLAR GAINS
```

```
SGdir = Fdir * G * Teff;
% DIFFUSE SOLAR GAINS
SGdiff = (1-Fdir) * G * Tdiff;
% TOTAL SOLAR GAINS THROUGH WINDOWS
SG = SGdir + SGdiff;
```

File name : solar_angles.m

```
function [theta, Fdir] = solar_angles(t,Lat,Beta,Psi,n, Month)

%-----------------------------------------------------------------
%%%% IMPORTANT NOTES:
% Function that calculates the direct (and diffuse) portion of daylight
% (Fdir) incident on the basement south windows. It also calculates
% the incidence angle of the sun-rays (theta).
% Clearness index model is used.
%-----------------------------------------------------------------

%------------
% DESCRIPTION OF INPUTS
% t:    Time of the day
% Lat:  Latitude of the Ecoterra house
% Beta: Tilt angle of the surface
% Psi:  Surface orientation
% Month: Month of the year

%GROUND REFLECTANCE
if Month > 3 &&  Month < 12
    rho = 0.2;  % no snow
else
    rho = 0.85; % winter with snow
end

%DECLINATION ANGLE (degrees)
sigma=23.45*sind(360*(284+n)/365);

%HOUR ANGLE
hd=(t-12)*60*0.25 ;          %(degress)

    % CORRECTION IN ORDER TO AVOID H/ABS(H)=0/0
if hd == 0
    hd=0.000001;
end

%SOLAR INCIDENCE ANGLE (degrees)
costheta    =   sind(sigma)*sind(Lat)*cosd(Beta)...
               -sind(sigma)*cosd(Lat)*sind(Beta)*cosd(Psi)...
               +cosd(sigma)*cosd(Lat)*cosd(Beta)*cosd(hd)...
               +cosd(sigma)*sind(Lat)*sind(Beta)*cosd(Psi)*cosd(hd)...
               +cosd(sigma)*sind(Beta)*sind(Psi)*sind(hd);
theta1=acosd(costheta);

if theta1 >= 90
```

```
    theta=90;
else
    theta=theta1;
end

% SOLAR ALTITUDE ANGLE (ALPHA) (Duffie & Beckman)
alpha1 = asind(cosd(Lat)*cosd(sigma)*cosd(hd) + sind(Lat)*sind(sigma));
if alpha1 > 0
    alpha = alpha1;
else
    alpha = 0;
end

% ZENITH ANGLE (Duffie & Beckman)
zenith1 = acosd(cosd(Lat)*cosd(sigma)*cosd(hd)+sind(Lat)*sind(sigma));

if zenith1 >= 90
    zenith=90;
else
    zenith=zenith1;
end

% SUNSET HOUR ANGLE (hs)
coshs = -tand(Lat)*tand(sigma);
coshs2 = -tand(Lat-Beta)*tand(sigma);
hs    = min([acosd(coshs) acosd(coshs2)]);

% ------------------------------------------------
% Kt method
% ------------------------------------------------

% MONTHLY CLEARNESS INDEX FOR MONTREAL
Kt = [0.45 0.51 0.50 0.48 0.49 0.49 0.52 0.49 0.49 0.41 0.35 0.38];

% EARTH'S SPIN RATE
we = 360/24;          % degrees/hour

% COLLARES_PEREIRA_RABL CORRELATIONS
a = 0.4090 + 0.5016*sind(hs-60);
b = 0.6609 - 0.4767*sind(hs-60);

k = a + b*cosd(we*(t-11.99))*Kt(1,Month);

if k>0
    kt=k;
else
    kt=0;
end

% HOURLY DIFFUSE CLEARNESS INDEX
%(ORGILL-HOLLANDS CORRELATION, DUFFIE & BECKMAN ,3nd edition)
if kt <0.35
    kd = (1.0 - 0.249*kt);
elseif kt>=0.35 && kt <0.75
    kd = (1.557 - 1.84*kt);
```

```
else
    kd = 0.177;
end

% HOURLY BEAM CLEARNESS INDEX
kb = kt - kd;

% EXTRATERRESTRIAL NORMAL SOLAR RADIATION
Io = 1353*(1 + 0.033*cosd(360*n/365));

% INCIDENT BEAM SOLAR RADIATION
Ib = Io*kb*cosd(theta);

% INCIDENT SKY DIFFUSE SOLAR RADIATION
Ids = Io*sind(alpha)*kd*(1+cosd(Beta))/2;

% GROUND REFLECTED DIFFUSE SOLAR RADIATION
Idg = Io*sind(alpha)*(kd + kb)*rho*(1-cosd(Beta))/2;

% RATIO OF DIRECT SR ON TOTAL SOLAR RADIATION
Itot = Ib + Ids + Idg;

if Itot == 0
    Fdir = 0;
else
    Fdir = Ib/Itot;
End
```

File name : TF_SOLDOM.m

```
function [DN_ARX_d] = TF_SOLDOM

%-------------------------------------------------------------------
%%%% TRANSFER FUNCTION CREATION FUNCTION: TF_SOLDOM.m
%-------------------------------------------------------------------

%-------------------------------------------------------------------
%%%% IMPORTANT NOTES:
% Function that identifies the best model between the following inputs:
%   a: Solar gains through windows;
%   b: Heat stored into the VCS, from the BIPV/T heated air;
%   c: Outside temperature.
% And the ouput:
%    a: Average surface temperature of the VCS.
% This model is used to characterize the VCS response to active
% and passive charging during the solar dominated period.
% Time step = 3600s
%-------------------------------------------------------------------
%-------------------------------------------------------------------
%   1 - LOAD OF THE MATFILE CONTAINING THE DATA USED TO IDENTIFY THE
%   POLYNOMIAL MODEL
%-------------------------------------------------------------------
```

```
SIDATA = load('..\ECOTERRA TRANSFER
FUNCTIONS\output_data\Mar13to17_2009', 'Ts',
'T_VCS','Text','SolarGains','QinVCS_BIPVT');
VALDATA = load('..\ECOTERRA TRANSFER
FUNCTIONS\output_data\Mar20to25_2009', 'Ts',
'T_VCS','Text','SolarGains','QinVCS_BIPVT');

TS       = SIDATA.Ts;

% IDENTIFICATION VECTORS
TEXT = SIDATA.Text;
TVCS = SIDATA.T_VCS;
SG   = SIDATA.SolarGains;
QINVCS = SIDATA.QinVCS_BIPVT;


% VALIDATION VECTORS
TEXTv   = VALDATA.Text;
TVCSv   = VALDATA.T_VCS;
SGv     = VALDATA.SolarGains;
QINVCSv = VALDATA.QinVCS_BIPVT;


%-------------------------------------------------------------------
%   2 - CREATION OF DATA OBJECTS (3 inputs - 1 outputs)
%-------------------------------------------------------------------
TVCSd  = downsample(TVCS,12);
TVCSvd = downsample(TVCSv,12);

DATAid = iddata(TVCSd,downsample([QINVCS SG TEXT] ,12), TS*12);
DATAvd = iddata(TVCSvd,downsample([QINVCSv SGv TEXTv],12), TS*12);

%-------------------------------------------------------------------
%   3 - IDENTIFICATION OF POLYNOMIAL MODEL
%-------------------------------------------------------------------

% ARX MODEL
marx = arx(DATAid,'na',8,'nb',[3 3 3 ],'nk',[1 1 1],'Focus','Stab');

%-------------------------------------------------------------------
%   4 - EXTRACTION OF NUMERATOR AND DENOMINATOR (DISCRETE TIME)
%-------------------------------------------------------------------

% ARX MODEL
[numA, denA] = tfdata(marx);
numTEXTA     = cell2mat(numA(1,3));
numSGA       = cell2mat(numA(1,2));
numQINVCSA   = cell2mat(numA(1,1));
denTEXTA     = cell2mat(denA(1,3));
denSGA       = cell2mat(denA(1,2));
denQINVCSA   = cell2mat(denA(1,1));
DN_ARX_d = {numTEXTA, numSGA, numQINVCSA, denTEXTA, denSGA,
denQINVCSA};
```

File name : SlabHeatAbsorption.m

```
function OUTPUT = SlabHeatAbsorption(Inputs)

%-------------------------------------------------------------------
%%%% IMPORTANT NOTES:
% Function that calculates the total air stream
% energy loss across the VCS slab at each time step.
% Assumptions:
% 1 - Slab temperatue over channels is assumed equal to surface
temperature
% 2 - An air temp. decrease of 2 deg C is assumed between VCS inlet
%     and entry of first channel
% 3 - An air temp. decrease of 5 deg C between entry of first channel
%     and entry of 19th channel is assumed
% 4 - The soil temperature under the insulation is assumed constant
% 5 - Heat exchange in manifold is not calculated
% 6 - Each channel is discretized into 10 elements
% 7 - Trapezoidal dimension of channel cross-section are: 115mm - 89mm
%     76mm (height)
%-------------------------------------------------------------------

%------------
% DESCRIPTION OF INPUTS
Tinlet = Inputs(1,1);
Tvcssurf = Inputs(2,1);
Tsoil = Inputs(3,1);
CFM = Inputs(4,1);
%------------

%------------
% NUMBER OF DISCRETIZED ELEMENTS PER CHANNELS
Nel = 10;
%------------
% AREA COVERED BY THE 19 CHANNELS
DIMEW = 9.144;   % m
%------------
% CHANNEL CROSS-SECTIONAL AREA
AREA_chn = 0.0077;  %m^2
%------------
% CONDUCTANCE UNDER THE METAL MESH PORTION (U value)
Uins = 1/1.7;     % W/(m^2*K)
%------------
% Cp AIR, AIR DENSITY
Cp_a = 1007;    % J/(Kg*K) for air at 300K
Rho_a = 1.1614; % kg/m^3 for air at 300K
%------------
% ENTRY TEMPERATURE OF EACH CHANNELS
Tentry = [(Tinlet-2):(-5/18):(Tinlet-7)]';
%------------
% AIR VELOCITY AND MASS FLOW RATE IN EACH CHANNELS
Vair = CFM/315;     %m/s - Relation taken from Xiang's thesis
Mdot = Vair * AREA_chn * Rho_a; % kg/s
%------------
% CONVECTIVE HEAT TRANSFER COEFFICIENT
Hc_vcs = 3.94*Vair + 5.45;
```

```
%------------
% AREA OF STEEL DECK SURROUNDING EACH CHANNEL ELEMENT (EXCEPT METAL
MESH
% SURFACE)
Achn = (DIMEW /Nel) * 0.2432;     % m^2
%------------
% AREA OF FACING SOIL FOR EACH STEEL DECK (METAL MESH)
Asoil = (DIMEW /Nel) * 0.115;     % m^2
%------------
% SOLUTION LOOP
Tslab  = Tvcssurf;
Qair = zeros(19,1);
Qair_soil = zeros(19,1);
Qair_slab = zeros(19,1);
Tair_out = zeros(19,1);  % Vector of temperatures at the exit of each
channel

if CFM==0
    Qinvcs = 0;
    Qtoslab = 0;
    Qtosoil = 0;
else
      for j=1:19;
        Ta_in = Tentry(j);
        %---------------
        for i = 1:Nel
            %ITERATION TO SOLVE SYSTEM OF EQUATION
            %---------------
            for k= 0:0.01:60

                Qair_a = Mdot*Cp_a*(k-Ta_in);
                Qair_b = Hc_vcs*Achn*(-k + Ta_in)/log((Tslab-k)/(Tslab-
Ta_in)) + Uins*Asoil*(-k + Ta_in)/log((Tsoil-k)/(Tsoil-Ta_in));

                if abs(Qair_a-Qair_b)<10 && isreal(Qair_a-Qair_b)==1
                    Qair_slab(j) = Qair_slab(j) + Hc_vcs*Achn*(-k +
Ta_in)/log((Tslab-k)/(Tslab-Ta_in));
                    Qair_soil(j) = Qair_soil(j) + Uins*Asoil*(-k +
Ta_in)/log((Tsoil-k)/(Tsoil-Ta_in));
                    Qair(j)= Qair(j) + (Qair_a + Qair_b)/2;
                    Ta_out = k;
                    break
                else
                    Ta_out = k;
                end

            end
            %---------------
            if Ta_out == 60;
                break
            else
                Ta_in = Ta_out;
            end


        end
```

```
        if Ta_out == 60;
            Qair = zeros(19,1);
            Qair_soil = zeros(19,1);
            Qair_slab = zeros(19,1);
            break
        else
            Tair_out(j,1) = Ta_out;
        end
        %---------------

    end
    Qinvcs = (-1)*sum(Qair);
    Qtoslab = (-1)*sum(Qair_slab);
    Qtosoil = (-1)*sum(Qair_soil);

end
%------------
% VCS OUTLET AIR TEMPERATURE
vdot=ones(19,1)* Vair * AREA_chn;
Tair_mix = zeros(19,1);

if CFM==0
    Toulet_VCS = 0;
else

Tair_mix(1,1) = Tair_out(1,1);

    for k = 2:19
        v_dot_t = sum(vdot(1:k,1));
        v_dot_a = sum(vdot(1:(k-1),1));
        v_dot_b = vdot(k,1);
        Tair_mix(k,1) = (v_dot_a*Tair_mix((k-1),1) +
v_dot_b*Tair_out(k,1))/v_dot_t;
    end

    Toulet_VCS = Tair_mix(19,1);
end
%------------
% VECTOR OF OUTPUTS
OUTPUT = [Qinvcs Qtoslab Toulet_VCS];
```

File name : ECOTERRA_BIPVT.m

```
function Tfinal  = ECOTERRA_BIPVT(RAD,Flowrate,Ti,To,Tattic,Wspeed)

%-----------------------------------------------------------------
%%%% IMPORTANT NOTES:
% Function that calculates the exit air temp. at the end of the BIPV/T
% roof channels of the Ecoterra house.
% Source:
% Candanedo, J. A. (2011).A Study of Predictive Control strategies for
% Optimally Designed Solar Homes(Doctoral). Concordia University,
% Montréal.
```

```
% The model was modified to accomodate the construction details of the
% Ecoterra house
%-----------------------------------------------------------------

eml.extrinsic('Integration_Tma')
% Final temperature of a BIPVT System
% Final_temp =  BIPVT(RAD,Flowrate,Ti,To,Tattic,Wspeed)
% Temperatures in Celsius
% Flowrate in CFM
% Windspeed in m/s
%-------------------------------------------------------------------------
----
To = To + 273.15;                               %Temperature in K
Ti = Ti + 273.15;                               %Temperature in K
Tattic = Tattic + 273.15;                        %Temperature in K
Flowrate = Flowrate/(2117.253);                  %Flowrate in m3/s
%-------------------------------------------------------------------------
----
%-----------------------------GEOMETRY OF THE ROOF---------------------
----
WidthPV = 10.4;              %Width of the BIPV/T roof
Total_length_slope = 6.74;  %Length of the system in the flow
dir.(upwards)
LengthPV = 6.73;             %Lenght of the PV in the flow dir.(upwards)
LengthGL = Total_length_slope - LengthPV;  %Length of the glazing
section
Gapsize = 0.038;             %Gap size
%-----------------------------SOME FLOW CALCULATIONS-------------------
----
ACS = WidthPV*Gapsize;             %Area cross section
Per = 2*(WidthPV+Gapsize);         %Perimeter
Dh = 4*ACS/Per;                    %Hydraulic diameter
sigma = 5.67E-8;                   %Stefan-Boltzmann constant
%-------------------------------AIR PROPERTIES-------------------------
----
Pr = 0.71;                                  %Prandlt number
M_air = 0.0289;                             %Molecular mass of air kg/mol)
R = 8.314;                                  %Ideal gas constant (J/K-mol)
Pressure = 101300;                          %Atmospheric pressure
air_density = Pressure*M_air/(R*Ti);        %Air density based on Ti
k_air = (0.002528*(Ti)^1.5)/(Ti+200); %Thermal cond. of air based on Ti
cp_air = 1000;                              %cp of air
b = 1.458E-6;
Su = 110.4;
visc = (b*(Ti)^1.5)/(Ti+Su); %Viscosity (Sutherland model)based on Ti
%-----------------------MASS FLOW AND REYNOLDS-------------------------
----
Vel_gap = Flowrate/ACS;                     %Velocity in the gap
MFR = Flowrate*air_density;                 %Mass flow rate
Jones = 2/3 + (11/24)*(Gapsize/WidthPV)*(2-Gapsize/WidthPV); %Jones'
corr.
Rey = air_density*Vel_gap*Dh/visc;  %Reynolds num.
Rey_corr = Rey*Jones;               %Correction Rey. number
%---------------------HEAT TRANSFER CONVECTIVE COEFFICIENT-------------

hc = 11 ;    %Assumed value of convective heat transfer coefficient
```

```
%-----------------------------Exterior heat transfer coefficient-------
hox = 5.7 + 3.8*Wspeed;
%-----------------------------SEGMENTS OF PV---------------------------
npv = 5;
DeltaPV=LengthPV/npv;
xPV=zeros(npv+2,1);
xPV(1) = 0;
for i=1:npv
    xPV(i+1)=i*DeltaPV-DeltaPV/2;  %Coord. of central pts. PV panels
end
xPV(npv+2)=LengthPV;
%-----------------------------SEGMENTS OF GLAZING----------------------
----
ngl = 4;
DeltaGL=LengthGL/ngl;
xGL=zeros(ngl+2,1);
xGL(1) = 0;
for i=1:ngl
    xGL(i+1)=i*DeltaGL-DeltaGL/2;   %Coord. of central pts. glz. panels
end
xGL(ngl+2)=LengthGL;
%-----------------------------SEGMENTS OF VERTICAL GLAZING-------------
%**********************************************************************
%*******************************MAIN CALCULATIONS**********************
%**********************************************************************
%----------------------------------PV SECTION--------------------------
e1 = 0.9;            %Emissivity of back of PV
e2 = 0.3;            %Emissivity of absorber plate
aPV = 0.92;          %Absorptance of PV panel
Afraction = 0.95;    %Eff. fraction of PV area actually occupied by PV
uins = 1;            %Conductance per unit area of insulation below
attic
%----------------------------------------------------------------------
%Guess value for C1 and C2 and eff
C1 = 0;
C2 = 0;
eff= 0;
%Guess temperatures
TPVguess = 50+273.15;
TABguess = 30+273.15;
Tmaguess = 40+273.15;
%convection coefficients in both sides
hcb = hc;
hcf = hc;
Tin = Ti;            %Initial Temperature
% Initialization of vector
PVMidpoints     = zeros(npv,1);
PVFinalpoints   = zeros(npv,1);
Gen             = zeros(npv,1);


for n=1:npv
     TPV = TPVguess;
     TAB = TABguess;
     Tma = Tmaguess;
```

```
    error_tol = 0.1;
    while abs(error_tol)>=0.001
        Tprevious = Tma;
        C1 = (hcf*TPV+hcb*TAB)/(hcf+hcb);
        C2 = (WidthPV*(hcf+hcb))/(MFR*cp_air);
        Tma = Integration_Tma(DeltaPV, C1, Tin, C2);
        Tmean = (TPV+TAB)/2;
        hrad = (4*sigma*Tmean^3)/(1/e1 + 1/e2 -1);
        eff = 0.12 - 0.00055*(TPV-(25+273.15));
        % efficiency of PV as a function of PV temp.
        TPV = (hox*To+hcf*Tma+hrad*TAB+RAD*Afraction*(aPV-eff))...
            /(hox+hcf+hrad);
        TAB = (Tma*hcb+Tattic*uins+TPV*hrad)/(hcb+uins+hrad);
        error_tol = (Tma-Tprevious)/Tprevious;
    end
    PVMidpoints(n) = Tma;
    PVFinalpoints(n) = C1 + (Tin-C1)*exp(-C2*DeltaPV);
    Gen(n) = eff*WidthPV*DeltaPV*Afraction*RAD;
    Tin = PVFinalpoints(n);
end
%-------------------------------------------------------------------------
%--------------------------------GLAZING SECTION-----------------------
----
e1 = 0.9;     %Emissivity of back of glazing (infrared)
e2 = 0.2;     %Emissivity of absorber plate (infrared)
taupv = 0.9;  %Transmittance of glazing
aAB = 0.9;    %Absorptance of absorber plate (overall)
uins = 1;     %Conductance per unit area of insulation below attic
%-------------------------------------------------------------------------
%Guess temperatures
TGLguess = 50+273.15;
TABguess = 30+273.15;
Tmaguess = 40+273.15;
%convection coefficients in both sides
hcb = hc;
hcf = 2.5*hc;
Tin = PVFinalpoints(npv); %Initial Temperature = final point of PV
% Initialization of vector
GLMidpoints     = zeros(ngl,1);
GLFinalpoints   = zeros(ngl,1);
for n=1:ngl
    TGL = TGLguess;
    TAB = TABguess;
    Tma = Tmaguess;
    error_tol = 0.1;
    while abs(error_tol)>=0.001
        Tprevious = Tma;
        C1 = (hcf*TGL+hcb*TAB)/(hcf+hcb);
        C2 = (WidthPV*(hcf+hcb))/(MFR*cp_air);
        Tma = Integration_Tma(DeltaGL, C1, Tin, C2);
        Tmean = (TGL+TAB)/2;
        hrad = (4*sigma*Tmean^3)/(1/e1 + 1/e2 -1);
        TGL =(hox*To+hcf*Tma+hrad*TAB)/(hox+hcf+hrad);
        TAB
=(Tma*hcb+Tattic*uins+TGL*hrad+RAD*taupv*aAB)/(hcb+uins+hrad);
        error_tol = (Tma-Tprevious)/Tprevious;
    end
```

```
     GLMidpoints(n) = Tma;
     GLFinalpoints(n) = C1 + (Tin-C1)*exp(-C2*DeltaGL);
     Tin = GLFinalpoints(n);
end
%---------------------------------RESULTS-----------------------------
Tfinal = GLFinalpoints(ngl)-273.15;
```

File name : Integration_Tma.m

```
function Tma = Integration_Tma(DeltaPV, C1, Tin, C2)

%--------------------------------------------------------------------
%%%% IMPORTANT NOTES:
% Integration function used to calculate the exitait air temperature of
% each control volume of the BIPV/T roof.
%--------------------------------------------------------------------

Tma = (1/(DeltaPV))*quad(@(x) (C1 + (Tin-C1)*exp(-C2*x)),0,DeltaPV);
```

APPENDIX IV

Use of the System Identification Toolbox® to Find Polynomial Models

This section presents an example showing how the System Identification Toolbox can be used to identify polynomial models describing dynamic systems. The case of the air supply fan dynamic system presented in Chapter 2 was kept for this demonstration.

Time	Electrical current (amps)	Volumetric flow rate (cfm)	Time	Electrical current (amps)	Volumetric flow rate (cfm)
0	0,0	50,0	**25**	0,0	124,6
1	0,0	55,0	**26**	2,5	338,0
2	2,0	221,9	**27**	0,0	107,7
3	2,0	259,1	**28**	4,0	504,4
4	0,0	77,7	**29**	4,0	574,9
5	3,5	436,9	**30**	0,0	172,6
6	0,0	112,4	**31**	3,5	506,2
7	4,0	512,1	**32**	0,0	156,8
8	3,0	464,1	**33**	2,0	299,4
9	0,0	151,5	**34**	0,0	109,3
10	2,0	316,8	**35**	2,0	268,2
11	0,0	109,4	**36**	3,5	465,1
12	2,0	269,6	**37**	0,0	127,1
13	0,0	86,0	**38**	4,0	530,5
14	4,0	492,2	**39**	0,0	149,8
15	4,0	565,7	**40**	2,5	354,6
16	0,0	168,1	**41**	2,0	327,2
17	0,0	123,0	**42**	0,0	110,9
18	2,5	342,2	**43**	2,0	284,4
19	3,0	413,3	**44**	2,0	295,7
20	0,0	125,1	**45**	3,5	475,6
21	2,5	352,2	**46**	0,0	143,6
22	3,0	431,9	**47**	4,0	536,7
23	0,0	129,9	**48**	0,0	153,4
24	3,0	414,0			

Table IV.1: Inline fan experimental data.

Table IV.1 shows a record of experimental data over a 48-hours period. The system variables were sampled hourly. This data will be used to build a model of the outlet volumetric flow rate. This model will allow identifying how the volumetric flow rate is affected by the fan electric current input. Therefore, the inline fan system is a single-input/single-output (SISO) dynamic system.

Data Preparation

It is important to use separate sets of data during the identification procedure. One will be used to estimate the model and the other will be used to validate the model. Experimental data should be transformed into data objects using the IDDATA function in order to be imported into the system identification tool. Using two data vectors, [I] and [CFM], the data object can be created with the following commands. Input and output signals can also be attributed names.

```
DATA = iddata(CFM,I,3600);
DATA.OutputName = {'volumetric flow rate'};
DATA.InputName = {'current};
```

The system identification tool is opened by typing "ident" in the command window. The data object created can be imported in the tool as shown here (Figure IV.1).

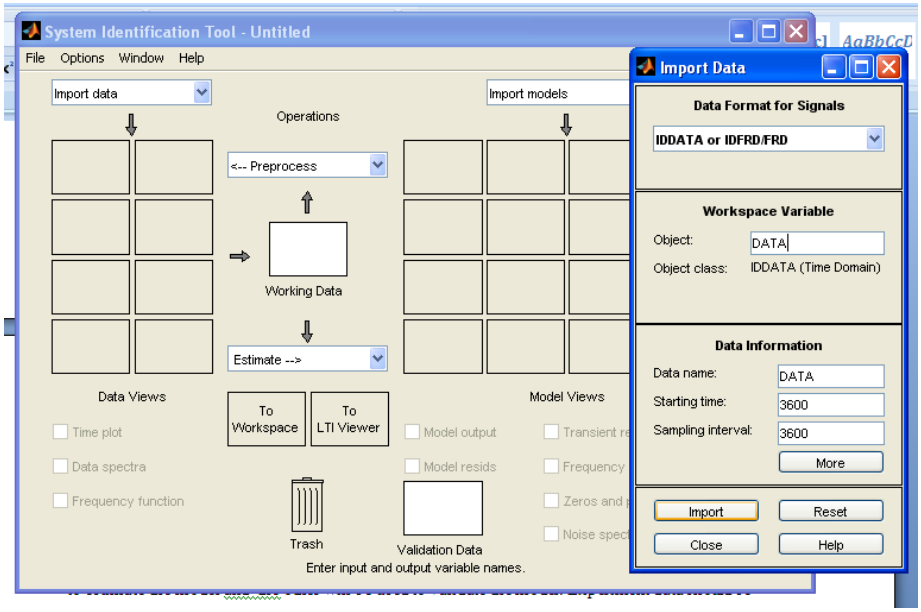

Figure IV.1: Data import into the system identification tool.

The data can be split into two distinct experimental data sets using the preprocessing function. By dragging and dropping the appropriate experiment, the working data and validation data can be respectively assigned (Figure IV.2).

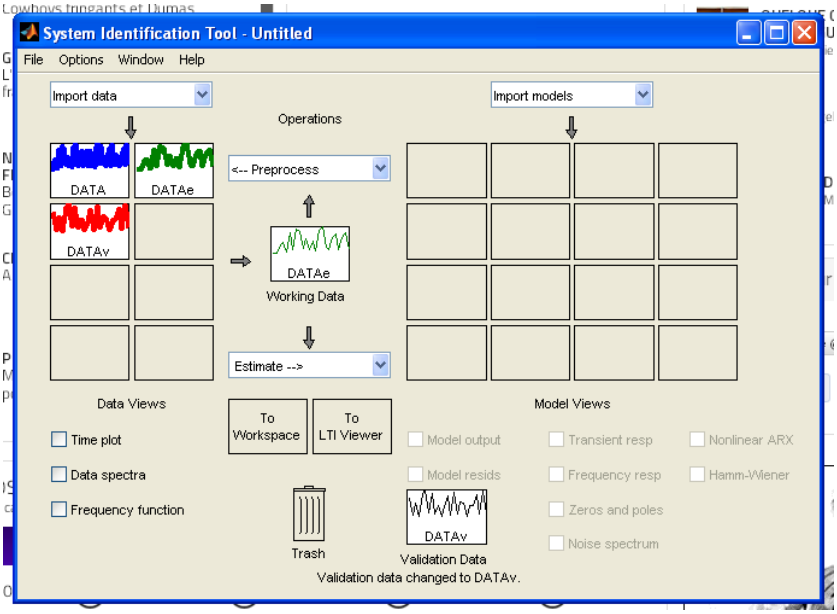

Figure IV.2: Selection of estimation and validation data subsets.

Model Structure Selection

In the current case, no a priori information about the inline fan system is known. However, it can be assumed that this system is linear and could be described by a low order model. It is worth trying to estimate a polynomial model having the simplest structure. For this example, the ARX model structure will be chosen. The ARX structure for polynomial models is characterized by only three integers, n_a, n_b and n_k (refer to Chapter 3 of this thesis).

Polynomial Order and Model Validation

The fit between the measured and simulated output can examined on the Model Output window (Figure IV.3). By default the first model estimated will be an ARX441 model. As observed, this model estimation results in a poor fit with the validation data and should be rejected.

It can be assumed that the air flow rate response to the electrical input does not include any significant delay. A second estimation should be performed, this time setting the delay parameter (n_k) to 0. This time, the fit between the model and the validation is almost perfect (Figure IV.4).

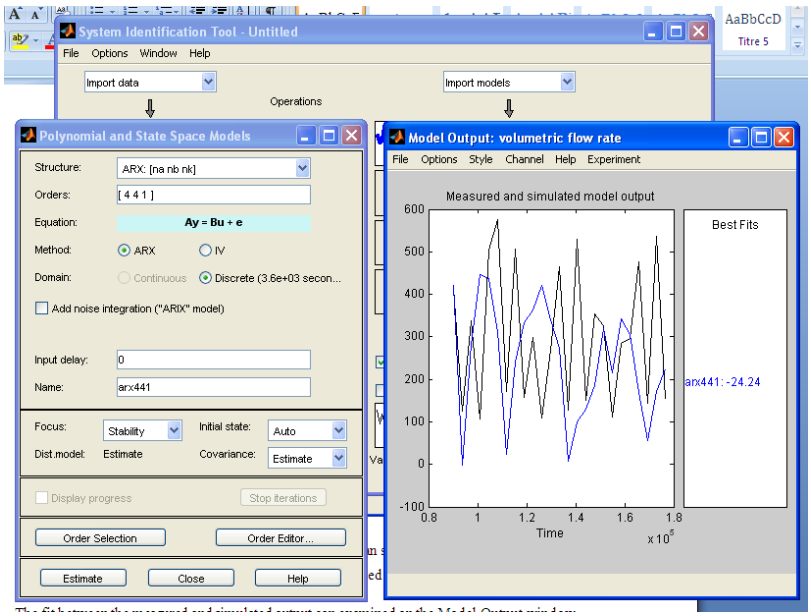

Figure IV.3: Model output and fit evaluation with validation data for the first model.

It is important to verify if a lower order model could perform as well as the ARX441. For that reason, the third order model ARX330 will be estimated and tested with the validation data. The fit results show that this model performs well (Figure IV.5).

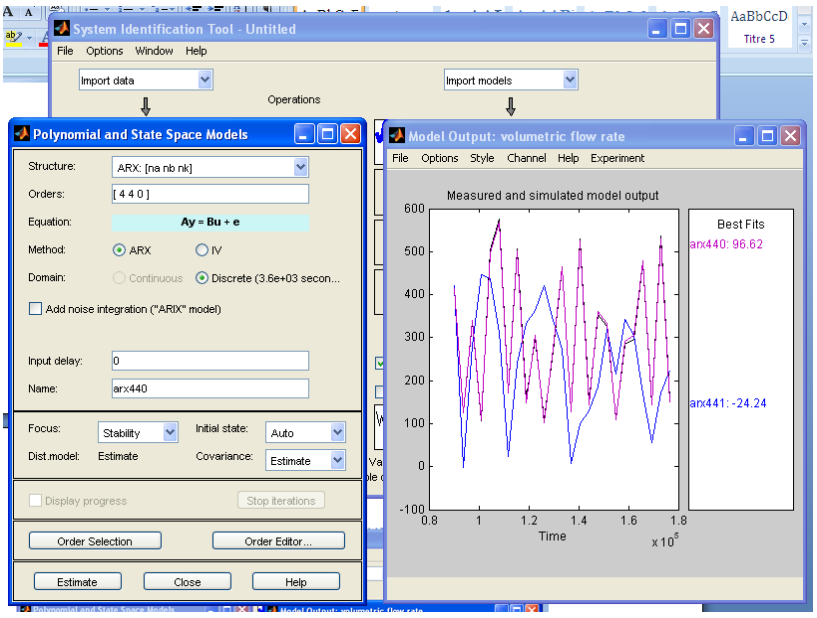

Figure IV.4: Model output and fit evaluation with validation data for the second model.

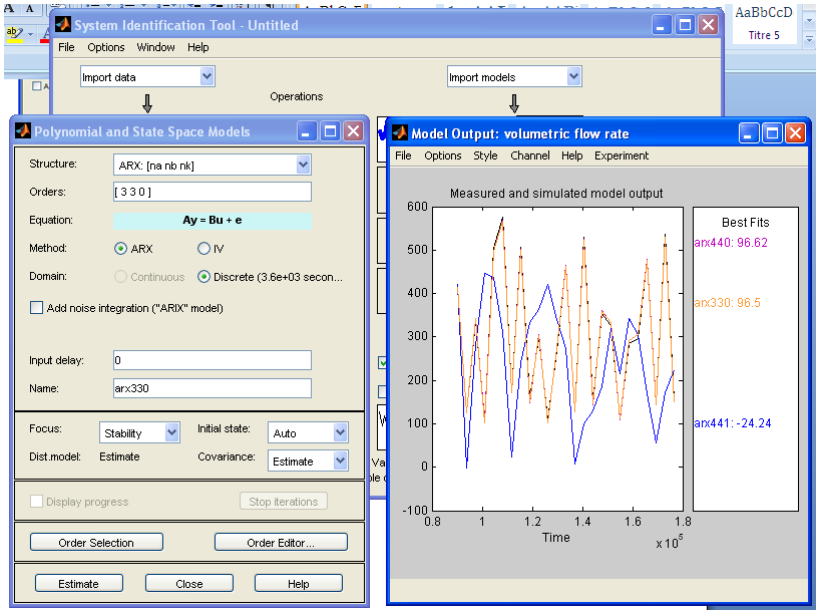

Figure IV.5: Model output and fit evaluation with validation data for the third model.

Before accepting this model as the best mathematical description of the inline fan system, future validation should be completed. A look at the model residuals will indicate if the model was able to catch all the system dynamics of the inline fan system. The residual analysis window will pop-up when the respective box is checked in the main system identification GUI. Residuals are the part of the data that the identified model

could not imitate. Residuals should therefore be free of any patterns that could be explained mathematically and should not be dependant of any previous inputs, i.e. uncorrelated. Here, the results confirmed that the residuals of the last ARX model (ARX330) are uncorrelated because they are well within the confidence intervals (dashed lines, Figure IV.6).

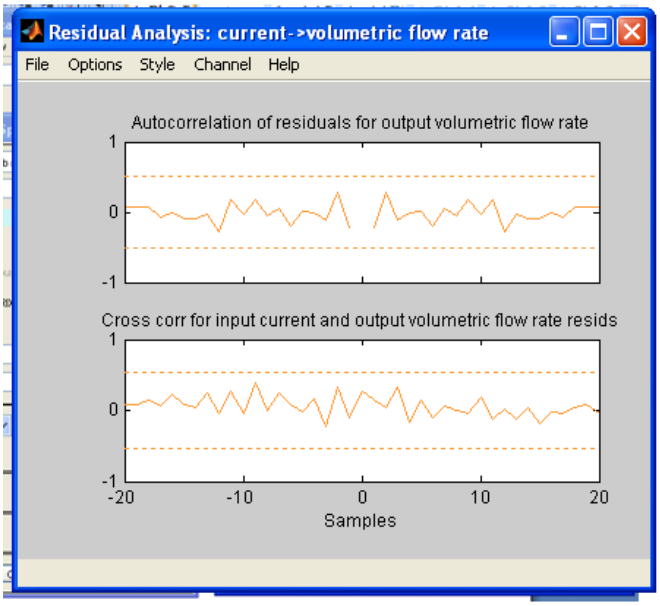

Figure IV.6: Residual analysis window.

The zeros and poles plot is displayed when the corresponding item is checked in the main GUI (Figure IV.7). Having all poles and zeros inside the unit circle confirms the stability of the ARX330 polynomial model.

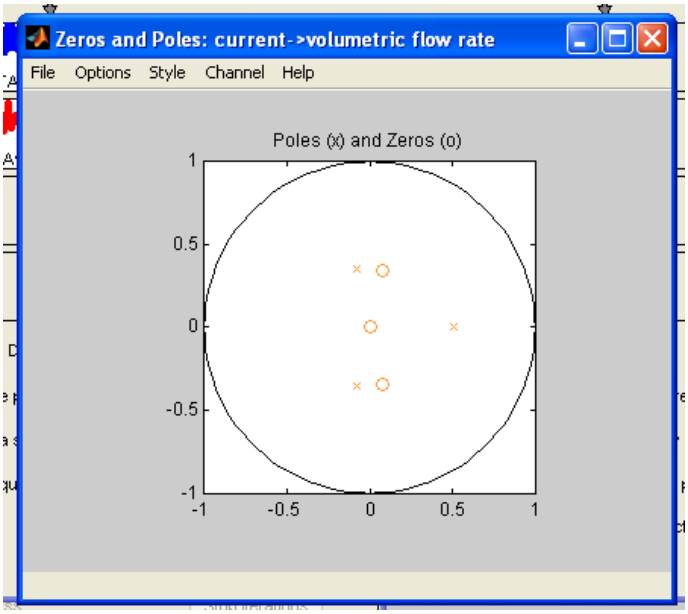

Figure IV.7: Pole and zero plot window.

Finally, by clicking on the final model box in the main system identification GUI, the value of the model parameters can be obtained (Figure IV.8).

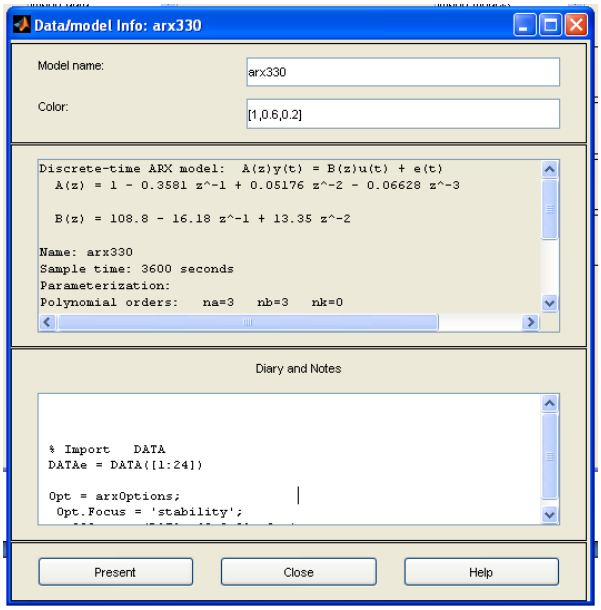

Figure IV.8: Model information window.

Special notes

The completion of this thesis required an important amount of successive system identification cycles. An important knowledge was accumulated and should be transmitted for future system identification studies. Here is a list of important information regarding the process of system identification.

- Sampling interval/Time step: The choice of sampling interval should be so that the information lost about the system dynamics is not significant. Also, it was found that increasing the time step of the identification data, most of the time, eases the identification process by limiting the identification to the relevant system dynamics. The time step should also be selected in accordance with the future use of the model.
- Choice of model structure: It is important to try most of the structures offered by the toolbox. Knowledge about the system to model should also be used to select the model structures that are most likely to serve for the system identification.
- Before starting the system identification process, the model acceptance criteria should be made clear. The intended use of the model should guide them. This includes knowing the form of the data that will be available when it will be used.
- Model size: The computational efforts required to calculate the model are an important aspect to consider. Therefore, for most cases, the model order/degree of the polynomials should be as low as possible. This will result in a model having a low computational “cost”.

System Identification: Theory for the User

Liennart Ljung is the man behind the System Identification Toolbox for MATLAB. His book (L. Ljung, 2009) is an essential reading before starting any system identification project using the System Identification Toolbox. This book provides information about the theory of system identification, the methodology to apply and practical guidance for system identification tasks.

APPENDIX V

Summary of the Energy Consumption Analysis of the Ecoterra™ house and Comparison of the Actual Energy Consumption Against Modeled Values

COMPARISON BETWEEN ENERGY USE MODELING AND ACTUAL CONSUMPTION FOR THE ÉCOTERRA™ HOUSE DURING 2010

June 06, 2011

Amélie Allard, M. A. Sc. Student (Building Engineering), Concordia University

Andreas Athienitis, Professor, Concordia University

1. INTRODUCTION

This report is a summary of the energy consumption analysis for the EcoTerra™ house. It compares actual energy consumption over a one year period (2010) against the modeled values determined prior to the house being built and occupied.

The modeled values were based on rules specified in Canada Mortgage and Housing's EQuilibrium™ Initiative competition of 2007. Those rules required that projections be based on the energy use of a "typical" Canadian family of two adults and two children with the usual complement of cooking, cleaning, entertainment, etc.

Information on actual energy consumption is derived from the data recorded by numerous sensors installed throughout the house. For this analysis, the recorded readings used were from the period of December 10, 2009 to December 9, 2010.

All values expressed, both modeled and measured, are believed to be accurate within 5%.

2. COMPARISON SUMMARY

A quick comparison of overall numbers shows that the net energy deficit during 2010 was almost five times the expected amount. Consumption was 231% of the projected value while production of electricity from the PV collectors achieved only 75% of expectations.

Table 1: Comparison Summary

	Modeled VALUES (kWh)	ACTUAL VALUES (kWh)
ANNUAL ENERGY CONSUMPTION	**5575**	**12 888**
ANNUAL PV GENERATION	**-3420**	**-2570**
NET ANNUAL ENERGY DEFICIT	**2155**	**10318**

3. REASONS FOR THE DIFFERENCES BETWEEN MODELED ENERGY PERFORMANCE AND ACTUAL PERFORMANCE

A. Energy Production Deficit

- Original projections were for the house to be fitted with a 3 kW PV array. During construction, it was determined that only 2.84 kW could be accommodated with the selected technology that emphasized building integration, and this even though a design change was made to increase the south facing roof surface by approximately 15% through the addition of a covered deck off the second bedroom.

  The problem stems from a design requirement to install individual PV collectors within the space defined by the standing seams of the metal roof. There was some concern for the potential of partial shading of the collectors by the standing seams, and because the metal roofing systems were only available in standard widths, a non-optimal spacing of the PV collectors was inevitable. Consequently, production shortfall from modeled values is in the neighbourhood of 228 kWh.
- The PV array appears to be operating at the expected levels of efficiency of production vs. insolation[1]. The remaining deficit on the production side (622 kWh) is assumed to be because of higher than expected snow cover of the array during the winter months due to; a) less than optimal roof pitch (30 degrees), b) higher than average snow fall amounts during the period, and c) less-than-average levels of insolation during the period.

[1] Amount of solar radiation received on a surface area at a given time (W/m^2).

Table 2: Differences Between Modeled And Actual Production

PRODUCTION	(kWh)
Projected Energy Production	**3420**
• **Smaller PV Array / Efficiency of the PV array**	**-228**
• **Snow Cover / Reduced Insolation / Tree shading**	**-622**
Net Energy Production	**2155**

B. Energy Consumption In Excess Of Modeled Values

a. Design issues

- The overall efficiency of the ground source heat pump was modeled using an assumed COP value including all required equipment (fans, dampers, etc.), and included allowing the temperatures within the dwelling to vary between 19°C and 22°C. The control strategy eventually implemented and now in effect, allows the distribution fan to run continuously, at low speed, even when no heating or cooling is occurring. The goal is to reduce thermal stratification throughout the house and increase occupant comfort. Additional consumption of approximately 1611 kWh is the result.
- An optimally sized heat pump was calculated to be 2.2 Ton; the smallest heat pump available was 3.0 Ton. Efficiency is lower and energy consumption is slightly higher than expected. Although peak power demand will be higher, total energy consumption will not be significantly different.
- The measured domestic hot water (DHW) energy consumption is approximately 625 kWh higher than the modeled value. This is due to; a) the heat delivered to the heat exchanger is not as high as expected because the BIPV/T fan is not being run at its highest speed in an effort to reduce fan noise, and b) the consumption of hot water is predominantly during the day. It was expected that higher utilization would be made at night, allowing for a better optimization of the available pre-heating energy sources.

b. Equipment failures/shortcomings

- An analysis of the collected data during the period led to the discovery that the dryer booster fan was not properly controlled and consequently, was running continuously. The fault was traced to a loose control system connection and was corrected in September 2010. The increased energy consumption resulting from this situation is estimated at 920 kWh.
- During the fall of 2010, customer feedback and collected data showed a more-or-less continuous, unexpected and unexplained, 500 W electrical load that began on July 23rd and disappeared without explanation on December 20th. In the spring of 2011, a similar load appeared and was traced to a faulty programming of the periodic temperature increase in the pre-heat reservoir of the domestic hot water system. This load has been estimated at 1,580 kWh during the measurement period.
- Integration of the control system is ongoing, has yet to be fully optimized, and has occasionally fallen off-line.
- The ducting of thermal energy from the roof to the various systems is not as efficient as expected (e.g. too many 90° turns), resulting in significant pressure drops and some energy loss.

c. Added equipment

- In the final stages of construction/commissioning, a decision was made to add an air cleaner to the ventilation system in order to ensure good indoor air quality. This item was not included in the original modeling exercise and represents an additional 429 kWh of energy consumption.

d. Modifications made by the occupants

- It was originally assumed that the garage would not be heated. However, in order to use that space as a workshop, the occupants subsequently added a 5 kW electric auxiliary heater. Consumption during the period has been estimated from the measured electricity profiles to be 763 kWh.

- The interior lighting originally provided was modest but adequate. The homeowners decided to increase interior lighting by approximately 15 low-energy light bulbs.

e. Variations from modeling rules under the EQuilibrium™ Initiative

- The contest rules of the EQuilibrium™ Initiative allowed heating set-points of 19°C and 21°C (without regard to the time of day), and a cooling set-point of 24°C. It was assumed that some behavioral change by the occupants would be forthcoming in the attainment of a zero-energy goal, and that the temperature of the home would be allowed to fluctuate in order to optimize the heating and cooling profile and the storage of solar gains in the building mass.

  However, comfort levels (both physical and financial) are subjective. The current occupants have determined that an acceptable comfort level is about 18°C during the night time and 22.5°C during the day (for heating), and no more than 23°C during the summer months. This change in the set-point temperatures contributes to increased energy consumption for space heating (the high set point), and adds a requirement for some cooling. The set-point change during the heating season is especially onerous as it forces the auxiliary electric coil to operate early in the morning, even though more-than-enough passive solar and/or thermal solar energy is often available to gradually raise the temperature from 18°C to 22.5°C within a few hours of daybreak.

Table 3: Differences Between Modeled And Actual Consumption

CONSUMPTION	(kWh)
Projected Energy Consumption	5575
Design Issues	
• Distribution Fan	1611
• Domestic Hot Water	625
Equipment Shortcomings	
• Dryer Fan	920
• Mystery load	1580
Added Equipment	
• Air Cleaner	429
Modifications	
• Garage Heater	763
Variations From EQuilibrium™ Rules	
• Set-point (Heating)	104
• Set-Point Changes (Cooling)	124
Other (Plug Loads, Etc.)	1157
Actual Energy Consumption	12888

4. VARIOUS OTHER CONSIDERATIONS AND CONCLUSIONS

- The additional energy consumed by increased interior lighting and garage heating is significant; more energy is consumed by these elements than that required to run the heat pump.
- The final, total net-energy consumption of the ÉcoTerra™ house at 10,318 kWh is approximately 28,000 kWh less than the national average for single family detached homes.
- The appliances, lighting and other electrical plug loads are higher than the design values. This item is difficult to predict because it is largely influenced by the occupant's lifestyle.
- The garage heater, the heat pump distribution fan, and the domestic hot water heating were found to be the main sources of the extra consumption. The dryer booster fan running continuously and the mystery load were caused by equipment failure and should not be considered as part of the normal energy consumption of the house.

5. LESSONS LEARNED

- The garage heater could be eliminated by utilizing BIPV/T air from the roof (when the BIPV/T air temperature is above 10^{o}C) ducted to the garage with a small duct of about 5 cm diameter. This would increase the heat used from the solar roof (currently, only BIPV/T air above 20^{o}C is useful).
- Use of a heat pump connected to the roof instead of a ground source heat pump would also decrease energy use while reducing cost (elimination of the ground loop).
- Reduction of the daytime set-point would further reduce consumption.
- Making the forced air circulation fan of the heat pump run only half of the time (or less) when heating is not required (i.e. in circulation mode) would be a good solution to reduce the net energy consumption of the ÉcoTerra™ house while maintaining a reasonable comfort level for the occupants.

- The system control display should provide feedback to the occupants to enable them to compare real-time energy consumption against the normal base load. This would help avoid a situation where equipment malfunctions go undetected as was the case of the mystery load from July to December. See attached example of a suggested display.
- The actual plug loads of the ÉcoTerra™ house are much more extensive than those modeled. See the attached original and actual equipment list.
- A similar house with a more optimized BIPV/T system, a heat pump linked to the BIPV/T source, and more efficient PV system (e.g. 15% efficiency as opposed to 6% efficiency for amorphous Si, collectors angled at an 40-50 degrees), should result in approximately net-zero energy consumption.

6. REFERENCE

Doiron, Matthew Antony. 2011. "Whole Building Energy Analysis and Lessons Learned for a Near NetZero Energy Solar House". Thesis, Montreal, Concordia University.

With thanks to Louise Laferrière and Gilles Drouin, owners of the ÉcoTerra™ house.